EÖTVÖS LORÁND GEOPHYSICAL INSTITUTE OF HUNGARY
MAGYAR ÁLLAMI EÖTVÖS LORÁND GEOFIZIKAI INTÉZET
ВЕНГЕРСКИЙ ГЕОФИЗИЧЕСКИЙ ИНСТИТУТ ИМ. Л. ЭТВЕША

GEOPHYSICAL TRANSACTIONS
GEOFIZIKAI KÖZLEMÉNYEK
ГЕОФИЗИЧЕСКИЙ БЮЛЛЕТЕНЬ

28/1

BUDAPEST
1982

ETO/UDC 550.3(061.6) (439 Budapest) (058)
HU ISSN 0016—7177

Felelős kiadó: MÜLLER Pál

Manuscripts and all correspondence to:
Editor, Geophysical Transactions, Eötvös Loránd Geophysical Institute
of Hungary, POB 35, Budapest, H-1440, Hungary.

CONTENTS

TARTALOM

СОДЕРЖАНИЕ

EDITORIAL

A number of basic changes in publishing policy were decided upon by the Editorial Board to bring Geophysical Transactions into line with the latest trends of scientific publications.

The most important task of our journal remains that of acquainting the world of geophysics with the latest results of Hungarian geophysicists. But at the same time we would like to broaden the scope of topics as well as the circle of authors by including papers of researchers of all countries. With this in mind, mention is made here that the present issue includes a paper from the GDR and a contribution from the USSR.

Geophysical Transactions has been published since 1952 and is sent on an exchange basis to 360 institutions of exploration geophysics in 59 countries. It is thus guaranteed that your work will reach an international audience. Geophysical Transactions is reviewed regularly in Applied Mechanics Reviews and Referativny Zhurnal. We are currently concerned with extending the reviewing possibilities to enable all information appearing in our journal to flow into the mainstream of worldwide information circulation.

In addition to the strong background indicated above we are able to offer:

— publication of accepted manuscripts (if necessary revised according to referees' opinion) within six months;

— charge-free supply of 25 separata; for more than two authors—on request—this figure can be doubled.

Starting with this issue, from now on English abstracts will be published at the beginning of the article; Hungarian and Russian abstracts will appear at the end of each paper. Figure captions are provided in three languages (English, Hungarian, Russian) for the benefit of a wider audience.

The Editor will be pleased to receive letters, comments and opinion from readers and contributors.

EÖTVÖS LORÁND GEOPHYSICAL INSTITUTE OF HUNGARY
GEOPHYSICAL TRANSACTIONS 1982
28/1 pp. 5–19

CERTAIN PROBLEMS OF SEISMIC AND ULTRASONIC WAVE PROPAGATION IN A MEDIUM WITH INHOMOGENEITIES OF RANDOM DISTRIBUTION. III. STATISTICS OF THE DIFFUSE REFLECTION SHADOW FOLLOWING A ROUGH REFLECTING BOUNDARY*

G. KORVIN**

It has been since long a basic problem of reflection seismics in Hungary that in many cases we can get only intricate diffuse reflections from the uneven surface of the basement. These diffuse reflections tend to make it difficult to accurately map the basin floor, diffraction arrivals from surface roughnesses follow the basement reflection as a "diffuse shadow" of a few hundred ms length interfering with eventual deeper arrivals.

The statistical properties of diffuse reflections arising from Gaussian differentiable, random surfaces are dealt with. The temporal amplitude behaviour of the diffuse reflection shadow is derived and an interesting analogy between two-dimensional Brownian motion and backscattering from random surfaces is pointed out.

Introduction

It has been since long a basic problem of Hungarian reflection seismics that in many cases we cannot get but intricated *diffuse* reflections from the uneven surface of the basement (Szénás and Ádám 1953). Due to these diffuse reflections it is rather difficult at some places to map the basin floor accurately: diffraction arrivals coming from the surface roughnesses follow the basement reflection as a "diffuse shadow" of a few hundred ms length so that it tends to be very difficult to detect eventual deeper reflections. The existence of the diffuse reflection shadow following rough boundaries has also been demostrated by model experiments (Voskresenskiy 1962, Leong et al. 1971). For a special non-differentiable random surface model the time-behaviour of the diffuse reflection shadow was theoretically investigated in the low-frequency limit by Biot (1957). In the present paper Gaussian differentiable, random surfaces will be considered for the case when the wavelength is much shorter than the characteristic size of the inhomogeneities. Surface-surface multiple scattering and corrections for the self-shadowing of the random surface (Beckmann 1965) will not be taken into account.

I will derive the expected temporal behaviour of the amplitude distribution of the diffuse reflection shadow, and call attention to an interesting analogy between the Brownian motion (two-dimensional random walk) and the backscattering from random surfaces. Connections with digital processing are to be dealt with in a separate paper.

The problem was called to my attention some 10 years ago by the late Dr. Gy. Szénás (see *Editorial note* to Korvin 1973). This paper is dedicated to his memory.

* The first two parts of this series of articles appeared in Geophysical Transactions, Vols. 21 (1973) and 24 (1977).

** Eötvös Loránd Geophysical Institute (ELGI) of Hungary

Manuscript received: 24. 9. 1981.

Statistics of the Diffuse Reflection Shadow

The measurement geometry utilized is shown in *Fig. 1*. The random surface is described by the function $\xi(x, y)$; it is supposed that $\xi(x, y)$ is homogeneous and isotropic (TATARSKI 1967) with

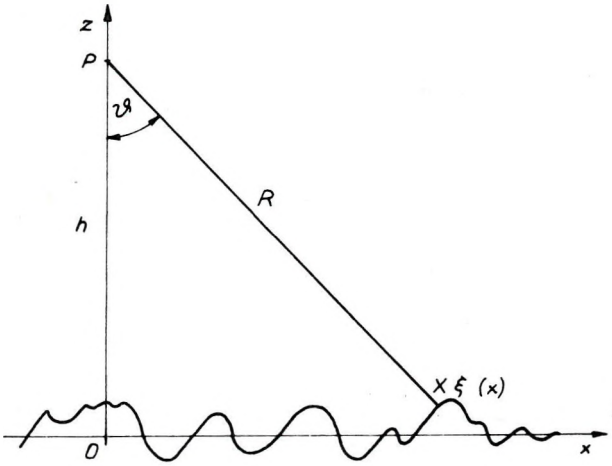

Fig. 1. Measurement geometry
1. ábra. Mérési geometria
Рис. 1. Геометрия измерительной установки

$$\langle \xi \rangle = 0, \quad \langle \xi^2 \rangle = \sigma^2,$$

further, that it is Gaussian with the distribution function

$$W(\xi) = \frac{1}{\sigma \sqrt{2\pi}} \exp\left(-\xi^2/2\sigma^2\right) \tag{1}$$

and correlation function

$$\langle \xi(x_1, y_1)\xi(x_2, y_2) \rangle = \sigma^2 \exp\left(-r^2/r_0^2\right), \tag{2}$$

where $r^2 = (x_1 - x_2)^2 + (y_1 - y_2)^2$; r_0 is termed the *correlation length*. If we consider a section of $\xi(x, y)$ along an arbitrary direction x the power spectrum of $\xi(x)$ is given by

$$E(k) = \frac{r_0}{2\sqrt{\pi}} \exp\left(-\frac{k_0^2}{4} r_0^2\right) \tag{3}$$

(cf. TATARSKI 1957). Suppose that $\xi(x)$ is at least twice continuously differentiable and introduce the new variables

$$\xi_1 = \frac{\partial \xi}{\partial x}, \quad \xi_2 = \frac{\partial^2 \xi}{\partial x^2}.$$

Obviously, ξ_1 and ξ_2 are also Gaussian and, by the general formula of RICE (1944, 1945), if $\xi_n = \dfrac{\partial^n \xi}{\partial \xi^n}$ exists, then

$$\langle \xi^2 \rangle = \gamma_n^2 = \int_0^\infty E(k) k^{2n} \, \mathrm{d}k. \tag{4}$$

Substituting Eq. (3) into (4) and making use of the integration formula 3.461.2 of GRADSHTEIN—RYZHIK (1963):

$$\gamma_n^2 = \langle \xi_n^2 \rangle = \frac{2^{n-1}(2n-1)!!}{r_0^{2n}} \cdot \sigma^2, \tag{5}$$

where, with the usual notation,

$$(2n-1)!! = 1 \cdot 3 \cdot 5 \ldots (2n-1). \tag{6}$$

Particularly,

$$\langle \xi_1^2 \rangle = \gamma_1^2 = \frac{\sigma^2}{r_0^2}, \tag{7}$$

$$\langle \xi_2^2 \rangle = \gamma_2^2 = \frac{6\sigma^2}{r_0^4}. \tag{8}$$

Now, suppose $\xi(x)$ is an arbitrary stationary stochastic process with zero mean and the autocorrelation function

$$R_{\zeta\zeta}(\tau) = \langle \zeta(x) \zeta(x+\tau) \rangle.$$

As is well known, if $\zeta(x)$ is continuously differentiable then

$$\left. \frac{\partial R_{\zeta\zeta}(\tau)}{\partial \tau} \right|_{\tau=0} = 0 \tag{9}$$

(see e.g. CHERNOV 1960).

Then

$$\left\langle \frac{\mathrm{d}\zeta(x)}{\mathrm{d}x} \zeta(x+\tau) \right\rangle = -\left\langle \zeta(x) \frac{\mathrm{d}\zeta(x+\tau)}{\mathrm{d}\tau} \right\rangle = -\frac{\mathrm{d}R_{\zeta\zeta}(\tau)}{\mathrm{d}\tau} \tag{10}$$

implying that

$$\left\langle \frac{\mathrm{d}\zeta(x)}{\mathrm{d}x} \cdot \zeta(x) \right\rangle = -\left. \frac{\mathrm{d}R_{\zeta\zeta}(\tau)}{\mathrm{d}\tau} \right|_{\tau=0} = 0,$$

that is ζ and $\frac{d\zeta}{dx}$ are uncorrelated.

Applying this result for ξ_1 and ξ_2, their covariance matrix will be

$$\langle \xi_i \xi_j \rangle_{i,j=1,2} = \begin{pmatrix} \gamma_1^2 & 0 \\ 0 & \gamma_2^2 \end{pmatrix}$$

i.e. the 2-dimensional joint distribution of (ξ_1, ξ_2) is

$$W(\xi_1, \xi_2) = \frac{1}{2\pi\gamma_1\gamma_2} \exp\left[-\frac{1}{2}(\xi_1^2/\gamma_1^2 + \xi_2^2/\gamma_2^2) \right]. \tag{11}$$

After these preliminaries we select on the (x, y) plane an arbitrary straight line passing through the origin, say the axis x. Measurements are performed by generating and receiving the waves at point $P = P(0, 0, h)$, lying on the z axis at a height h above the plane (x, y) (this case corresponds to NMO corrected seismograms or time-sections). It is supposed that P lies high above the random surface, that is

$$\sigma^2 < h^2. \tag{12}$$

Let X denote the point $\xi(x)$, let $R = \overline{PX}$ (Fig. 1). We obtain a reflection from point X if and only if x is a stationary point of the function $R(x) = PX$, i.e.

$$\frac{\partial R}{\partial x} = \frac{\partial}{\partial x}\sqrt{(h-\xi)^2 + x^2} = \frac{x + \xi\xi_1 - h\xi_1}{R} = 0,$$

i.e. if

$$\xi_1\left(1 - \frac{\xi}{h}\right) = \frac{x}{h}. \tag{13}$$

If we introduce the notation $\varkappa = 1/h$ and neglect the second term on the l.h.s. of Eq. (13) on the strength of assumption (12), the necessary and sufficient condition of a reflection from $X = \xi(x)$ will be the validity of

$$\xi_1(x) = \varkappa x. \tag{14}$$

Denote by $N(x)\,dx$ the probability of a reflection arrival from some surface point $\xi(x)$ above the interval $(x, x + dx)$.

$N(x)$ will be determined by means of the method of KUZNETSOV et al. 1954 (see also BASS and FUKS 1972, LONGUET—HIGGINS 1960):

Suppose $\zeta(x)$ is an arbitrary differentiable random function, $\varphi(x)$ a differentiable deterministic function. Denote by

$$w(\zeta = \varphi(x); \dot{\zeta} = \gamma) \Delta\zeta \Delta\dot{\zeta} \left(\dot{\zeta} = \frac{d\zeta}{dx} \right) \tag{15}$$

the probability of the event that the function $z=\zeta(x)$ intersects the vertical line segment

$$\varphi(x) \leqq z \leqq \varphi(x)+\Delta\zeta \tag{16}$$

in such a manner that the slope at the crossing remains within the limits

$$\gamma \leqq \dot{\zeta} \leqq \gamma+\Delta\dot{\zeta}. \tag{17}$$

As seen from *Fig. 2* this occurs, for a sufficiently small $\Delta\zeta$, if and only if $\zeta(x)$ and $\varphi(x)$ cross each other within the interval

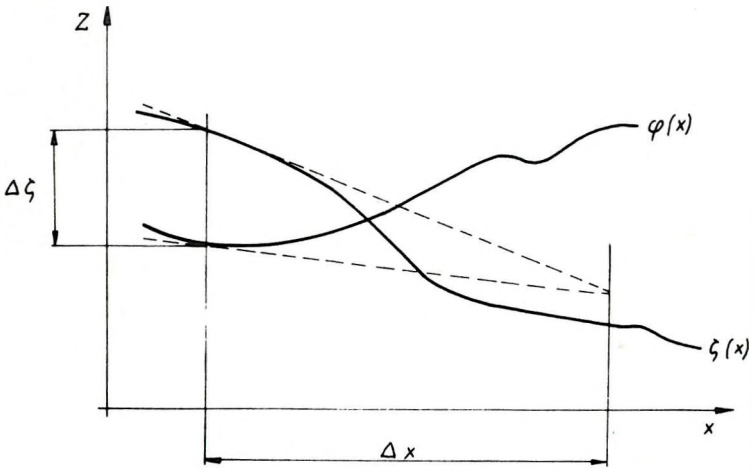

Fig. 2.
2. ábra
Рис. 2.

$$\Delta x = \frac{\Delta\zeta}{|\dot{\zeta}-\dot{\varphi}|}.$$

Consequently,

$$w(\zeta=\varphi(x);\ \dot{\zeta}=\gamma)\,|\dot{\zeta}-\dot{\varphi}|\,\Delta\dot{\zeta}\Delta x \tag{18}$$

is the probability that $\zeta(x)$ intersects $\varphi(x)$ while its derivative $\dot{\zeta}$ stays within $\gamma \leqq \dot{\zeta} \leqq \gamma+\Delta\dot{\zeta}$.

So, the probability of ζ crossing φ in the interval $(x, x+\mathrm{d}x)$ is given by

$$P = \mathrm{d}x \int_{-\infty}^{\infty} w(\varphi(x), \gamma)\,|\gamma-\dot{\varphi}(x)|\,\mathrm{d}\gamma. \tag{19}$$

Taking, in view of Eq. (14), $\zeta(x)=\xi_1(x)$, $\dot{\zeta}(x)=\xi_2(x)$, $\varphi(x)=\chi x$ the probability of having a reflection from $\xi(x')$ $(x \leqq x' \leqq x+\mathrm{d}x)$ is given by

$$N(x)\,dx = \frac{dx}{2\pi\gamma_1\gamma_2}\int_{-\infty}^{\infty}\exp\left[-\frac{1}{2}(\chi^2x^2/\gamma_1^2+\xi_2^2/\gamma_2^2)\right]|\chi-\xi_2|\,d\xi_2. \tag{20}$$

Performing the integration in Eq. 20 we obtain

$$N(x) = \frac{1}{\pi\gamma_1}\exp\left[-\frac{1}{2}\chi^2x^2/\gamma_1^2\right]\cdot\left\{\chi\int_0^{\alpha}\exp\left(-\frac{1}{2}\tau^2\right)d\tau+\gamma_2\exp\left(-\frac{1}{2}\alpha^2\right)\right\}, \tag{21}$$

where I introduced the notation

$$\alpha = \frac{\chi}{\gamma_2} = \frac{1}{h\gamma_2} = \frac{1}{\sqrt{6}}\frac{r_0^2}{h\sigma}. \tag{22}$$

Assuming that

$$\frac{\alpha}{h} = \frac{1}{\sqrt{6}}\frac{r_0^2}{h^2\sigma} < 1 \tag{23}$$

we can neglect the first term in the wavy brackets of Eq. (21), so that

$$N(x) \approx \frac{1}{\pi}\frac{\gamma_2}{\gamma_1}\exp\left(-\frac{\alpha^2}{2}\right)\exp\left(-\frac{1}{2}\chi^2x^2/\gamma_1^2\right) =$$

$$= \frac{\sqrt{6}}{\pi r_0}\exp\left(-\frac{1}{12}\frac{r_0^4}{h^2\sigma^2}\right)\exp\left[-\frac{1}{2}\chi^2x^2/\gamma_1^2\right]. \tag{24}$$

Let us now determine the expected number of reflections $\mathfrak{N}(x)\,dx$ scattered from the ring between the radii x and $x+dx$ around the origin 0 of the (x, y) plane. If v is the propagation speed of sound waves above the plane (x, y) and $R \approx \sqrt{x^2+h^2}$, then $\mathfrak{N}(x)\,dx$ is the expected number of reflection arrivals from the surface ξ, at the time instant $t = 2R/V$.

Denote by C_x the circle of radius x around 0, let e be an arbitrary line through the origin that intersects C_x at pont Q, and C_{x+dx} at point Q'. Let us define a function $\varepsilon(Q)$ along the circle C_x in the following way:

$\varepsilon(Q)=1$ if there is a reflecting point on surface ξ, above the segment $\overline{QQ'}$,

$\varepsilon(Q)=0$ otherwise.

Evidently

$$\mathfrak{N}(x)\,dx = \left\langle \oint_{C_x}\varepsilon(Q)\,ds\right\rangle;$$

on the other hand, because of the isotropy and ergodicity of the random surface ξ:

$$\left\langle \frac{\oint_{C_x} \varepsilon(Q)\,\mathrm{d}s}{2\pi x} \right\rangle = N(x)\,\mathrm{d}x$$

that is

$$\mathfrak{N}(x)\,\mathrm{d}x = 2\pi x N(x)\,\mathrm{d}x. \tag{25}$$

By Eq. (24):

$$\mathfrak{N}(x) = 2\sqrt{6}\frac{1}{r_0}\exp\left(-\frac{1}{12}\frac{r_0^4}{h^2\sigma^2}\right)\times\exp\left(-\frac{1}{2}\chi^2x^2/\gamma_1^2\right) \tag{26}$$

i.e. the expected number of reflections at the time instant $t = 2R/v$ from the random surface ξ is

$$\mathfrak{N}(x)\,\mathrm{d}x = Ax\exp\left(-\frac{1}{2}\chi^2x^2/\gamma_1^2\right)\mathrm{d}x, \tag{27}$$

where

$$A = 2\sqrt{6}\frac{1}{r_0}\exp\left(-\frac{1}{12}\frac{r_0^4}{h^2\sigma^2}\right). \tag{28}$$

Since A is a bounded function of depth h:

$$A = A(h) = O(1) \tag{29}$$

and γ_1^2 is independent of h, the *expected total number of reflections from the Gaussian random surface* $\xi(x, y)$ is

$$N = A\int_0^\infty x\exp\left(-\frac{1}{2}\chi^2x^2/\gamma_1^2\right)\mathrm{d}x = \frac{A\gamma_1^2}{2\chi^2} = O(h^2) \tag{30}$$

i.e. a finite value of the order h^2, in agreement with the result of LONGUET—HIGGINS (1960).

The function

$$x\exp\left(-\frac{1}{2}\chi^2x^2/\gamma_1^2\right)$$

attains its maximum for x_{max}, where

$$\frac{x_{\max}^2}{h^2} = \gamma_1^2 \tag{31}$$

that is

$$x_{\max} = \pm h(\gamma_1). \tag{32}$$

Since, by Eq. (7), γ_1^2 is the mean square slope of the surface $\xi(x)$, Eq. (32) allows the following simple geometric interpretation *(Fig. 3)*:

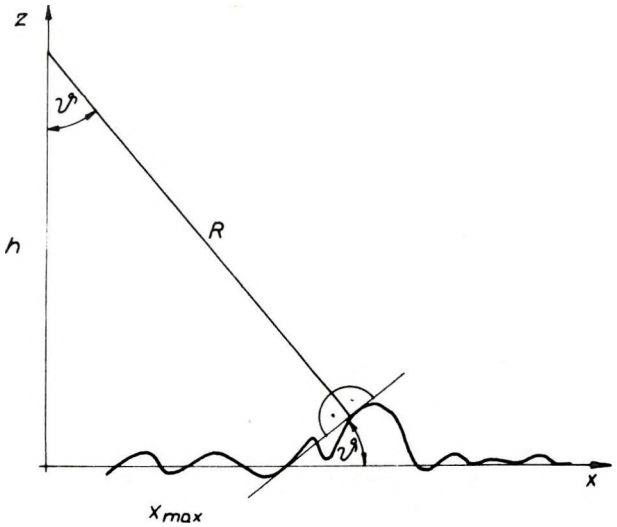

Fig. 3. Condition of maximal energy return from a random Gaussian surface

3. ábra. Véletlen felületről várható maximális reflexió feltétele

Рис. 3. Условие максимального отражения от случайной поверхности

The greatest number of reflections from the random surface $\xi(x, y)$ will be obtained for the angle of incidence ϑ for that

$$\operatorname{tg}^2 \vartheta = \left\langle \left(\frac{\partial \xi}{\partial x} \right)^2 \right\rangle = \gamma_1^2 = \frac{\sigma^2}{r_0^2}. \tag{33}$$

The corresponding distance $R_{\max}$ will be, by Eq. 31:

$$R_{\max} \approx h\sqrt{1+\gamma_1^2} \tag{34}$$

or, in terms of two-fold arrival times, the maximum number of backscattered reflections is to be expected at

$$t_{\max} \approx t_0\sqrt{1+\gamma_1^2}, \tag{35}$$

where $t = 2R/v$, $t_0 = 2h/v$, v is the propagation speed above the plane (x, y).

If the propagating wave has the dominant frequency f, the corresponding wavelength is

$$\lambda = \frac{v}{f} \tag{36}$$

and the first Fresnel zone on the (x, y) plane has the radius

$$x_1 = \sqrt{\lambda h/2}.$$

As is well known, the scattering has no important effect unless

$$r_0 \ll x_1, \tag{37}$$

in this case the *total energy* of the diffuse reflections coming from the circle of radius x will also be proportional to their total number $\mathfrak{N}(x)\,dx$ (cf. CLAY and LEONG in HAMPTON, 1974).

For the applicability of geometrical optics we require the following conditions

$$\lambda < r_0 \tag{C.1}$$

$$\lambda < h \tag{C.2}$$

a further evident geometrical restriction that

$$\sigma^2 \ll h^2 \quad \text{(cf. Eq. 12)} \tag{C.3}$$

should hold.

The condition of significant diffuse reflection noise is Eq. (37) i.e.

$$r_0 \ll \sqrt{\frac{\lambda h}{2}}. \tag{C.4}$$

In the neglection made in expression (21) we assumed (cf. Eq. 23) that

$$\frac{1}{h^4} \ll \gamma_2^2 = \langle \xi_2^2 \rangle = \frac{6\sigma^2}{r_0^4}. \tag{C.5}$$

If we are given the geometry (σ^2, r_0) of the random surface ξ, it is only condition C.1 that implies a restriction on the wavelength, all the other conditions C.2—C.5 are automatically satisfied for sufficiently large depths h.

With regard to the width of the diffuse reflection shadow, it begins at the distance

$$x=0$$

assumes its maximum at

$$x^2=h^2\gamma_1^2 \quad \text{(cf. Eq. 31)}$$

and it practically dies out for

$$x^2 \approx 3h^2\gamma_1^2. \tag{38}$$

The corresponding distances R are given by

$$\begin{aligned} R_0 &= h, \\ R_{\max} &\approx h\sqrt{1+\gamma_1^2}, \\ R_{\text{end}} &\approx h\sqrt{1+3\gamma_1^2}. \end{aligned} \tag{39}$$

In terms of two-fold travel times, the shadow exists between

$$t_0 \leqq t \leqq t_0\sqrt{1+3\gamma_1^2}$$

it starts with zero expected energy, its energy gradually builds up, attains its maximal value around

$$t_{\max} = t_0\sqrt{1+\gamma_1^2}$$

and from that point on it decreases faster than exponentially until it disappears around

$$t_{\text{end}} \approx t_0\sqrt{1+3\gamma_1^2}.$$

As an example consider the case of $v = 4000$ m/s; $f = 40$ Hz; $h = 4000$ m; $r_0 = 250$ m; $\sigma^2 = 5000$ m^2 ($\lambda = 100$ m). It is easy to check that conditions C.1—C.5 are met. The time-behaviour of the diffuse reflection shadow is characterized by:

$$t_0 = \frac{2h}{v} = 2 \text{ s},$$

$$t_{\max} \approx 2.078 \text{ s},$$

$$t_{\text{end}} \approx 2.228 \text{ s}.$$

Connections with Two-Dimensional Random Walk

Equation (26) can be re-written, by means of Eqs. (28) and (30), as

$$\mathfrak{N}(x)\,dx = N\frac{x}{\gamma_1^2 h^2}\exp\left(-\frac{1}{2}\frac{x^2}{\gamma_1^2 h^2}\right)dx, \tag{40}$$

where N is the expected total number of reflections from the random surface ξ.

It will be shown that Eq. (40) has an interesting physical interpretation.

Let us consider a particle walking randomly along the (x, y) plane in such a way that it starts at $t=0$ then performs its *Brownian motion with a free path-length decreasing inversely with time.* More exactly we are going to solve the following problem, by a generalization of RAYLEIGH's (1877) method.

Denote $v(t, x, y)$ the probability distribution of the event that the particle starting out from the origin at $t=0$ arrives to the point (x, y) at time t. This can only happen *(Fig. 4)* if at the time-instant $(t-\Delta t)$ the particle had been at some of the equally probable points of the circle of radius $a(t)$ centred around (x, y):

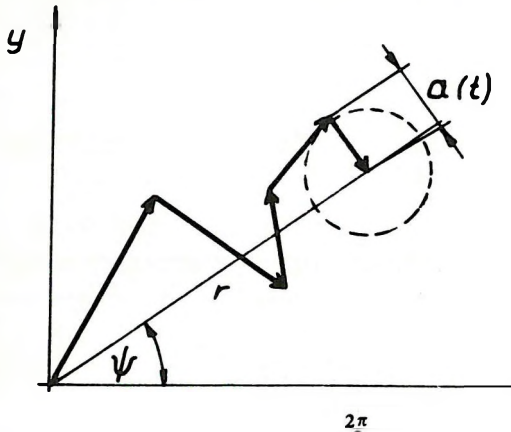

Fig. 4. Generalized Brownian motion
4. ábra. Általánosított Brown-mozgás
Рис. 4. Обобщенное броуновское движение

$$v(t, x, y) = \int_0^{2\pi} v(t-\Delta t, x-a\cos\varphi, y-a\sin\varphi)\frac{d\varphi}{2\pi}. \tag{41}$$

Developing the integrand into series according to the powers of $a\cos\varphi$ and $a\sin\varphi$ and performing the integration with respect to φ:

$$v(t, x, y) = v(t-\Delta t, x, y) + \frac{a^2(t)}{4}\left(\frac{\partial^2 v}{\partial x^2} + \frac{\partial^2 v}{\partial y^2}\right) + O(a^3). \tag{42}$$

If we assume that the free path-length decreases in inverse proportion with time:

$$\lim_{\Delta t\to 0}\frac{a^2(t)}{\Delta t} = \frac{2B}{(t+1)^2}, \tag{43}$$

where B is constant and we let $\Delta t \to 0$, Eq. (42) leads to the following 2-dimensional diffusion equation with time-variant diffusion coefficient:

$$\frac{\partial v}{\partial t} = \frac{B}{2(t+1)^2}\left(\frac{\partial^2 v}{\partial x^2} + \frac{\partial^2 v}{\partial y^2}\right). \tag{44}$$

It is easy to check that the solution to Eq. (44), subject to the initial condition $v(t=0, x, y) = \delta(x)\delta(y)$, is

$$v(t, x, y) = \frac{t+1}{2\pi Bt} \exp\left[-\frac{t+1}{2Bt}(x^2+y^2)\right]. \tag{45}$$

Introducing polar coordinates r, ψ by

$$x = r\cos\psi,$$

$$y = r\sin\psi$$

we have

$$v(t, x, y)\,\mathrm{d}x\,\mathrm{d}y = \exp\left[-\frac{t+1}{2Bt}r^2\right]\frac{t+1}{Bt}\,\frac{r\,\mathrm{d}r\,\mathrm{d}\psi}{2\pi} \tag{46}$$

that is the probability that the randomly walking particle would be a distance r from the origin at the time instant t is given by

$$v(t, r)\,\mathrm{d}r = \exp\left[-\frac{t+1}{2Bt}r^2\right]\frac{t+1}{Bt}\,r\,\mathrm{d}r. \tag{47}$$

Asymptotically, for $t \to \infty$, the moving particle slows down and its location will finally be distributed on the (x, y) plane according to the law

$$\lim_{t\to\infty} v(t, r)\,\mathrm{d}r = \frac{r}{B}\exp\left(-\frac{r^2}{2B}\right)\mathrm{d}r. \tag{48}$$

The similarity of our result (40) and the limiting distribution (48) is evident, by taking

$$B = \gamma_1^2 h^2.$$

Consequently, the backscattering effect of the Gaussian surface $\xi(x, y)$ can be substituted by the following Brownian motion model.

Suppose that at $t=0$ N randomly walking particles start out from the origin 0 of the (x, y) plane, where N is a finite number of $O(h^2)$, defined by Eq. (30). Suppose the particles perform their Brownian motion independently of each other, with unit velocity and with a gradually decreasing path length

$$\frac{\gamma_1 h}{t+1}. \tag{49}$$

Asymptotically, for $t\to\infty$ and for a sufficiently large N, the particles will be distributed on the (x, y) plane according to (48), with

$$B=\gamma_1^2 h^2.$$

If we now consider the particles as small mirrorlike monopoles of frequency- and direction-independent backscattering coefficient, the backscattered radiation observed at $P(0, 0, h)$ will be the same for $t>1$ than that received from the original random surface $\xi(x, y)$. Strictly speaking, the above substitution of random surfaces by the random walk of monopoles on the (x, y) plane is only valid for sufficiently high frequencies satisfying conditions C.1, C.2.

However, as observed by many researchers (MARSH 1961, LANGLEBEN 1970) the backscattering coefficient is frequency-independent for a very broad range of frequencies. It seems very likely that our main result (26) and the Brownian-motion model of random surfaces can be extended from the case $\lambda<r_0$ up to the wavelengths $\lambda\approx r_0$. In the low frequency limit ($\lambda>r_0$) there appears a coherent specular reflection coming from the mean surface $\langle\xi\rangle$ (TOLSTOY and CLAY 1966)—followed by a diffuse echo trail *of exponentially decaying density* (BIOT 1957). The time-constant of the exponential density decay is—in contradistinction to our results—frequency dependent for low frequencies: it is proportional to the square of the wave number (BIOT *op. cit.* §§. 4, 5).

It should be noted that the proposed Brownian motion model of wave scattering from random surfaces is in good agreement with the recently recognized interconnection of random wave propagation and Brownian motion (see e.g. BERCKHEMER 1970, FRISCH 1968, SULEM and FRISCH 1972).

REFERENCES

BACKUS, M., BURG, J., BALDWIN, D., BRYAN, E., 1964: Wideband extraction of mantle P waves from ambient noise. Geophysics, **29**, 5, pp. 672–692

BASS, F. G., FUKS, I. M. 1972: Wave Scattering from Statistically Uneven Surfaces. Nauka, Moscow (In Russian)

BECKMANN, P. 1965: Shadowing of random rough surfaces. IEEE Trans. AP–13 No. 3, pp. 384–388

BERCKHEMER, H. 1970: A possible scattering mechanism for lunar seismic waves. Zeitschr. für Geoph., **36**, 5, pp. 523–529

BIOT, M. A. 1957: Reflection on a rough surface from an acoustic point source. Journal Acoust. Soc. Am. **29**, No. 11, pp. 1193–1200

CHERNOV, L. A. 1960: Wave Propagation in a Random Medium. McGraw-Hill, New York
FRISCH, U. 1968: Wave Propagation in Random Media. *In:* Probabilistic Methods in Applied Mathematics. I. (Ed. BHARUCHA–REID, A. T.). Acadamic Press, New York–London, pp. 75–198
GRADSHTEIN, I. S., RYZHIK, I. M. 1963: Tables of Integrals, Sums and Products. Fiz. Mat. Lit. Moscow (In Russian)
HAMPTON, L. (Ed.) 1974: Physics of Sound in Marine Sediments. Plenum Press, New York–London
KORVIN, G. 1973: Certain problems of seismic and ultrasonic wave propagation in a medium with inhomogeneities of random distribution. Geoph. Trans., **21,** pp. 5–34
KORVIN, G. 1978: Correlation properties of source generated seismic noise, scattered on velocity inhomogeneities. Acta Geod. Geoph. Mont. Acad. Sci. Hung. **13,** Nos 1–2, pp. 201–210
KUZNETSOV, P. I., STRATONOVICH, V. L., TIKHONOV, V. I. 1954: Duration of the overshots of a random function. Zhurn. Tehn. Fiz., **24,** No. 1, 103 (In Russian)
LANGLEBEN, M. P. 1970: Reflection of sound at the water—sea ice interface. Journal Geoph. Res., **75,** 27, pp. 5243–5246
LEONG, W. K., KAN, T. K., CLAY, C. S. 1971: Use of acoustic scattering theory to interpret marine geophysical data. Univ. Wisconsin Geoph. and Polar Research Center, Research Rept. 71–7
LONGUET—HIGGINS, M. S. 1960: Reflection and refraction at a random moving surface. II. Number of specular points in a Gaussian surface. J. Opt. Soc. Am., **50,** 9, pp. 845–850
MARSH, H. W. 1961: Exact solution of wave scattering by irregular surfaces. Journal Acoust. Soc. Am., **33,** 3, pp. 330–333
RAYLEIGH, J. W. S. 1877: The Theory of Sound. Macmillan, London 2nd reprint Ed.: Dover, New York, 1945
RICE, S. O. 1944, 1945: The mathematical analysis of random noise. Bell Syst. Techn. J. **23,** No. 3 (1944); **24,** No 1 (1945)
RISTOW, D., JURCZYK, D. 1975: Vibroseis deconvolution. Geoph. Prosp., **23,** 2, pp. 363–379
SULEM, P. L., FRISCH, U. 1972: Total reflection of a plane wave by a semi-infinite random medium. J. Plasma Phys., **8,** 2, pp. 217–229
SZÉNÁS, GY., ÁDÁM, O. 1953: Seismo-geological conditions in SW-Hungary. Geof. Közl., **2,** pp. 73–89 (In Hungarian)
TATARSKI, V. I. 1967: Wave Propagation in a Turbulent Medium. Dover Publ. Inc. New York
TOLSTOY, I., CLAY, C. S. 1966: Ocean Acoustics: Theory and Experiment in Underwater Sound. McGraw-Hill, New York
VOSKRESENSKIY, YU. N. 1962; A three-dimensional model study of seismic wave reflection from non-mirrorlike boundaries. Izv. ANSSSR Ser. Geof., No 5, pp. 620–629 (In Russian)

KORVIN GÁBOR

A VÉLETLEN KÖZEGEK ELMÉLETE ÉS A SZEIZMIKUS, VALAMINT ULTRASZONIKUS HULLÁMTERJEDÉS NÉHÁNY PROBLÉMÁJA. III. AZ EGYENETLEN FELSZÍNŰ REFLEXIÓS HATÁRFELÜLETEKET KÖVETŐ DIFFÚZ REFLEXIÓS ÁRNYÉK STATISZTIKAI TULAJDONSÁGAI

A magyarországi reflexiós szeizmika régi problémája, hogy a bonyolult felületű medencealjzatról sok esetben csak diffúz reflexiót kapunk. A diffúz reflexió helyenként az aljzat pontos kimutatását is megnehezíti, az aljzat felületi egyenetlenségeiről jövő beérkezések pedig néhol több száz ms hosszú „árnyékként" követik az aljzatról származó reflexiót, megnehezítve az esetleges mélyebbről jövő beérkezések kimutatását.

A dolgozat a Gauss-eloszlású, véletlen, differenciálható felületekről való diffúz hullámvisszaverődés statisztikai tulajdonságaival foglalkozik. Levezeti a diffúz reflexiós árnyék amplitúdójának időbeli lefutását és felhívja a figyelmet a véletlen felületekről való hullámvisszaverődés és a kétdimenziós Brown-mozgás közötti analógiára.

A dolgozat legfontosabb eredményét a (26) egyenlet tartalmazza, a levezetéseknél alkalmazott közelítéseket a (C.1)—(C.5) feltételek foglalják össze.

Г. КОРВИН

ТЕОРИЯ СЛУЧАЙНЫХ СРЕД И НЕКОТОРЫЕ ПРОБЛЕМЫ РАСПРОСТРАНЕНИЯ СЕЙСМИЧЕСКИХ И УЛЬТРАЗВУКОВЫХ ВОЛН
III.
СТАТИСТИЧЕСКИЕ ОСОБЕННОСТИ ДИФФУЗНОЙ ТЕНИ ОТРАЖЕНИЙ, ПРОСЛЕЖИВАЮЩЕЙ НЕРОВНЫЕ ОТРАЖАЮЩИЕ ГРАНИЦЫ

Одна из проблем сейсморазведки МОВ в Венгрии давно заключается в получении в ряде случаев только диффузных отражений с основания бассейна при сложном построении его рельефа. Диффузное отражение местами также затрудняет точное выявление основания, а вступления с неровной поверхности основания появляются в качестве «тени» длиной до нескольких сотен мс, затрудняя выявление случайных вступлений от более глубоко залегающих горизонтов.

В работе обсуждаются статистические особенности диффузного отражения волн от случайных по гаусову распределению поверхностей, которые поддаются дифференциалу. Дается вывод временной характеристики амплитуды тени диффузного отражения и обращается внимание на аналогию между отражением волн от случайных поверхностей и двухмерным броуновским движением.

Важнейший результат работы представлен уравнением (26), а применяемые для выводов аппроксимации подытоживаются в условиях (С.1)–(С.5).

EÖTVÖS LORÁND GEOPHYSICAL INSTITUTE OF HUNGARY
GEOPHYSICAL TRANSACTIONS 1982
28/1 pp. 21–32

SIMPLE TECHNIQUE FOR MODELLING AND RECOMPRESSING SH TYPE CHANNEL WAVES

T. BODOKY*, E. CZILLER*, A. KÖRMENDI**

The increasing importance of in-seam seismic techniques used in coal mines necessitates a better understanding of seismic channel waves. To achieve this goal different numerical modelling techniques have been developed for studying the different types of these waves under arbitrary conditions.

A simple numerical model of SH type channel waves is presented and utilized to derive a recompressing filter to remove dispersion of the waves.

Simple model of SH type waves in a seismic wave guiding channel

When studying the propagation of SH type waves in a seam we can use a similar scheme of the raypaths to that used by BURG et al. to explain seismic repetitive patterns in shallow water *(Fig. 1)*. We consider the wave propagation in a seam having parallel plain boundaries and a thickness H. The distance between the source and the receiver is x. For simplicity's sake we assume symmetry in the model, i.e. both the source and the receiver are placed in the middle of the seam and the distortional waves have the same velocity both in the upper- and underlying layers. If this velocity is V_2 and that in the seam V_1, then $V_2 > V_1$.

There are a great number of possible raypaths between the source and the receiver because of the reflections on boundaries of the seam. Thus, at the receiver, the wavelets, which have propagated along different raypaths and have different arrival times, are subjected to interference and this interference is recorded as a seamwave wavelet. In the formation of this interference, two factors play important roles:

a) a series of "geometrical delays" coming from the geometrical length of raypaths,

b) phase shifts occurring at total reflections. The lengths of the raypaths and the travel times belonging to them are given by the geometry of the model. If the travel times are represented by τ, then in the case of n reflections

$$\tau_n = \frac{1}{V_1}\sqrt{(nH)^2 + x^2}. \tag{1}$$

The phase shifts are independent of frequency at the total reflection of SH type waves and are given by the formula

* Eötvös Loránd Geophysical Institute (ELGI) of Hungary.
** Tatabánya Coal Mines.
Paper presented at the 43rd EAEG Meeting, Venice, 25–29. May, 1981.

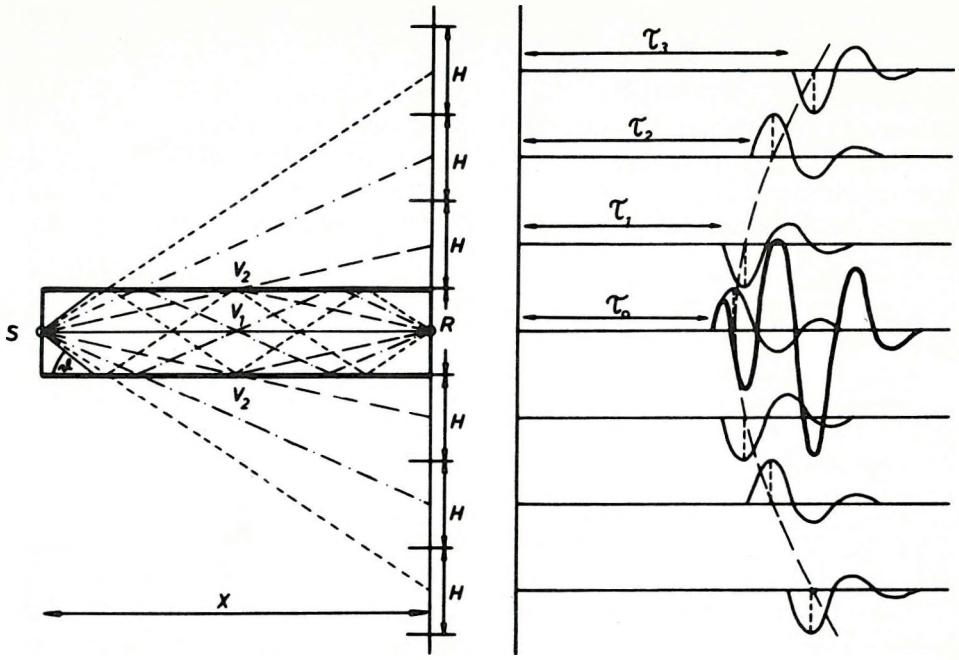

Fig. 1. A scheme of the raypaths and the "geometrical delays" in a wave guiding channel
1. ábra. A geometriai késleltetések vázlata egy hullámvezetőben
Фиг. 1. Схема геометрических задержек в волноводе

$$\psi(\vartheta) = -2 \arctan \left(\frac{\varrho_2 V_2}{\varrho_1 V_1} \frac{\sqrt{\frac{V_2^2}{V_1^2}\cos^2 \vartheta - 1}}{\sin \vartheta} \right), \tag{2}$$

where ψ is the phase shift, ϑ the angle made by the raypath with the boundary of the seam, and ϱ is the density.

If a raypath involves n total reflections then its total phase shift is

$$\psi_n = n\psi(\vartheta_n), \tag{3}$$

where ϑ_n comes also from the geometry of the model:

$$\vartheta_n = \arctan \frac{nH}{x}. \tag{4}$$

Now, if we denote the source signal as $S(t)$, the Fourier series of $S(t)$ can be written as

$$S(t) = \frac{A_0}{2} + \sum_k A_k \cos(\omega k t + \varphi_k), \tag{5}$$

where the series A_k is the amplitude spectrum and the series φ_k is the phase spectrum of $S(t)$.

From the source signal the dispersed in-seam wavelet can be derived by summing all source signals propagating along the possible raypaths and undergoing the attendant phase shifts. If the dispersed wavelet is denoted as $W(t)$ then

$$W(t) = S(t) + 2 \sum_{n=1}^{m} \sum_k A_k \cos[\omega k(t-\tau_n) + \varphi_k + \psi_n]. \tag{6}$$

The number of summands (m) can be determined from the critical angle. The summation has to be continued to the last direction having a ϑ_n smaller than the critical angle, viz.

$$\vartheta_m \leqq \arccos\frac{V_1}{V_2} \leqq \vartheta_{m+1}.$$

The model can be made better by weighting the summands proportionally to their source angles and inversely proportionally to the length of their raypaths. So the last form of the model is

$$W(t) = \sum_{n=0}^{m} \frac{b_n}{\tau_n} \sum_k A_k \cos[\omega k(t-\tau_n) + \varphi_k + \psi_n], \tag{7}$$

where b_n is given by the formulae

$$b_0 = 1$$

$$b_n = \frac{\beta_n - \beta_{n-1}}{\beta_0} \quad \text{if} \quad n = 1, 2, \ldots, m.$$

$$\beta_n = \arctan\frac{(2n+1)H}{2x}.$$

Formula (7) describes what we call the numerical model of the dispersed SH type channel wave wavelet. In the following we try to decompose the interference wavelet on the basis of this formula.

Simple recompression filter derived from the described model

The effect of the series of geometrical delays may be described as a convolution with a $G(x)$ function, where $G(x)$ takes the form

$$G(x) = \sum_{n=0}^{m} \frac{b_n}{\tau_n} \delta(\tau_n), \tag{8}$$

where δ denotes the Dirac function.

The $G(x)$ function has a special feature: its autocorrelation function is characterized by a sharp impulse-like main peak with comparatively very small side lobes. This behaviour can be used to eliminate the effect of geometrical delays, namely if $W(t)$ is correlated by $G(x)$ then the "short" autocorrelation function of $G(x)$ will step into the place of the "long" $G(x)$ function in the original convolution. Thus the dispersed wavelet will be significantly shorter, it will be decompressed.

In real practice however, the source-receiver (source image-receiver) distance, x, is not known therefore we have substituted the t variable for the fixed x value using the $x = tV_1$ equation. Neglecting the coefficients of delta functions, in this way the following filter operator is obtained:

$$g(t) = \sum_{n=0}^{m} \delta(\tau_n). \tag{9}$$

To see the effect of this filter a model using phase inversion instead of phase shifts was computed and filtered.

Figure 2 shows the source signal, the dispersed wavelet and the filtered result. As can be seen, the dispersed wavelet is not only recompressed by the filter in an effective manner but also placed exactly where it could have been expected if it had propagated as a regular *S* type bodywave.

The elimination of the phase shift of a single frequency can be done in a similar way. The phase shifts have to be converted into time delays and these have to be built into the filter operator.

$$U_{nk} = \frac{\psi_n}{2\pi} T_k,$$

where T_k is the period of the given f_k single frequency:

$$g(t, f_k) = \sum_{n=0}^{m} \delta(\tau_n + U_{nk}). \tag{10}$$

For accuracy, the measured trace must be reduced to its frequency components and the filtering must be performed on each component with the appropriate operator. After filtering, the components have to be summed again.

The solution described above is correct, but it is by no means simple. For this reason we decided to use the following approach:

the measured trace is filtered by several band-pass filters. The band-pass filters are zero-phase filters possessing triangle-shaped transfer functions. The

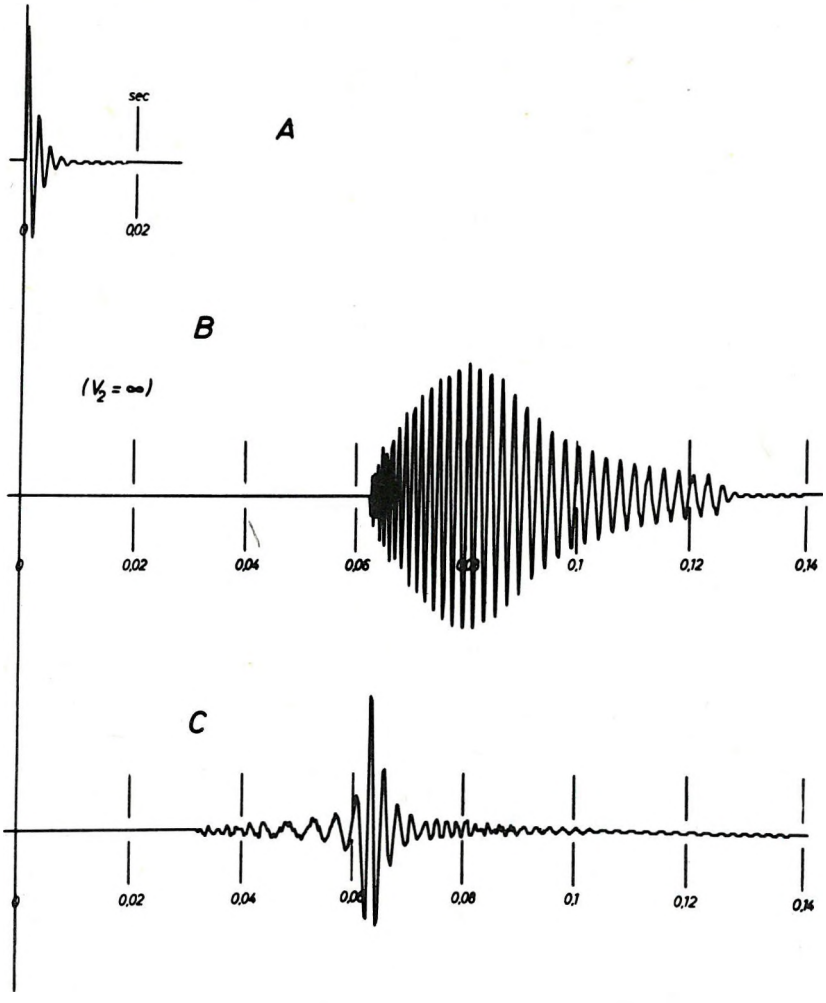

Fig. 2. A — source signal; B — dispersed wavelet; C — filtered wavelet

2. ábra. A — indulójel; B — diszperz csatornahullám; C — szűrt csatornahullám

Фиг. 2. А — Исходный сигнал; В — Дисперсная канальная волна; С — Отфильтрованная канальная волна

lower and upper frequency limits of the transfer functions fall to the peak frequency of the neighbouring ones *(Fig. 3)*. The band-pass filtered versions are correlated by the above described $g(t, f_k)$ operator, in which f_k is the peak frequency of the applied band-pass filter. After the correlation the different versions are summed and the result can then be band-pass filtered again.

This simplified way means that the original task is solved exactly only at the peak frequencies of the band-pass filters. All other frequency components of the filtered trace are obtained as a sum from the two neighbouring filtered versions.

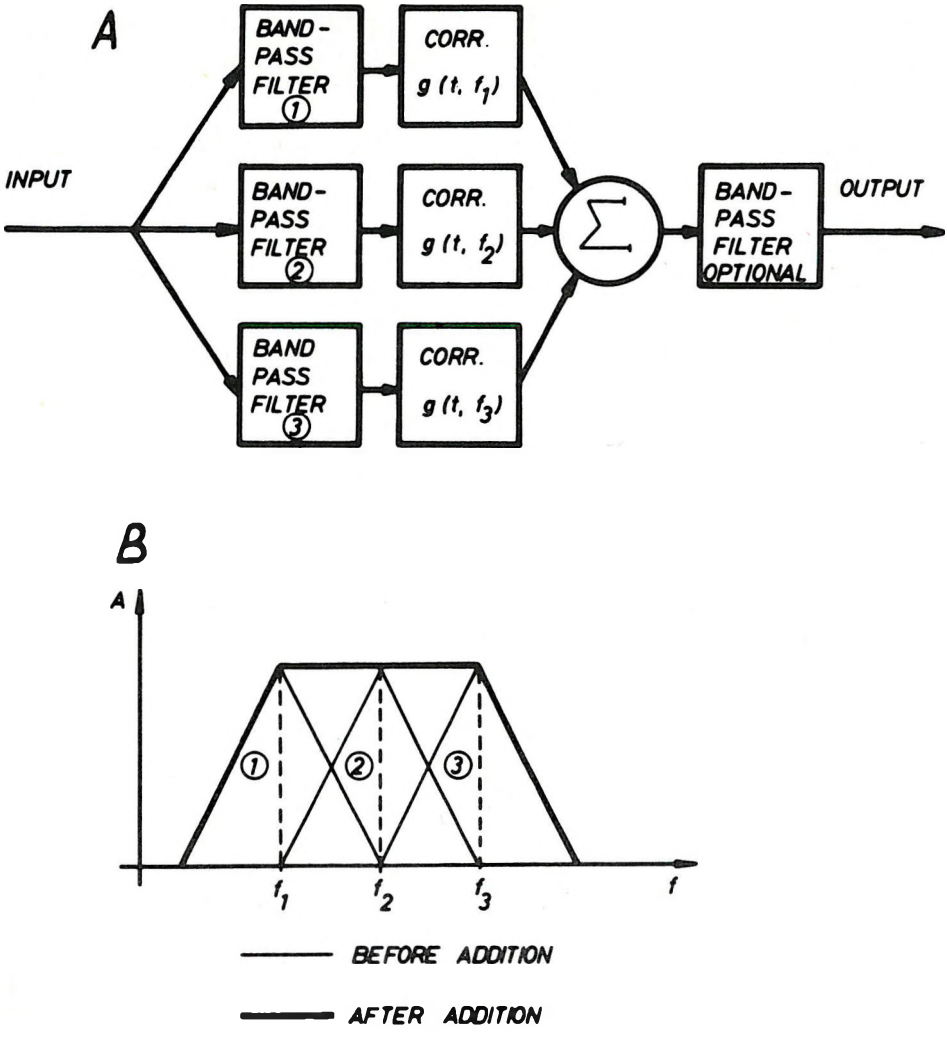

Fig. 3. The scheme of the proposed filtering
A — block diagram; B — transfer functions

3. ábra. A javasolt szűrési eljárás vázlata
A — blokkdiagram; B — átviteli függvények

Фиг. 3. Схема предложенного способа фильтрации А — Блок-схема; В — Частотные характеристики

To illustrate the effectiveness of the procedure three dispersed wavelet models and their filtered versions are shown. For the model computations the source signals were different but the other parameters were the same: ($x = 100$ m, $H = 2.5$ m, $V_1 = 1{,}600$ m/s, $V_1/V_2 = 0.5$ and $\varrho_1/\varrho_2 = 0.5$).

In *Fig. 4* the spectrum of the source signal expands from 100 to 400 Hz. The dispersed wavelet model is significantly delayed compared with the expected

arrival time of an S type bodywave propagating with velocity V_1, but it is not attenuated very much. For its filtering, five band-pass filters were used. As a result of the applied procedure the main peak of the filtered wavelet indicates precisely the arrival time belonging to V_1, and the wavelet has become shorter. If the processed wavelet is compared with the source signal it can be seen that the former is no more than 50% longer than the latter.

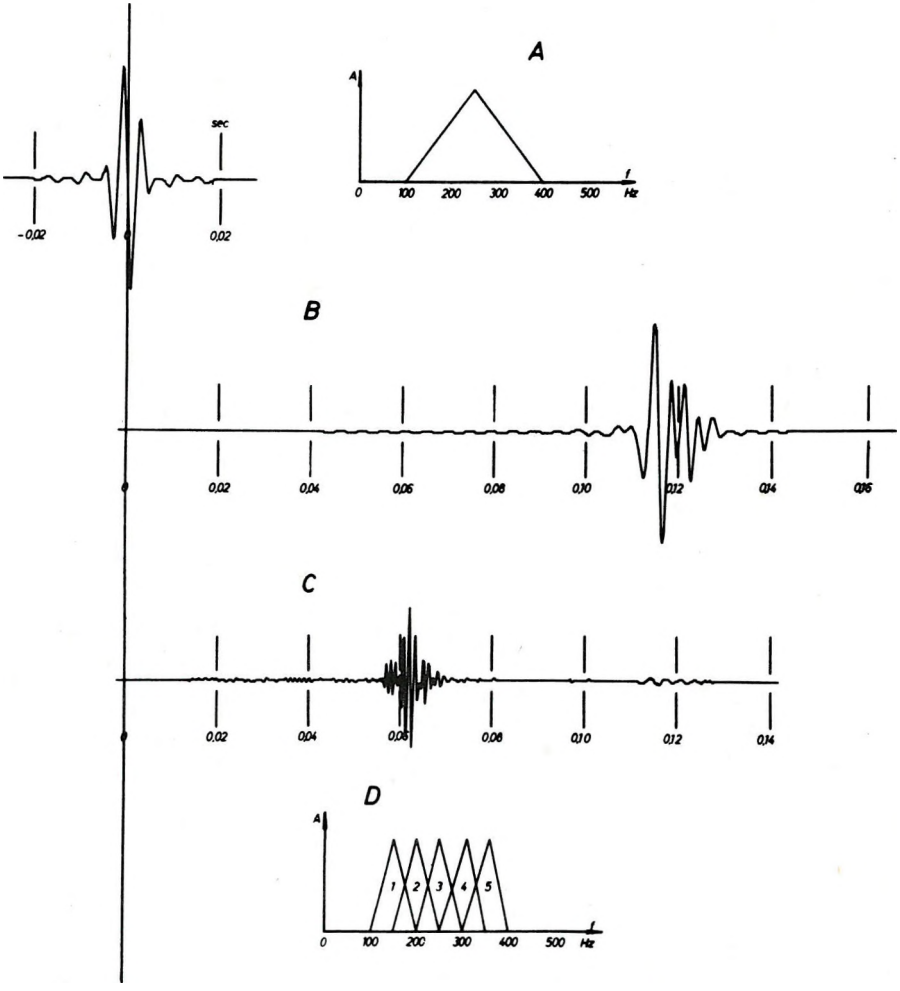

Fig. 4. A — source signal and its spectrum; B — dispersed wavelet; C — filtered wavelet; D — transfer functions of the used bandpass filters

4. ábra. A — az indulójel és spektruma; B — diszperz csatornahullám; C — szűrt csatornahullám; D — a használt sávszűrők átviteli függvényei

Фиг. 4. A – Исходный сигнал и его спектр; B – Дисперсная канальная волна; C – Отфильтрованная канальная волна; D – Частотные характеристики использованных полосовых фильтров

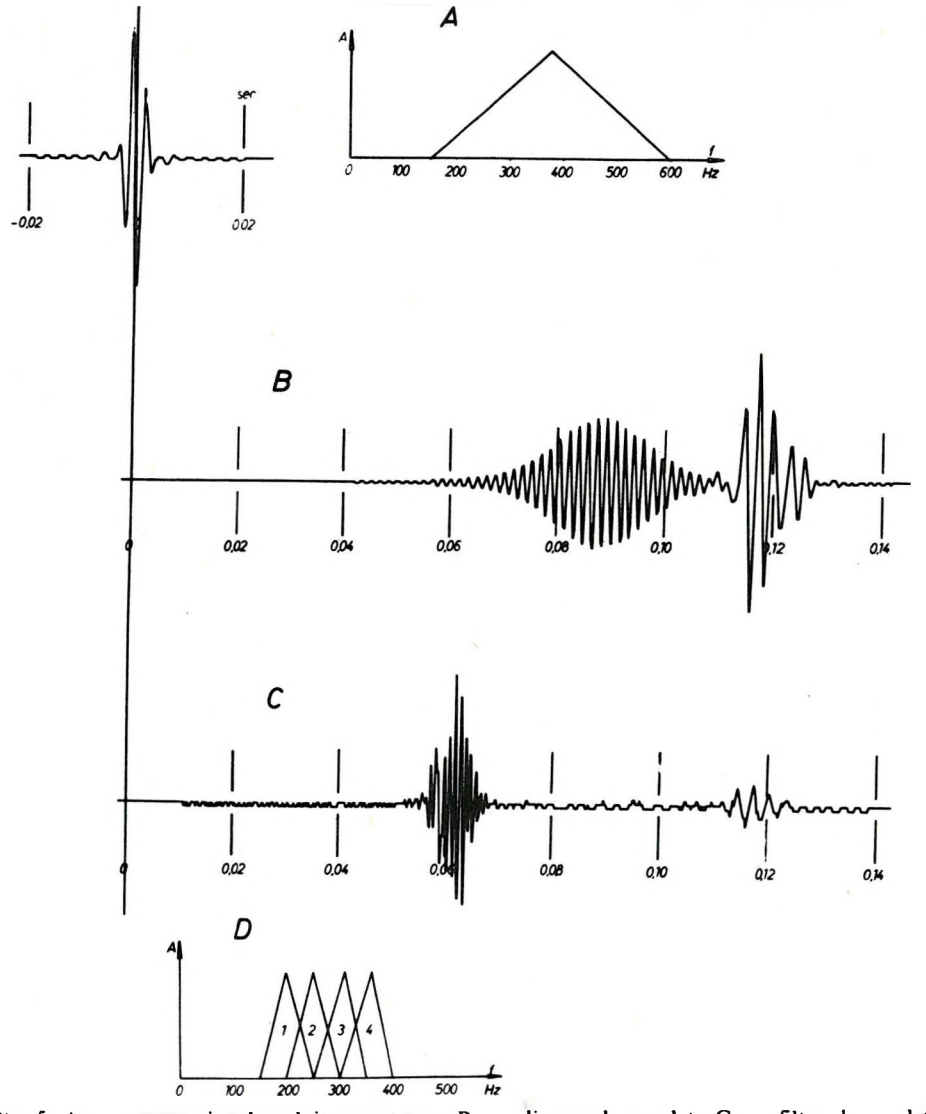

Fig. 5. A — source signal and its spectrum; B — dispersed wavelet; C — filtered wavelet; D — transfer functions of the used bandpass filters

5. ábra. A — az indulójel és spektruma; B — diszperz csatornahullám; C — szűrt csatornahullám; D — a használt sávszűrők átviteli függvényei

Фиг. 5. A – Исходный сигнал и его спектр; B – Дисперсная канальная волна; C – Отфильтрованная канальная волна; D – Частотные характеристики использованных полосовых фильтров

In *Fig. 5* the spectrum of the source signal expands from 150 to 600 Hz. The dispersed wavelet model is definitely attenuated and high amplitudes appear at its end. Four band-pass filters were used for filtering but their total width did not cover the complete signal spectrum. The main peak of the filtered wavelet indi-

cates again the precise expected arrival time of *S* bodywaves. The wavelet is definitely recompressed in spite of the restricted bandwidth.

Figure 6 shows that the spectrum of the source signal expands from 250 to 1,000 Hz. In the first part of the dispersed wavelet model the high frequency sig-

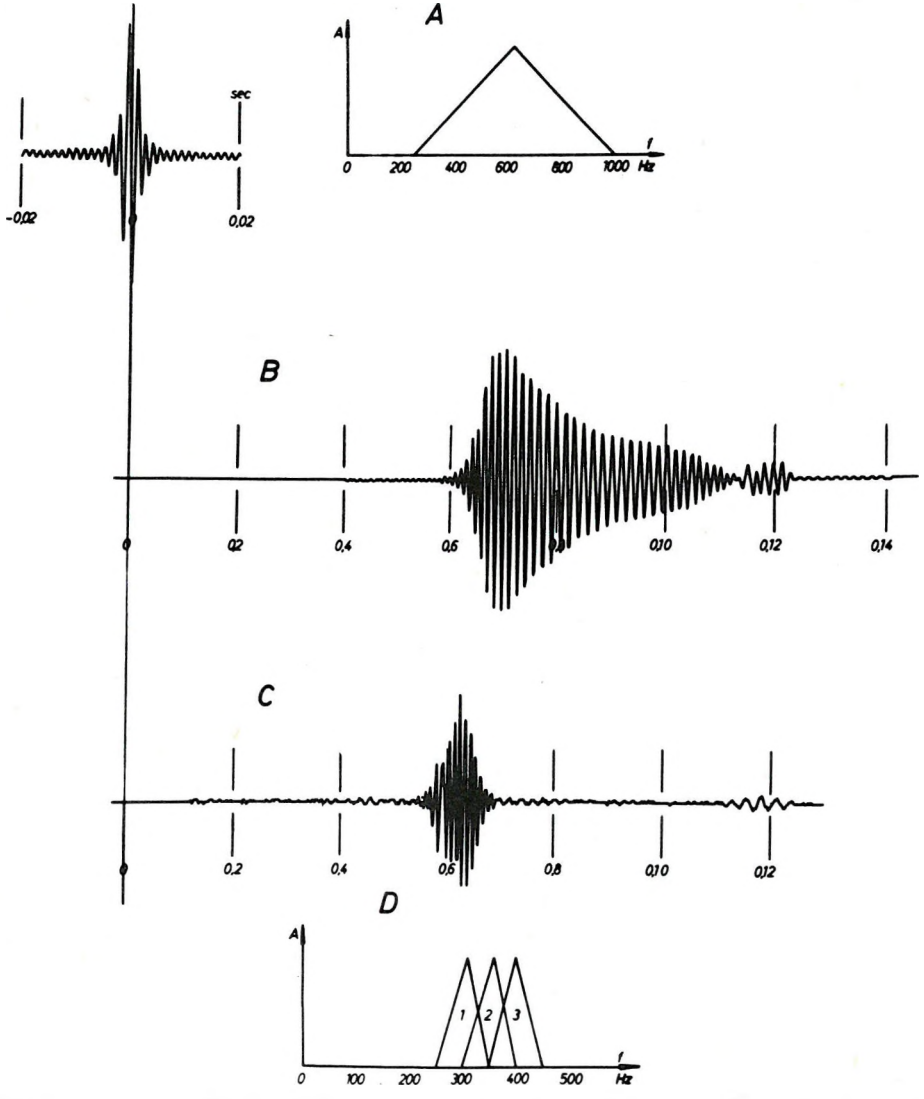

Fig. 6. A — source signal and its spectrum; B — dispersed wavelet; C — filtered wavelet; D — transfer functions of the used bandpass filters

6. ábra. A — az indulójel és spektruma; B — diszperz csatornahullám; C — szűrt csatornahullám; D — a használt sávszűrők átviteli függvényei

Фиг. 6. A – Исходный сигнал и его спектр; B – Дисперсная канальная волна; C – Отфильтрованная канальная волна; D – Частотные характеристики использованных полосовых фильтров

nal has very high amplitudes whereas at the end of the wavelet the amplitudes are weak. For the filtering, three band-pass filters were used with a total bandwidth much narrower than that of the source signal. In spite of the narrow band-pass the result is satisfactory: the filtered wavelet is not more than 60% longer than the source signal.

Domain of validity

To check the validity of the above described numerical model its dispersion curves were computed and compared with the theoretical curves.

Figure 7 shows three different sets of dispersion curves: the curves of the model using calculated phase shifts (1A, 1B), the curves of the model using phase inversion instead of phase shifts (2), and the theoretical curves (3).

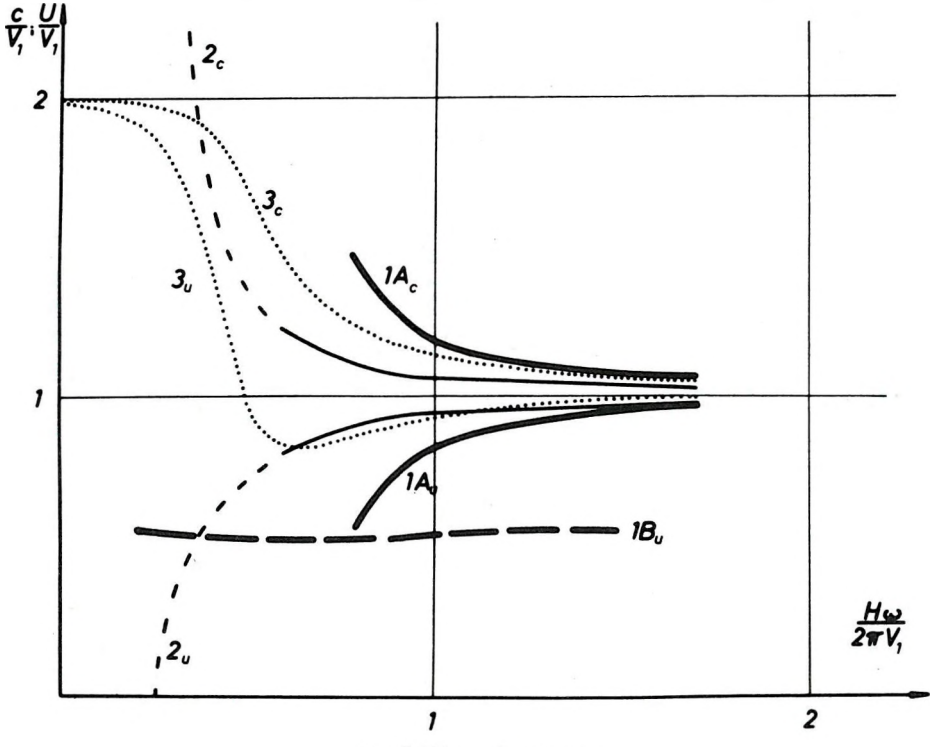

Fig. 7. Dispersion curves
1A, 1B — curves of the model using calculated phase shifts; 2 — curves of the model using phase inversion instead of phase shifts; 3 — theoretical curves

7. ábra. Diszperziós görbék
1A, 1B — a fázistolásokat figyelembe vevő modell diszperziós görbéi; 2 — a fázistolás helyett fázisfordításokat alkalmazó modell diszperziós görbéi; 3 — elméleti diszperziós görbék

Фиг. 7. Дисперсионные кривые
1A, 1B — модели с учетом смещений по фазе; 2 — модели, применяющей инверсию фазы вместо смещения по фазе; 3 — теоретические дисперсионные кривые

Studying the curves it can be seen that the model using calculated phase shifts produces two separated wavelets denoted by 1A and 1B. Wavelet 1A is similar to the vibration of a free plate, except for the low-frequency end of the dispersion curve which is missing because the length of the wavelet is limited by the critical angle. Wavelet 1B is a low velocity wavelet almost without dispersion. The average amplitude ratio of 1A to 1B is 20–25 dB. The two separated wavelets can be seen well in Fig. 5 (where the amplitude of wavelet 1A is attenuated because of the input spectrum), and in Fig. 6. In Fig. 4 none of the possible frequency components of wavelet 1A is present therefore here only wavelet 1B is to be seen.

The model using phase inversion corresponds to the vibration of a plate between two infinitely rigid half spaces except for the low frequency end of the dispersion curve, which is also truncated by the limited wavelet length.

Now, to answer the question of validity, one may say that wavelet 1A of the model using phase shifts gives an acceptable approximation of reality at frequencies above the ratio

$$\frac{Hf}{V_1} = 1.$$

In this frequency range wavelet 1B, which has nothing to do with reality, can be treated as background noise because of its significantly smaller amplitudes.

The model using phase inversion provides a worse approximation of the theoretical phase velocity curve, its group velocity curve fits better.

Conclusions can be drawn as follows:

— numerical models of seismic channel waves which are constructed on the basis of geometrical optics have similar characteristics to those of vibrations in a plate even if phase shifts are introduced into the model,

— similarity of the model to the vibrating plates introduces strong frequency limitations if a recompressional filter is derived from it.

BIBLIOGRAPHY

BURG, K. E., EWING, M., PRESS, F., STULKEN, E. J., 1951: A Seismic Wave Guide Phenomenon. Geophysics, **16,** pp. 594–613.

BOOER, A. K., CHAMBERS, J., MASON, I. M., 1977: Fast numerical algorithm for the recompression of dispersed time signals. Electronics Letters, **13,** 16, pp. 433–455.

BUCHANAN, D. J., 1979: The location of Faults by Underground Seismology. Colliery Guardian Annual Review, August 1979.

EWING, W. M., JARDETZKY, W. S., PRESS, F., 1957: Elastic Waves in Layered Media. McGraw-Hill Book Co., London, 1957.

FREYSTÄTTER, S., 1974: Modellseismische Untersuchungen zur Anwendung von Flözwellen für die untertätige Vorfelderkundung im Steinkohlenbergbau. Berichte des Institutes für Geophysik der Ruhr-Universität Bochum, Nr. 3., Bochum.

KREY, T. C., 1963: Channel Waves as a Tool of Applied Geophysics in Coal Mining. Geophysics, **28**, 5, pp. 701–714.
MESKÓ, A., 1977: Szeizmika. Tankönyvkiadó, Budapest, 1977.
SAVARENSKY, E., 1975: Seismic Waves. Mir Publishers, Moscow, 1975.
TOLSTOY, I., USDIN, E., 1953: Dispersive Properties of Stratified and Elastic and Liquid Media: a Ray Theory. Geophysics, **18**, pp. 844–870.

BODOKY TAMÁS, CZILLER ESZTER, KÖRMENDI ALPÁR

EGYSZERŰ ELJÁRÁS AZ SH TÍPUSÚ CSATORNAHULLÁMOK MODELLEZÉSÉRE, ILLETVE DISZPERZITÁSUK MEGSZÜNTETÉSÉRE

A dolgozat a két végtelen féltér közé ágyazott rugalmas hullámvezetőben létrejövő SH típusú csatornahullámok geometriai optikai eszközökkel történő modellezésével foglalkozik.

A bemutatott egyszerű, sugárutakra épülő modellből olyan szűrési eljárást vezet le, amellyel a diszperz SH típusú csatornahullámok közelítően nem diszperz, impulzusszerű jellé alakíthatók. Befejező részében vizsgálja a modell diszperziós görbéit, majd összehasonlítva ezeket az elméleti görbékkel, meghatározza a bemutatott modellezési és szűrési eljárások érvényességi tartományát.

A tárgyalt témát a szénbányákban végzett telephullám-szeizmika terjedése és feldolgozási problémái teszik időszerűvé.

Т. БОДОКИ, Э. ЦИЛЛЕР, А. КЁРМЭНДИ

ПРОСТОЙ СПОСОБ ДЛЯ МОДЕЛИРОВАНИЯ КАНАЛЬНЫХ ВОЛН ТИПА SH И ДЛЯ УСТРАНЕНИЯ ИХ ДИСПЕРСИИ

В работе обсуждаются вопросы моделирования при помощи средств геометрической оптики канальных волн типа SH, возникших в упругом волноводе, залюченном между двумя бесконечными полупространствами.

По изложенной простой модели, построенной на траекториях, выводится способ фильтрации, при помощи которого дисперсные канальные волны типа SH преобразуются в приблизительно недисперсные импульсные сигналы. В заключении рассматриваются дисперсионные кривые модели, затем сопоставив их с теоретическими кривыми, определяется диапазон действия приведенных способов моделирования и фильтрации.

Актуальность обсуждаемой темы вызывают распространение сейсморазведки с использованием пластовых волн в угольных шахтах и проблемы обработки получаемых данных.

EÖTVÖS LORÁND GEOPHYSICAL INSTITUTE OF HUNGARY
GEOPHYSICAL TRANSACTIONS 1982
28/1 pp. 33–46

CURVED RAY ALGEBRAIC RECONSTRUCTION TECHNIQUE APPLIED IN MINING GEOPHYSICS

L. HERMANN,* L. DIANISKA* AND J. VERBŐCI**

A proper understanding of the stress conditions in mines is of utmost importance for economy and for safety. Because the velocity of seismic waves in rocks is a function of pressure, the velocity distribution can be used to predict stress conditions.

A method is described that can be considered as a novel version of the Algebraic Reconstruction Technique. The procedure starts out from some initial velocity field and performs ray tracing based on the vectorial form of the Snellius–Descartes principle. By comparing the measured and computed travel times the velocity field is modified and new raypaths are computed until the deviations become less than some prescribed tolerance. The velocity field obtained represents the velocity distribution of the site studied.

Repeatedly performed transmission measurements yield information on the possible changes of the pressure conditions.

Introduction

Economic and safety considerations have made it an important task in several Hungarian coal mines to get detailed knowledge of the changes in the state of the surrounding rock formations. Because of mining activities the stability of these rock masses that have evolved through geological times becomes disturbed; these stress changes then cause different kinds of destructive phenomena. The proper tracing of these phenomena in space and time can be done only by a joint application of the different measuring methods. The Research Department of the Mecsek Coal Mines have elaborated a mining detection and control system [1] involving a method which contains—among other features—the repeated application of seismic transmission. This transmission technique is based on a measuring arrangement where the spatial domain to be studied lies within the sources and detectors; the acquisition of information is generally based on transmitted seismic waves [2], [3]. The processing and interpretation of the measurement results raise a number of mathematical and physical problems in view of which Mecsek Coal Mines and ELGI agreed to cooperate in an endeavour to solve these problems. The method elaborated and some preliminary results are presented here.

* Eötvös Loránd Geophysical Institute (ELGI) of Hungary.
** Research Department of the Mecsek Coal Mines
Paper presented at the 43rd EAEG Meeting, Venice, 25–29. May, 1981.

1. Basic principles of the transmission ("transillumination") method

The propagation of elastic waves (direction, velocity, energy absorption and spectrum) is determined by the parameters of the medium; during propagation the waves accumulate the integral effects of all these parameters. So, at least in principle, there should be a way to determine the physical properties of a given rock formation from the observed parameters of the transmitted waves.

The transit time between a source-detector pair is given by

$$T_1 = \int_{R_l} \frac{\mathrm{d}s}{V_l(\underline{r})}, \qquad T_2 = \int_{R_t} \frac{\mathrm{d}s}{V_t(\underline{r})}. \tag{1a, 1b}$$

Observed amplitudes are described by

$$A_l = A_{ol} \Gamma_l \exp\left(-\int_{R_l} \gamma_l(\underline{r})\,\mathrm{d}s\right), \tag{2a}$$

$$A_t = A_{ot} \Gamma_t \exp\left(-\int_{R_t} \gamma_t(\underline{r})\,\mathrm{d}s\right), \tag{2b}$$

where

— R_l and R_t are the paths of propagation of the longitudinal and transverse waves, respectively;

— $V_l(\underline{r})$ and $V_t(\underline{r})$ the corresponding (scalar) velocities;

— A_l, A_t the observed amplitudes;

— A_{ol}, A_{ot} the generated amplitudes;

— Γ_l, Γ_t spherical divergence;

— $\gamma_l(\underline{r})$, $\gamma_t(\underline{r})$ are absorption coefficients.

In homogeneous media the determination of the constants V_l, V_t and γ is straightforward.

In inhomogeneous media the inversion of the above integrals raise two problems:

a) For given raypaths there exists an infinity of functions satisfying the integral expressions; this means that the distribution of the parameters cannot be determined,

b) In inhomogeneous media the raypaths R_l, R_t also depend on the velocity fields.

2. The reconstruction algorithm

2.1. General properties of the reconstruction technique

In recent years the problem has been approached by several variants of three basic methods (direct matrix method, analytical methods and the so-called Algebraic Reconstruction Technique (ART)) [4]. The common root of these methods goes back to the classical work of RADON [5] who justified that any

two-dimensional domain can unambiguously be reconstructed by an infinite series of its one-dimensional projections. All known methods, however, assume straight-line integration paths, which means that they are not generally applicable for sufficiently complex geologies. While Bois [6], [7] did use curved raypaths, his iterative velocity determination is based on the rather inconvenient direct matrix method [8]. Our algorithm has been developed on the basis of the works of Bois and of Gordon and Herman [8], [9], see *Fig. 1.*

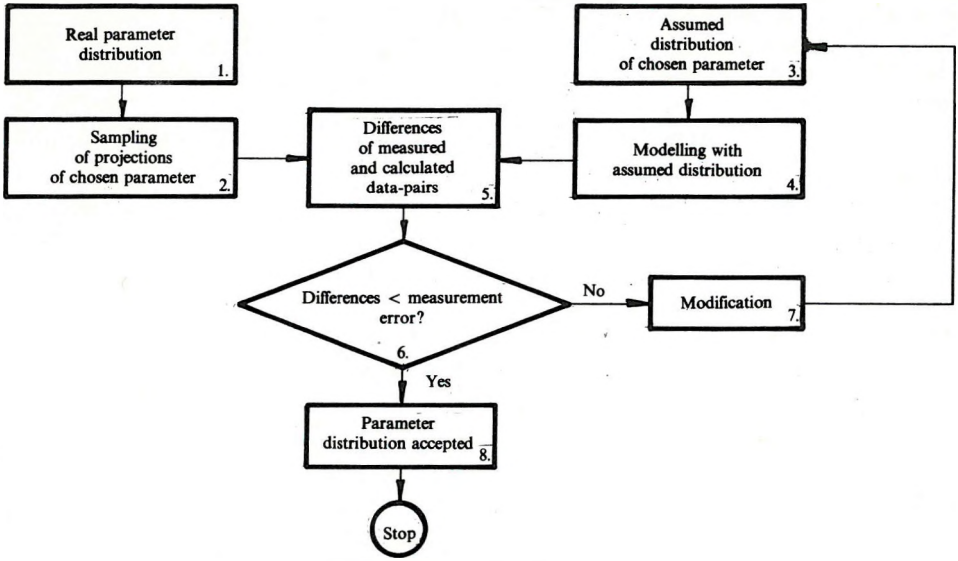

Fig. 1. Flow chart of the process

1. ábra. A kifejlesztett eljárás folyamatábrája

1 — a valóságban kialakult paramétereloszlás; 2 — egy választott paraméter vetületeinek mérése (mintavételezés); 3 — a választott paraméter feltételezett eloszlása; 4 — a mérés modellezése a feltételezett eloszlással; 5 — a mért és számított értékpárok különbsége; 6 — különbség < mérési hiba? 7 — módosítás; 8 — a paraméter eloszlása megfelel a valóságnak

Фиг. 1. Блок-схема разработанной процедуры

1 — Дествительное распределение параметров; 2 — Измерение проекции одного выбранного параметра (дискредитация); 3 — Предполагаемое распределение выбранного параметра; 4 — Моделирование измерения с помощью предполагаемого распределения; 5 — Разность вычисленных и измеренных параметров; 6 — Разность ошибка измерения? 7 — Исправление поля; 8 — Распределение соответствует истине

The spatial domain to be studied is "transilluminated" by transecting wave paths, sources and receivers being placed in the galleries.

The measurement results yield sampled values of the projections of distributions, burdened with measurement errors. From the finite number of values we can determine only a finite number of parameters of the velocity field—the number of determined parameters and the number of observed values not necessarily being equal (e.g. these parameters can be values of the velocity distribution at discrete grid points). The better the accuracy and the greater the quantity of the values along transecting raypaths the better will be the reconstruction.

According to the ART principle we compute by means of some supposed model the series of values corresponding to an assumed parameter distribution and to the measurement geometry. This data series is, of course, subject to modelling errors. Wave propagation is described by the laws of geometrical optics, absorption is computed by Eqs. 2a–2b.

The next step is to compare the measured and computed series of data. Our basic assumption—as in all iterative approaches of this kind—is that two distributions agree if and only if all of their projections agree.

If the deviations are greater than the measurement error the algorithm modifies the hypothetical parameter distribution toward the direction of a better agreement, then proceeds again with raypath modelling. So, from among the infinite number of possible fields it looks, by successive approximations, for that fitting best the measurements results.

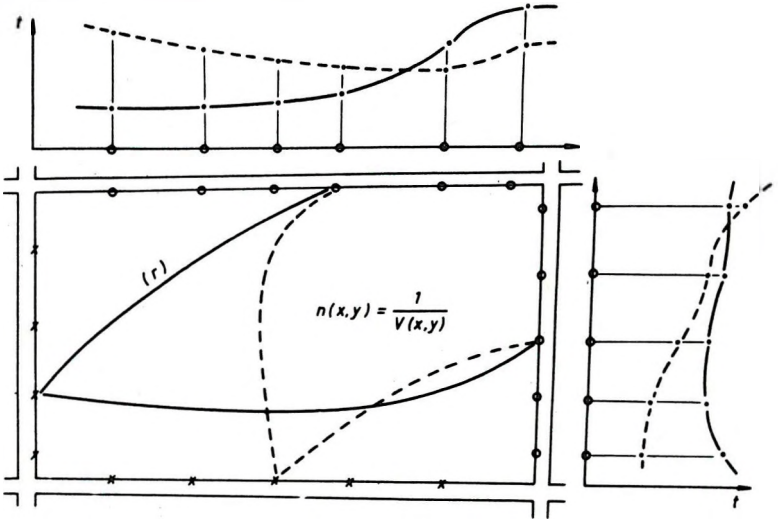

$$t_r = \int_{(r)} n(x,y)\,ds \qquad r = 1,2 \ldots\ldots R(=\Sigma \cdot \Gamma)$$

Fig. 2. Characteristic scheme of a measuring pattern

2. ábra. Egy jellegzetes mérési elrendezés vázlata

Фиг. 2. Схема характеристической измерительной установки

The parameter field found will be considered as the best approximation of the real distribution, within the possibilities of the algorithm and the measurement errors.

Figure 2 presents a typical transmission measurement geometry used in mines. The projections to be used for the reconstruction are first-arrival times registered by the geophones, the parameter to be determined is the velocity distribution $V(x, y)$ inside the domain studied.

2.2. Computation of the transit times and amplitudes

By the basic equation of geometrical optics, as expressed by SOMMERFELD [13],

$$\operatorname{curl}(n\underline{s}) = 0, \tag{3}$$

where

$n(\underline{r}) = \dfrac{1}{V(\underline{r})}$ is the index of refraction,

$\underline{s}(\underline{r})$ is the normal to the wave-front.

Since, in the general case, this equation is not integratable, we have to compute separately all the wave paths corresponding to the different shot point-geophone pairs. Starting out from the shot points we launch a diversity of rays through the velocity field then select those that "hit" the individual geophones.

The rays can be computed, by Eq. 3, as

$$\mathrm{d}\underline{s}(k) = \frac{1}{n(k)}[[\underline{s}(k) \times \operatorname{grad} n(k)] \times \underline{s}(k)], \tag{4}$$

$$\underline{s}(k+1) = \underline{s}(k) + \mathrm{d}\underline{s}(k). \tag{5}$$

Here, k is the serial number of the steps of length Λ along the ray, the values $n(k)$ and grad $n(k)$ are computed by cubic interpolation from adjacent grid points;

$$n(k) = \sum_{hij} c_{hij}^{(k)} n_{hij}, \tag{6}$$

$$\operatorname{grad} n(k) = \sum_{hij} c_{hij}^{*(k)} \tag{7}$$

(the coefficients $c_{hij}^{(k)}$ and $c_{hij}^{*(k)}$ differ from zero in the neighbourhood of $4 \times 4 \times 4$ of point (k)). The vectorial form can easily be treated in 3 dimensions as well. The cubic interpolation fairly well describes the refraction, does not increase significantly the computation time and takes into account the fact that the wave only "feels" a neighbourhood of limited size of point (k).

For a more complex velocity field several rays could belong to the same shot point-geophone pair; from these that having the smallest transit time will be selected.

For a given ray (r) the transit time is given by

$$T_r^c = \Lambda \sum_{(r)} n(k) = \Lambda \sum_{k} \sum_{hij} c_{hij}^{(k)} n_{hij}, \tag{8}$$

On the basis of the raypaths the spherical divergence [Γ, (2a), (2b)] can also be determined; its value is proportional to the ray density in the immediate vicinity

of the geophone. By these factors, and by the assumed distribution γ_{hij} the computed amplitude ratios for the raypaths of the first arrivals will be

$$F_r^c = \ln\left(\frac{A_r^c}{A_0}\right) = \ln \Gamma_r - \Lambda \sum_k \sum_{hij} c_{hij}^{(k)} \gamma_{hij}. \tag{9}$$

2.3. *Modification of the parameter distributions*

Modification of the hypothetical parameter distributions is carried out on the basis of the difference between the measured and computed results:

$$\Delta T_r = T_r^m - T_r^c; \qquad \Delta F_r = F_r^m - F_r^c. \tag{10}$$

From Eqs. (8), (9), by differentiation:

$$\delta T_r^c = \Lambda \sum_{hij} n_{hij} \left(\sum_k \delta c_{hij}^{(k)}\right) + \left(\sum_k c_{hij}^{(k)}\right) \delta n_{hij} \tag{11}$$

and

$$\delta F_r^c = \delta(\ln \Gamma_r) - \Lambda \sum_{hij} \left[\gamma_{hij} \left(\sum_k \delta c_{hij}^{(k)}\right) + \left(\sum_k c_{hij}^{(k)}\right) \delta \gamma_{hij}\right]. \tag{12}$$

The terms $\delta c_{hij}^{(k)}$ and $\delta(\ln \Gamma_r)$ describe the effect of the change in the raypath. Since these terms cannot be computed, they should be neglected. (This neglection is justifiable because the first arrival is the minimum time on all possible raypaths.)

Consequently

$$\delta T_r^c \cong \Lambda \sum_{hij} \left(\sum_k c_{hij}^{(k)}\right) \delta n_{hij} \tag{13}$$

and

$$\delta F_r^c \cong -\Lambda \sum_{hij} \left(\sum_k c_{hij}^{(k)}\right) \delta \gamma_{hij}. \tag{14}$$

The computed modification of the distributions at the grid point (hij) will be

$$\Delta n_{hij} = \sum_r^R d_{hij}^{(r)} \Delta n_{hij}^{(r)} = \frac{1}{\Lambda} \frac{\sum_r^R \sum_k (c_{hij}^{(k,r)}) \dfrac{\sum_k c_{hij}^{(k,r)}}{\sum_{hij} \left(\sum_k c_{hij}^{(k,r)}\right)^2} \Delta T_r}{\sum_r^R \sum_k (c_{hij}^{(k,r)})} \tag{15}$$

and

$$\Delta\gamma_{hij} = \sum_{r}^{R} d_{hij}^{(r)} \Delta\gamma_{hij}^{(r)} = -\frac{1}{\Lambda} \frac{\sum_{r}^{R} \sum_{k} (c_{hij}^{(k,r)}) \frac{\sum_{k} c_{hij}^{(k,r)}}{\sum_{hij} \left(\sum_{k} c_{hij}^{(k,r)}\right)^2} \Delta F_r}{\sum_{r}^{R} \sum_{k} (c_{hij}^{(k,r)})}. \tag{16}$$

It can be seen that the modification in a given grid point is the weighted and normalized algebraic sum of the modifications computed along the individual raypaths, on the basis of the difference between the theoretical and measured values. The weighting is made, basically, in inverse proportion to the "distance" of the given ray from the grid point.

The algorithm modifies the field values in the following way:

$$a) \quad \Delta n_{hij}^{w(r)} = 0 \quad \text{and} \quad \Delta\gamma_{hij}^{w(r)} = 0 \tag{17}$$

if for ray r

$$|\Delta T_r| < \mu(T) \quad \text{and} \quad |\Delta F_r| < \mu(F) \tag{18}$$

$\mu(T)$ and $\mu(F)$ are the errors of the time- and amplitude measurements, respectively.

$$b) \quad n_{hij}^{w+1} = \text{MIN}\{\text{MAX}[n_{\min}; n_{hij}^{w} + \Delta n_{hij}^{w}]; n_{\max}\} \tag{19}$$

and

$$\gamma_{hij}^{w+1} = \text{MIN}\{\text{MAX}[\gamma_{\min}; \gamma_{hij}^{w} + \Delta\gamma_{hij}^{w}]; \gamma_{\max}\}, \tag{20}$$

where

— w is the number of iterations;

— the indices "min" and "max" denote the plausible lower and upper boundaries of the given parameter;

— the operators MIN and MAX refer to the selection of the respective minimum and maximum values.

The above restrictions ensure, besides the physical reality of the computed fields (as, for example, $n>0$) the rapid convergence of the algorithm [10]. In the course of the modifications it is obviously possible to take into account the boundary values of the distributions, known *a priori* from other measurements.

The change of the field due to a single iteration step is shown by *Fig. 3*. The reference times are given as if there were an infinitely large velocity jump concentrated to one grid square at the centre of a homogeneous velocity field (the unit of velocity is grid-size/time, the value of the homogeneous field is 3). The effect of this inhomogeneity is distributed in a star-like manner along the rays passing through the centre. The more distant rays, not affected by the velocity jump, try to counteract the spread of the modification, causing splits in the arms of the star.

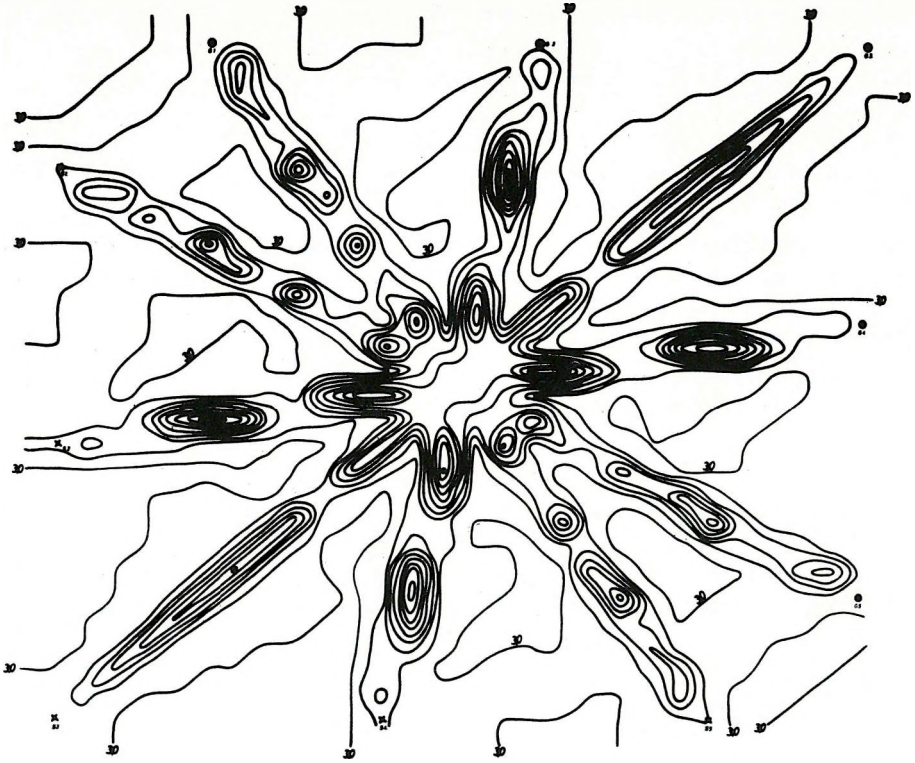

Fig. 3. Effect of one step in the iteration process *3. ábra.* Egy iterációs lépés hatása
Фиг. 3. Влияние шага итерации

3. Preliminary testing of the algorithm

The seismic waves giving the first arrivals propagate only in special cases in the plane of measurement (velocity fields perpendicularly homogeneous to the plane; measurements in waveguides, [11]). Even though our approach is applicable to 3-dimensional reconstructions on the strength of Eq. (4), this would necessitate spatial measurements. Since at present we have no reliably interpretable (i.e. sufficiently dense) spatial data and the algorithm works much more simply in the plane, we have restricted ourselves to reconstructing 2-dimensional distributions.

In order to judge the applicability of any iterative procedure, the following properties should be checked:

— convergence or divergence of the algorithm;
— rate of convergence;
— unambiguity, uniqueness of the limiting point.

In the literature the unambiguity of the seismic inverse problem has been proved rigourously only for some simple distributions [12]. In the case of iterative reconstruction techniques it is advisable to check the objectivity of the resulting distribution by a regeneration method [10]: the more surprising configurations of the result field should be deleted after which the iteration should be started again; if the deleted part reappears it is really due with a fair likelihood to the measured data.

A result from among our convergence studies is shown in Figs. 4, 5 and 6. The reference times refer to the velocity field of value 3, the initial distribution had the value of 4. The closeness of the approximation is measured by the quantities

$$(\overline{\delta t})^2 = \sqrt{\frac{1}{R}\sum_{r}^{R}\left(\frac{T_r^c - T_r^m}{T_r^m}\right)^2}, \tag{21}$$

$$(\overline{\delta t}) = \frac{1}{N}\sum_{ij}\left(\frac{V_{ij}^c - V_{ij}^m}{V_{ij}^m}\right), \tag{22}$$

$$(\overline{\delta V})^2 = \sqrt{\frac{1}{N}\sum_{ij}\left(\frac{V_{ij}^c - V_{ij}^m}{V_{ij}^m}\right)^2} \tag{23}$$

(cf. Fig. 4). It can be seen that the iteration gradually improves up to 4th–5th step. Similar results have been reported in [8], for straight raypaths.

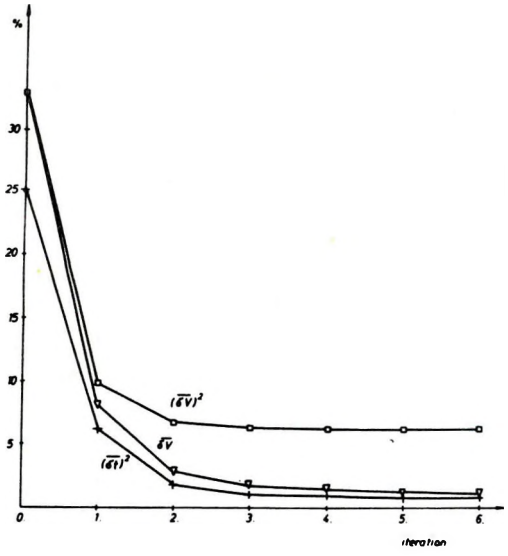

Fig. 4. Convergence curves of the process

4. ábra. Az eljárás konvergenciája

Фиг. 4. Сходимость процедуры

The histograms of velocity values *(Fig. 5)* show a similar convergence. The finite width of the histograms might be due to the following:

— the step size is of the order of 0.5 grid size; the computed times and the corresponding modifications have a statistical scatter;

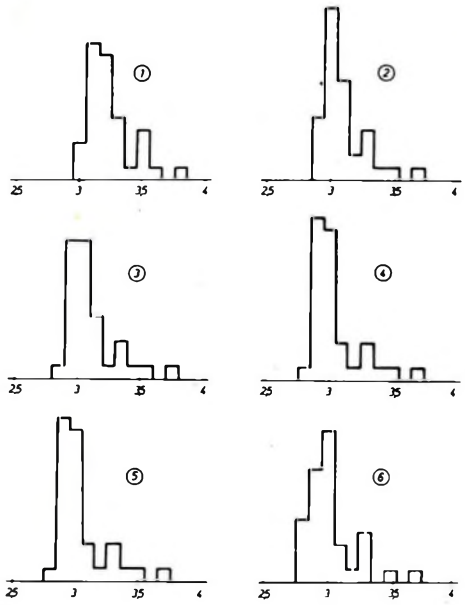

Fig. 5. Frequency histogram of velocity values

5. ábra. A sebességértékek gyakorisága (hisztogram)

Фиг. 5. Частота значений скоростей (гистограмма)

— there is a pronounced boundary effect due to the small size of the field.

The boundary effect is also striking in *Fig. 6a,* representing the velocity fields computed in iteration steps 1, 4 and 7: the algorithm cannot change properly the boundaries of the field and this causes an overshoot even at the very centre of the field.

To reduce these effects and to study the uniqueness of the solution we have also initiated another approximation of the reference field, starting out from the opposite side, with velocity 2. As seen, this series of iterations also tends to the reference field; the boundary effect and the overshoot are opposite in sign *(6b).* These results suggest that in actual cases it is worth while to compute 3–4 iteration steps starting out from initial distributions overestimated from below and from above, respectively, then carry out 1–2 more iterations with the average of the above results *(6c).*

Figure 7 illustrates a processing result. Reproduced by permission of the Research Department of the Mecsek Coal Mines. On the respective fields A, B and C we carried out, practically at the same time, separate measurements of the longitudinal first arrival times (all in all 26 shot points and 78 receivers). The boundary effects are due to the special measuring geometry; the main structure of the three fields, however, fits together fairly well.

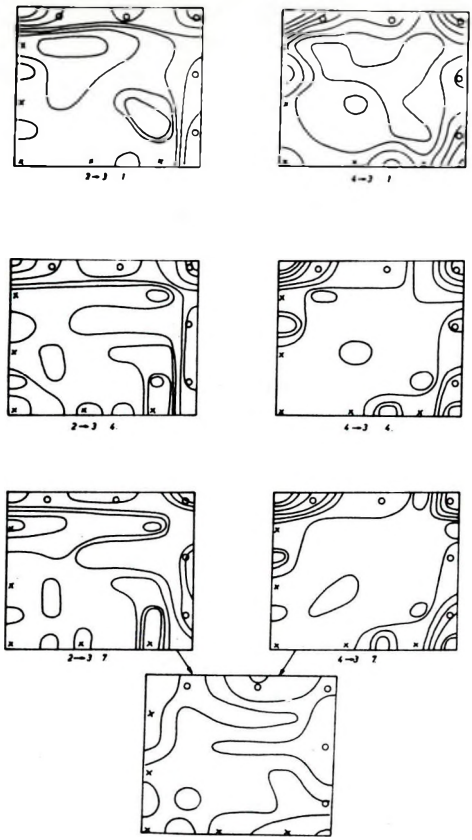

Fig. 6. Example of the reconstruction of a homogeneous velocity field
6. ábra. Kísérlet homogén sebességmező rekonstrukciójára
Фиг. 6. Проба восстановления поля однородных скоростей

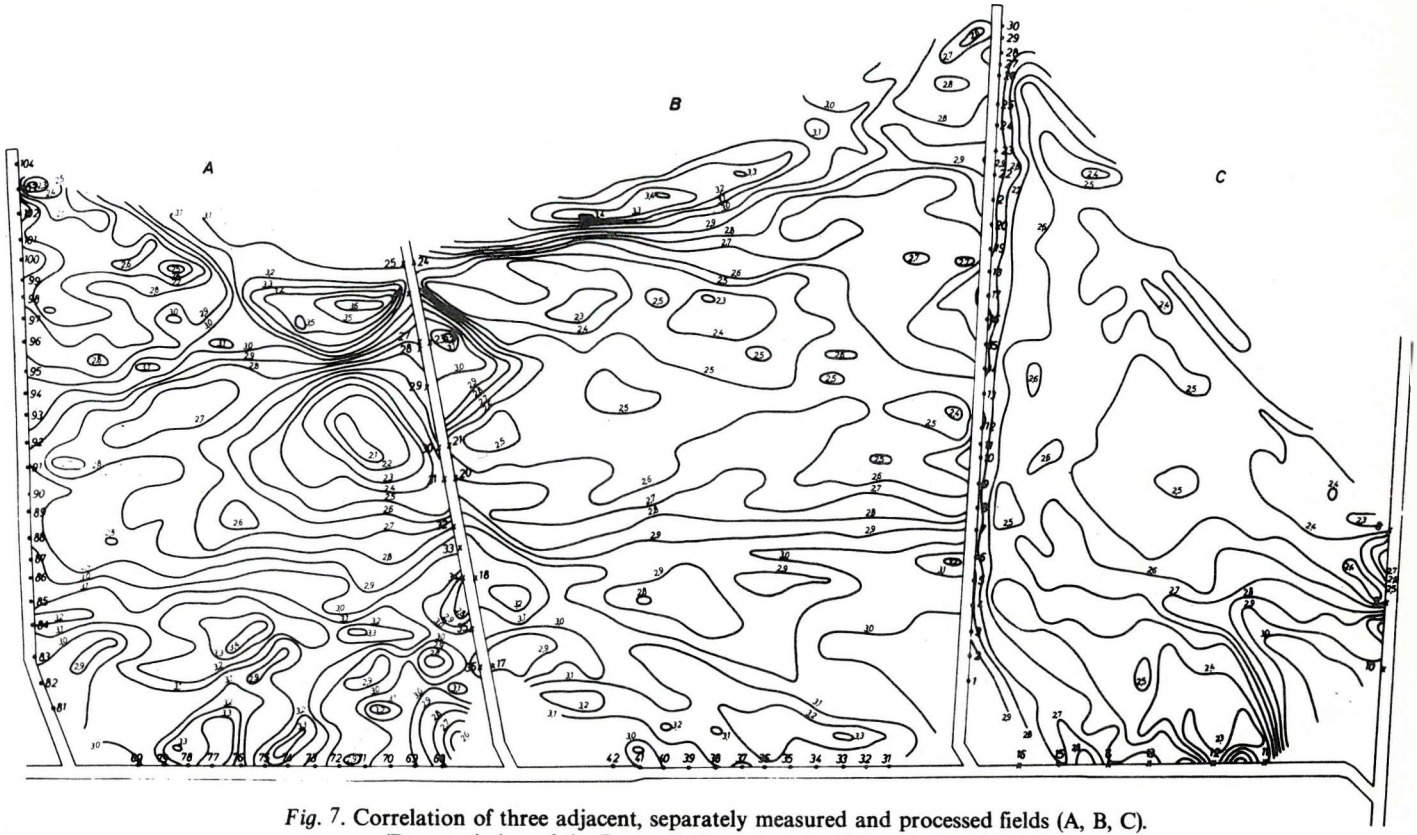

Fig. 7. Correlation of three adjacent, separately measured and processed fields (A, B, C).
(By permission of the Research Department of Mecsek Coal Mines)

7. ábra. Három, külön-külön végzett és feldolgozott mérés (A, B, C) korrelációja
(közölve a Mecseki Szénbányák Kutatási Osztályának engedélyével)

Фиг. 7. Корреляция трех, отдельно выполненных и обработанных измерений (A, B, C)
(С разрешением Отдела Исследований Мечекских Угольных Шахт)

Acknowledgements

Thanks are due to Mecsek Coal Mines for their kindly permitting publication of the method and some actual results; to Dr. T. Bodoky for many stimulating discussions; and to our referees, Mr. A. Körmendi and Mr. T. Ormos for their useful advice.

We are also grateful to all of our colleagues who helped in the preparation of the figures and the manuscript.

REFERENCES

[1] Mecseki Szénbányák Vállalat 34.328/KL találmány: Eljárás adott földtani rendszer bányászati tevékenység folytán bekövetkező vagy bekövetkezhető állapotváltozásainak kívánt befolyásolására.

[2] Barton, D. C., 1929: The Seismic method of mapping Geologic Structures. Trans. Am. Inst. Min. Met. Eng., **81,** pp. 572–624.

[3] Bodoky, T., et al. The predetection of andesite intrusions with seismic measurements. Bányászat **109,** pp. 671–675.

[4] Special Issue on Acoustics Imaging. Proc. IEEE, **67,** No. 4.

[5] Radon, J., 1917: Über die Bestimmung von Funktionen durch ihre Integralwerte längs gewisser Mannigfaltigkeiten. Ber. Saech. Akad. der Wiss., **69,** pp. 262–277.

[6] Bois, P. et al., 1971: Essai de Détermination Automatique des Vitesses Sismiques par mesures entre Puits. Geoph. Prosp., **19,** pp. 42–83.

[7] Bois, P. et al., 1972: Well-to-well seismic measurements. Geophysics, **37,** pp. 471–480.

[8] Gordon, R. et al., 1970: Algebaic Reconstruction Techniques (ART) for Three-dimensional Electron Microscopy and X-ray Photography. J. Theor. Biol., **29,** pp. 471–481.

[9] Herman, G. et al., 1971: Resolution in ART. J. Theor. Biol., **33,** pp. 213–223.

[10] Herman, G. et al., 1973: Three methods for reconstructing objects from X-rays: a comparative study. Comp. Graph. and Image Proc., **2,** pp. 157–178.

[11] Mason, I., 1981: Algebraic reconstruction of a two-dimensional velocity inhomogeneity in the High Hazles seam of Thoresby colliery. Geophysics, **46,** pp. 298–308.

[12] Алексеев, А. С. и др., 1979: Обратные кинематические задачи взрывной сейсмологии. «Наука», Москва, 1979.

[13] Sommerfeld, A. et al., 1911: Anwendung der Vektorrechnung auf die Grundlagen der geometrischen Optik. Annalen der Physik, **35,** pp. 277–298.

HERMANN LÁSZLÓ, DIANISKA LÁSZLÓ, VERBŐCI JÓZSEF

BÁNYABELI SZEIZMIKUS SEBESSÉGELOSZLÁS MEGHATÁROZÁSA A FESZÜLTSÉGELOSZLÁS MEGVÁLTOZÁSÁNAK KÖVETÉSÉHEZ

A bányabeli feszültségviszonyok ismerete biztonsági és gazdasági szempontból igen fontos. Mivel a szeizmikus hullámok sebességét a kőzetekben a nyomás befolyásolja, ezért a sebességeloszlás-adatokból következtethetünk a feszültségviszonyokra.

Az ismertetett módszer az ún. Algebraic Reconstruction Technique egyik változatának tekinthető. Egy kezdeti sebességmezőből kiindulva az eljárás sugárutakat követ a Snellius—Descartes-törvény vektorális formája alapján. A mért és számított futási idők összehasonlítása után — ha szükséges — módosítja a sebességmezőt, és újrakezdi a sugárút számítását. Az iterációs eljárás akkor fejeződik be, amikor a mért és számított időadatsor egy előre megadott értéknél kevésbé tér el egymástól. Az így kapott sebességmezőt fogadjuk el a vizsgált terület sebességeloszlásának. Rendszeresen végzett átvilágító mérésekkel és kiértékeléssel a vizsgált területen figyelemmel kísérhető a nyomásviszonyok alakulása.

Л. ХЕРМАН, Л. ДИАНИШКА, Й. ВЕРБЁЦИ

ОПРЕДЕЛЕНИЕ РАСПРЕДЕЛЕНИЯ СКОРОСТЕЙ СЕЙСМИЧЕСКИХ ВОЛН В ШАХТАХ ДЛЯ ПРОСЛЕЖИВАНИЯ ИЗМЕНЕНИЙ В РАСПРЕДЕЛЕНИИ НАПРЯЖЕНИЙ

Знание условий напряженности в шахтах представляет большой интерес с точки зрения безопасности и экономичности. Так как скорость сейсмических волн в горных породах подвергается влиянию давления, поэтому по данным распространения скоростей можно сделать вывод об условиях напряженности.

Излагаемый способ может рассматриваться как один из вариантов т. н. Algebraic Reconstruction Technique. Исходя из некоторого начального поля скоростей, процедура прослеживает траектории по векторальной форме закона Snellius-Descartes. После сопоставления измеренных и расчетных времен пробега — при необходимости — поле скоростей модифицируется и вычисление траектории начинается заново. Итерационная процедура заканчивается, когда расхождение между сериями измеренных и расчетных данных о временах пробега будет меньше заранее определенной величины. Регулярное выполнение работ по прослеживанию и интерпретации позволяет наблюдать изменения в условиях давления на изучаемом участке.

EÖTVÖS LORÁND GEOPHYSICAL INSTITUTE OF HUNGARY
GEOPHYSICAL TRANSACTIONS 1982
28/1 pp. 47–57

THEORY OF MATCHING SURFACE NON-EXPLOSIVE SEISMIC ENERGY SOURCES TO GEOLOGICAL MEDIUM

A. S. SHAGINYAN*

The source-medium matching theory represents a major section of the general seismic source theory. This paper deals with a technique of analytical investigations aimed at studying the conditions of matching impulse and vibration seismic sources to the geological medium under which the maximum possible amount of energy can be transmitted within an effective frequency range. The technique proposed can be used for solving optimization problems in the development of seismic energy sources.

The use of surface non-explosive seismic energy sources of various operating principles for studying the Earth's structure, and for seismic prospecting in particular, has aroused considerable interest in the source-medium interaction problems. This interest is largely explained by the desire to obtain higher seismic efficiency of the sources mentioned whose power is still rather low.

Geophysicists relate possibilities of a high-resolution deep study of the Earth's structure with the necessity of transmitting into the medium a certain attainable maximum energy (power) of a given spectrum.

Accordingly, recent years have seen intensive development of new seismic sources accompanied by theoretical and experimental research [CHICHININ 1973; NEKRASOV et al. 1976; SHAGINYAN 1977, 1979, 1980] and the introduction of new or modernized survey systems, etc. Much consideration in research is being given to the problems of matching seismic energy sources to the geological medium.

The condition of transmitting maximum active power from a source to a receiver (medium) is a well-known feature of the electrical engineering. As shown in the research made with an oscillating sphere model [CHICHININ 1973] the same also applies to seismic sources. It is reduced to minimizing the source internal resistance and the sum of imaginary components of the source resistance Z_s and those of the receiver-medium resistance Z_m.

In the principle equivalent circuit of the "source-medium" system (see *Fig. 1*) these resistances are shown in series with the source of force P.

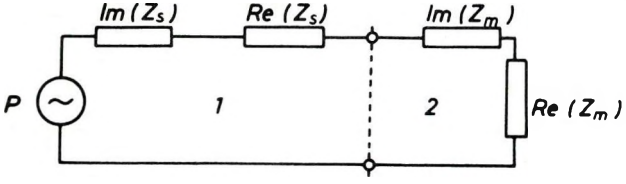

Fig. 1. Source—medium (1–2) system, equivalent circuit

1. ábra. A vibrátor—talaj (1—2) rezgőrendszerrel ekvivalens áramkör

Фиг. 1. Схема замещения системы «источник-среда»

* Special Design Office of Seismic Engineering, Gaidar Lane 2, Gomel 246020, USSR.
Paper presented at the 26th Geophysical Symposium, Leipzig, 22–25. September, 1981.

For the given equivalent circuit the condition of the source-medium matching to transmit maximum power to the medium can be written as

$$\begin{aligned} &\mathrm{Im}\,(Z_s)+\mathrm{Im}\,(Z_m)=0,\\ &\mathrm{Re}\,(Z_s)\to\min., \end{aligned} \tag{1}$$

where $\mathrm{Im}\,(Z_s)$ and $\mathrm{Im}\,(Z_m)$ are reactive components of the source and the medium resistances, respectively, and $\mathrm{Re}\,(Z_s)$ is the active component of the source internal resistance.

From the circuit in Fig. 1 the source power expended in oscillating the medium is

$$N=\frac{P^2[\mathrm{Im}\,(Z_m)+\mathrm{Re}\,(Z_m)]}{[\mathrm{Im}\,(Z_s)+\mathrm{Re}\,(Z_s)+\mathrm{Im}\,(Z_m)+\mathrm{Re}\,(Z_m)]^2}. \tag{2}$$

Its active component transformed into elastic waves, for condition 1, is maximum and equals

$$N_{\max}=\frac{P^2\,\mathrm{Re}\,(Z_m)}{[\mathrm{Re}\,(Z_s)+\mathrm{Re}\,(Z_m)]^2}. \tag{3}$$

If active losses in the source are low in relation to active losses in the medium, the magnitude $\mathrm{Re}\,(Z_s)$ can be neglected, and Eq. (3) can be written as

$$N_{\max}=\frac{P^2}{\mathrm{Re}\,(Z_m)}. \tag{3'}$$

Thus, the task assigned can be solved after securing the definite ratio of the components of the source's and the medium's complex impedance. This impedance for a given operating source and a real medium is determined experimentally enabling one to estimate the efficiency of employing the source in a given prospecting area. In designing new sources we tackle the problem of obtaining the source internal resistance correlated with the medium in a would-be prospecting area by selecting the source parameters with respect to predetermined medium parameters.

Let us first of all list the most general notions of complex impedances of the source proper (its internal resistance) and the soil to derive general equations and area by selecting the source parameters with respect to predetermined medium parameters.

lowing equation:

$$Z_s=\frac{P_{rg}}{V_{sc}}, \tag{4}$$

where P_{rg} is the complex amplitude of the source's force in the idling mode of operation when the source is acting on an absolutely rigid ground;

V_{sc} is the complex amplitude of the baseplate displacement velocity in the "short-circuit" mode with the baseplate off the ground.

The geological medium's complex impedance in the most general form is obtained from the equation

$$Z_m = \frac{P}{V}, \tag{5}$$

where P is the complex amplitude of the acting force which is equal to the reaction force of the soil;

V is the complex area-mean amplitude of the displacement velocity of the earth's particles under the baseplate.

Experimental verification of frequency characteristics $P_{r\theta}(\omega)$, $V_{sc}(\omega)$, $P(\omega)$ and $V(\omega)$ makes it possible to determine the resistances sought, that is, $Z_s(\omega)$ and $Z_m(\omega)$.

The procedure to calculate theoretically these resistances depends on the models selected to schematically represent the source and the medium. Thus, if the soil is represented in the form of a homogeneous half-space with its parameters concentrated at the baseplate [CHICHININ 1975], then the soil resistance becomes

$$Z_m = \frac{P}{V} = \frac{m_m\ddot{Z} + h_m\dot{Z} + C_mZ}{\dot{Z}}, \tag{6}$$

where m_m, h_m, C_m are the soil mass coupled to the baseplate, the damping coefficient, and the soil stiffness, respectively;

Z, $\dot{Z}$, $\ddot{Z}$ are the displacement, the velocity, and the acceleration of the baseplate (and of the earth's particles beneath.

The soil's complex impedance can be determined for more sophisticated models of the medium from the solution of dynamic contact problems of the elasticity theory [BABESHKO et al. 1981]. One of these methods makes it possible to establish a relationship between the acting force and the velocity of the particles beneath the baseplate for a variety of medium models, e.g. homogeneous elastic half-space, two-layer or multi-layer elastic half-space, etc.:

$$V(t) = \dot{Z}(t) = \frac{n}{q} \cdot L_t P(t), \qquad L_t = \sum_{k=0}^{N} a_k \frac{d^k}{dt^k}, \tag{7}$$

where n, q are coefficients possessing dimensions of length and force;

L_t is the differential operator;

a_k is the constant dimensionless coefficient;

N, k are the coefficients governing the operator's order.

Proceeding to frequency domain L_t, we get L_ω

$$Z_m(\omega) = \frac{q}{nL_\omega}. \tag{8}$$

Procedures for theoretically determining the source internal resistance involves the making up of a set of differential equations, the soil resistance is taken as a mechanical load. The source internal resistance is obtained from formula (2) by solving the set of equations for the complex amplitude of the source-developed force in the "idling" mode and for the complex amplitude of the baseplate velocity in the "short-circuit" mode. Varying the design parameters we obtain optimal matching between the source and the medium.

As an example, consider the theoretical determination of the source internal resistance for a seismic vibrator. Vibration seismic sources with electrohydraulic drive systems interact with the geological medium via hydraulic actuators. *Figure 2* shows models of a hydraulic actuator and the geological medium, with their parameters summarized in Table 1 (for seismic vibrators of the SV-10/100 and SV-10/150 types). The soil parameters are in accordance with known data.

Consider models of the actuator and the medium as a control element wherein the spool displacement X is the input action and the force P and the velocity $V=Z$ are the output:

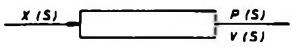

The transfer function of the actuator-medium system in the operator form becomes

$$W_P(S) = \frac{PS}{X(S)}, \tag{9}$$

$$W_v(S) = \frac{V(S)}{X(S)}, \tag{10}$$

where $S=j\omega$.

It is readily seen that the source resistance is derived from Eqs. (9) and (10) when two modes of the actuator-medium interaction are realized, i.e.

— "idling" mode characterized by $C_m=\infty$ and $Z=0$,

— "short-circuit" mode characterized by $C_m=0$ and $P=0$.

The transfer function equations are derived from the flow and force equations obtained with the conditions of the above-stated modes allowed for:

$$W_{P_{rg}}(S) = \frac{P_{rg}(S)}{X(S)} = \frac{C_{oil}F_{bp}K_q(m_cS+h_c)}{AS^2+BS+C}, \tag{11}$$

where

$$A = m_2 \cdot F_p,$$

$$B = C_{oil}m_c(K_l+K_v)+h_cF_p^2,$$

$$C = C_{oil}h_c(K_l + K_v).$$

$$W_{vsc}(S) = \frac{V_{sc}(S)}{X_p(S)} = \frac{C_{oil}F_pK_q(m_cS + h_c)}{S(T_1S^2 + T_2S + T_3)}. \tag{12}$$

$$T_1 = m_pm_cF_p^2,$$

$$T_2 = m_pF_ph_c + C_{oil}m_pm_c(K_l + K_v),$$

$$T_3 = C_{oil}F_p^2(m_p + m_c) + C_{oil}m_ph_c(K_l + K_v).$$

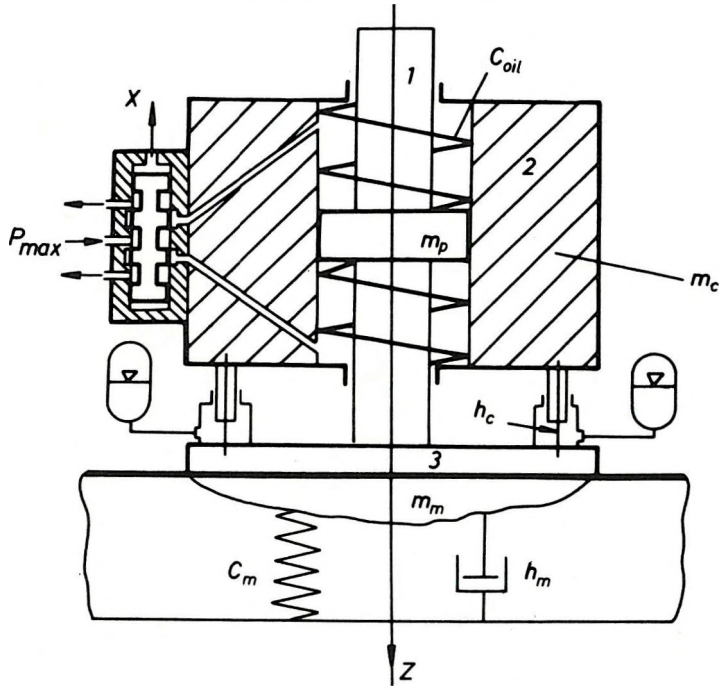

Fig. 2. Actuator—geological medium interaction
2. ábra. A vibrátor—talaj rendszer csatolása
Фиг. 2. Схема взаимодействия источником средей

By dividing Eq. (11) by Eq. (12) we obtain the sought vibrator resistance in the operator form:

$$Z_s(S) = \frac{S(T_1S^2 + T_2S + T_3)}{AS^2 + BS + C}, \tag{13}$$

where $S = j\omega$, and coefficients T_1, T_2, T_3 and A, B, C depend on the parameters in Table I.

Table I.

Nos.	Parameters	Symbols	Units	Magnitude	
				Vibrator	
	1. Hydraulic Actuator			SV-10/100	SV-10/150
1.1	Piston (1) area	F_p	m^2	$5.34 \cdot 10^{-3}$	$5.34 \cdot 10^{-3}$
1.2	Maximum supply pressure	P_{max}	N/m^2	$2 \cdot 10^7$	$2 \cdot 10^7$
1.3	Mass of:				
	— piston (1) plus baseplate	m_p	Ns^2/m	2.330	1.350
	— cylinder (2) (reaction mass)	m_c	Ns^2/m	2.500	2.500
1.4	Baseplate (3) area	F_{bp}	m^2	2.5	2.52
1.5	Stiffness of fluid in the cylinder and supply ports	C_{oil}	N/m	10^8	$1.4 \cdot 10^8$
1.6	Coefficients of:				
	— leakage	K_l	m^5/Ns	$8 \cdot 10^{-13}$	$8 \cdot 10^{-13}$
	— hydraulic amplifier internal conductivity	K_v	m^5/Ns	$1.3 \cdot 10^{-10}$	$1.3 \cdot 10^{-10}$
	— gain relative to the hydraulic amplifier flow rate	K_q	m^2/s	4.1	4.1
	— cylinder (2) damping	h_c	Ns/m	$2 \cdot 10^4$	$2 \cdot 10^4$
	2. Geological Medium			Source I	Point II
2.1	Soil density	ϱ	kg/m^3	$1.5 \cdot 10^3$	$1.8 \cdot 10^3$
2.2	Velocity of transverse	V'	m/s	50	200
	and longitudinal waves	V	m/s	100	400
2.3	Ratio $\frac{V'}{V}$	γ		0.5	0.5

Substituting respective parameters of the SV-10/100 and the SV-10/150 vibrators from Table I into Eq. (13) and the soil parameters into Eq. (6) and substituting $j\omega$ for S we can calculate actual Re and imaginary Im resistance components of the source and the medium.

The theory of matching impulse seismic sources to the geological medium is similar to that described before.

Figures 3 and *4* show characteristics Re (Z_s), Im (Z_s), Re (Z_m); Im (Z_m) computed for the SV-10/100 and SV-10/150 vibrators and the medium for the parameters in Table I.

Figures 5 and *6* illustrate computed resistance characteristics of the SI-32 and the SI-40 impulse seismic energy sources versus the resistance of the medium.

Considering the curves in Figs. 3 and 4 the following conclusions can be drawn:

— A perfect match between the vibrators' internal resistance and the resistance of the medium at a given source point is attainable only over a narrow band of frequencies. In designing vibration-type seismic sources it is essential that these frequencies be within the useful frequency range of a given prospecting area.

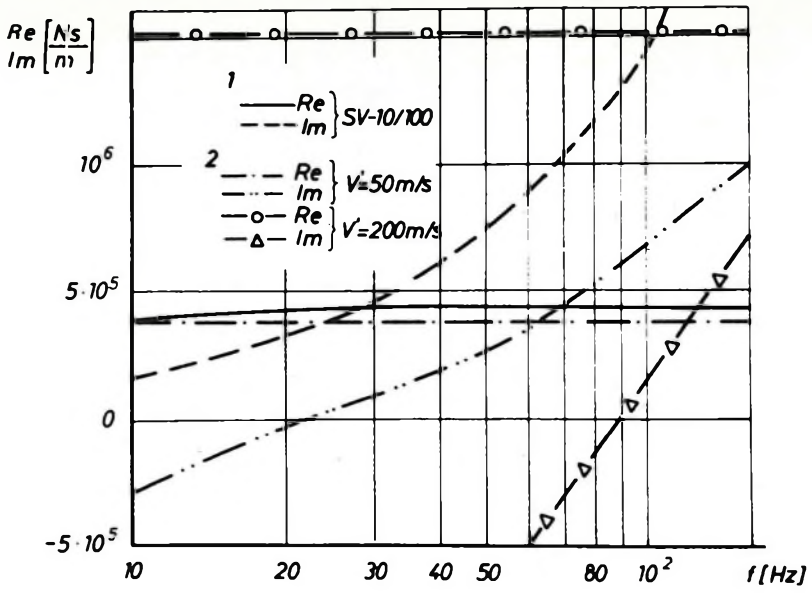

Fig. 3. Frequency characteristics of the SV-10/100 vibrator—medium system
1 — source; 2 — medium

3. ábra. Az SV—10/100 vibrátor—talaj rendszer frekvencia karakterisztikája
1 — forrás; 2 — közeg

Фиг. 3. Графики реальных Re и мнимых Im частотных характеристик виброисточника СВ-10/100 и среды
1 — источник; 2 — среда

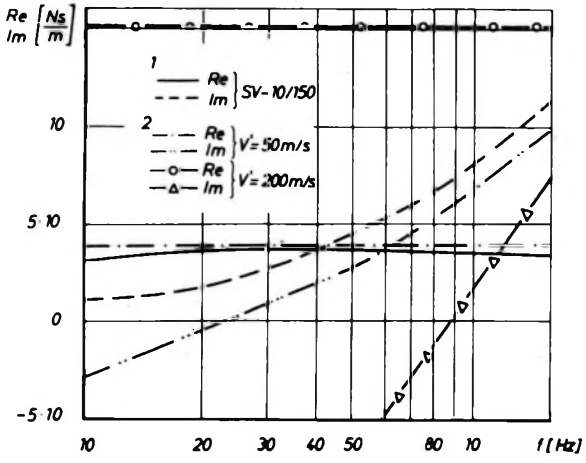

Fig. 4. Frequency characteristics of the SV-10/150 vibrator—medium system
1 — source; 2 — medium

4. ábra. Az SV—150 vibrátor—talaj rendszer frekvencia karakterisztikája
1 — forrás; 2 — közeg

Фиг. 4. Графики реальных Re и мнимых Im частотных характеристик виброисточника СВ-10/150 и среды
1 — источник; 2 — среда

— The matching between the SV-10/100 and the SV-10/150 seismic vibrators and the medium is the best on soft soils characterized by low propagation rates of elastic waves in the baseplate-earth contact zone (with V' equal to 50 m/s).

— The band of frequencies for securing a perfect match between the SV-10/100 vibrator's parameters and the resistance of the medium lies within 10 and 15 Hz on soft ground (with V' equal to 50 m/s) and within 45 and 50 Hz on harder ground (with V' equal to 200 m/s).

— The same is typical for the SV-10/150 vibrators, with the difference that a perfect match between their parameters and the medium will be obtained at higher frequencies, i.e. between 15 and 20 Hz on soft ground and between 55 and 60 Hz on hard ground, with the source reactive resistance Im (Z_s) being substantially reduced at a higher-frequency range.

Considering the curves in Figs. 5 and 6 the following can be concluded:

— As with the vibrators, impulse seismic sources have definite band of frequencies over which a perfect match can be obtained between their internal resistance and the medium at a given source point.

— Matching between the SI-32 and the SI-40 sources and the medium (see Table I for parameters) is the best between 10 and 30 Hz on soft ground (with V' equal to 50 m/s) and between 80 and 100 Hz on harder grounds (with V' equal to 200 m/s).

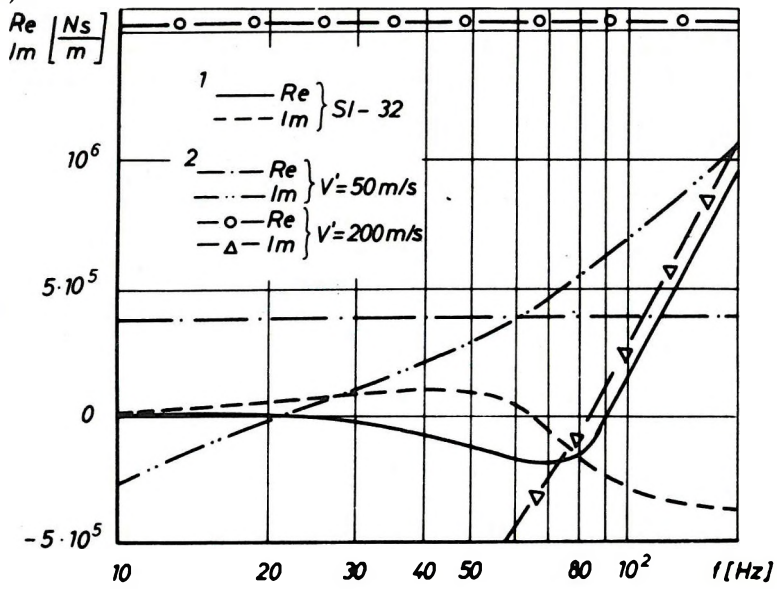

Fig. 5. Frequency characteristics of the SI-32 impulse source—medium system
1 — source; 2 — medium

5. ábra. Az SI—32 vibrátor—talaj rendszer frekvencia karakterisztikája
1 — forrás; 2 — közeg

Фиг. 5. Графики реальных RE и мнимых Im частотных характеристик источника СИ-32 среды
1 — источник; 2 — среда

— For the soils under consideration, the SI-40 sources have a lower-frequency band of matching as compared with the SI-32 sources. Hence it will be understood that the SI-40 type source may prove to be more efficient on harder ground, the SI-32 source will be more efficient on soft soils.

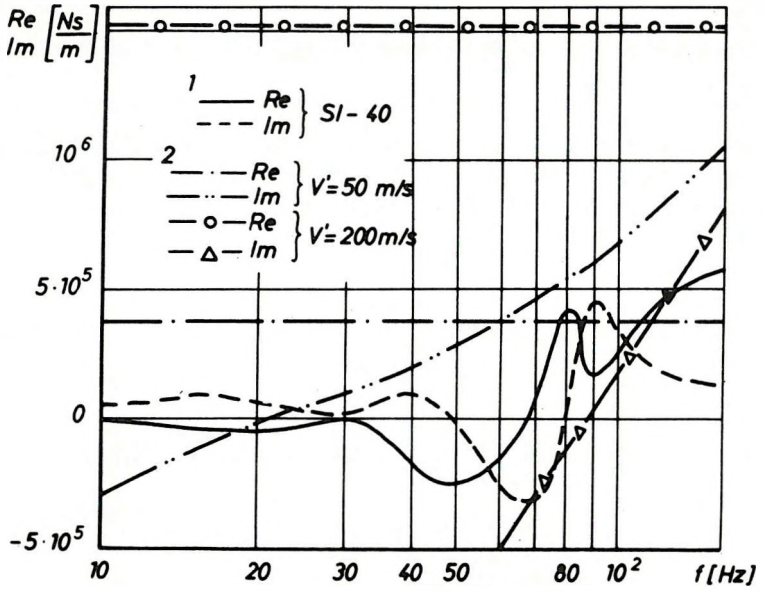

Fig. 6. Frequency characteristics of the SI-40 impulse source—medium system
1 — source; 2 — medium

6. ábra. Az SI—40 vibrátor—talaj rendszer frekvencia karakterisztikája
1 — forrás; 2 — közeg

Фиг. 6. Графики реальных Re и мнимых Im частотных характеристик источника СИ-40 и среды
1 — источник; 2 — среда

Conclusions

1. The source-medium matching theory proposed in this paper enables one to set an exact mathematical relationship between dynamic parameters of the source and the medium, and to determine the conditions for transmitting maximum active power from the source to the load, i.e. to the geological medium.

2. The theory proposed may be of use in both designing new seismic energy sources and operating existing ones.

3. The theory proposed may help engineers to solve the source parameter optimization problems arising from preset medium parameters; it can be adapted to optimize the transmission of maximum active power into the medium of a given spectrum corresponding to the frequency spectrum of useful waves in assigned prospecting areas.

4. The analysis of the SI-32 and the SI-40 impulse sources and of the SV-10/100 and the SV-10/150 vibration sources, made on the basis of the theory proposed, has demonstrated the effectiveness of the sources discussed since the frequency range and shear wave propagation rate V' taken are typical of most geological regions in the USSR.

5. Attempts to transmit maximum power into the medium within the useful frequency range may in some cases be at variance with the desire to have a high machine efficiency of the source. For instance, greater baseplate mass results in higher losses in overcoming the forces of gravity and inertia within the source. However, in the process we may obtain a better matching and a higher seismic efficiency of the source. In some cases it would be advisable to slightly reduce the source machine efficiency in order to get substantially higher total efficiency.

REFERENCES

Чичинин И. С.: Исследование механизма формирования продольных и поперечных волн сейсмическим источником... В сборнике «Измерительная аппаратура для разведочной геофизики», изд. СО АН СССР, Новосибирск, 1973.

Чичинин И. С.: О методике испытаний невзрывных источников сейсмических сигналов. Вибрационная сейсморазведка на продольных и поперечных волнах. Труды СНИИГГиМС и ИГиГ, СО АН СССР, вып. 219, Новосибирск, 1975.

Некрасов Г. А., Седин А. М., Шагинян А. С.: Результаты опробывания невзрывных источников. Вопросы возбуждения сейсмических волн вибрационным источником, сборник научных трудов, СО АН СССР, ИГиГ, Новосибирск, 1976.

Шагинян А. С.: Создание вибрационных источников большой мощности для глубинного зондирования Земли. Проблемы ВПЗ, Наука, Москва, 1977.

Шагинян А. С.: Исследование динамических характеристик поверхностных источников сейсмических сигналов. Труды 24 Международного геофизического симпозиума, Краков, 1979.

Шнеерсон М. Б., Майоров В. В.: Наземная сейсморазведка с невзрывными источниками колебаний. «Недра», Москва, 1980.

Бабешко В. А., Селезнев М. Г., Шагинян А. С.: Об одном методе уточненного учета реакции упругой среды при гармоническом воздействии. Прикладная геофизика, «Недра», Москва, 1981.

Бабешко В. А., Калинчук В. В., Селезнев М. Г.: Обзор методов излучения волновых полей, возбуждаемых в упругих средах вибрирующими штампами. Исследование Земли невзрывными сейсмическими источниками, изд. «Наука», Москва, 1981.

Шагинян А. С.: Динамика сейсмических вибраторов с электрогидравлическим сервоприводом. Исследование Земли невзрывными сейсмическими источниками, изд. «Наука», Москва, 1981.

Шагинян А. С.: О выборе оптимальных параметров газодинамических импульсных источников сейсмических сигналов. Исследование Земли невзрывными сейсмическими источниками, изд. «Наука», Москва, 1981.

ALBERT SHAGINYAN

A FELSZÍNI, NEM ROBBANTÁSOS, SZEIZMIKUS RENGÉSKELTŐK ÉS A FÖLDTANI KÖZEG CSATOLÁSÁNAK ELMÉLETE

A szeizmikus hullámforrások és a földtani közeg csatolásának elmélete a szeizmikus energiaforrások általános elméletének egyik legfontosabb fejezete.

Jelen munka az impulzusos és a vibrációs rengéskeltők, valamint a földtani közeg olyan csatolási feltételeinek analitikus vizsgálati módszerével foglalkozik, amelyek mellett megvalósítható a maximális energiaátadás a hasznos frekvenciatartományban. A szerző kimutatja, hogy az ajánlott módszer felhasználható optimalizálási feladatok megoldására a rengéskeltők fejlesztésénél.

АЛЬБЕРТ С. ШАГИНЯН

ТЕОРИЯ СОГЛАСОВАНИЯ ПОВЕРХНОСТНЫХ НЕВЗРЫВНЫХ ИСТОЧНИКОВ СЕЙСМИЧЕСКИХ СИГНАЛОВ С ГЕОЛОГИЧЕСКОЙ СРЕДОЙ

Теория согласования источников сейсмических сигналов с геологической средой относится к одному из наиболее важных разделов общей теории сейсмических источников. В настоящей работе излагается методика аналитических исследований условий согласования импульсных и вибрационных источников с геологической средой, при которых может быть осуществлена передача максимума энергии в среду в рабочем диапазоне частот. В работе показано, что предложенная методика может использоваться для решения оптимизационных задач при создании источников.

EÖTVÖS LORÁND GEOPHYSICAL INSTITUTE OF HUNGARY
GEOPHYSICAL TRANSACTIONS 1982
28/1 pp. 59–71

CONNECTION BETWEEN PSEUDO VELOCITY LOG AND SONIC LOG

I. SZULYOVSZKY*

In an ideal case any channel of the pseudo velocity log section—computed from a suitable preprocessed seismic section—is very similar to the sonic log measured in the place of the corresponding seismic channel.

Models are used to study the influence of the deconvolved signal bandwidth and that of the nonlinear transformation on the connection between the computed and sonic velocities. The computed velocity log has the same character as the sonic log, filtered by the seismic wavelet. The similarity is especially strong in the seismic frequency band.

The application of pseudo velocity logs is demonstrated by field examples.

1. Introduction

In the last few years direct hydrocarbon detecting methods have become customary. The basic element of these methods is the true amplitude processing. Following true amplitude recovery, pseudo velocity log sections can be computed. In the literature different names are used, viz. pseudo velocity log, velog, seislog, synlog; in the following, we use the name "seislog". The negative velocity anomaly has become accepted as a criterion for directly indicating hydrocarbon—as well as the amplitude anomaly, and the polarity change due to the liquid boundary. In theory, the seislog can also be considered as a direct hydrocarbon prospecting method because the presence of gas and oil causes a negative acoustic impedance anomaly that appears in the seislog in advantageous cases. The basis assumptions of a good quality seislog are as follows: perfect quality of the seismic section, minimum noise background, no multiples, a proper deconvolution and an acoustic log connected to the seismic line.

All of these assumptions are realized very rarely. Therefore the interpretation of seislogs needs an interpreter with considerable practice, with reliable concepts about the survey area.

The basic principles

In case of plane waves the reflection coefficient c for horizontal plane boundaries is given by the well-known formula

$$c = \frac{\varrho_i v_i - \varrho_{i+1} v_{i+1}}{\varrho_i v_i + \varrho_{i+1} v_{i+1}}, \tag{1}$$

* Geophysical Exploration Company, Budapest, Hungary.
Presented at the 26th Geophysical Symposium, Leipzig, 22–25. September, 1981.

where ϱ_i is the density, v_i the velocity in the i-th layer. By a simple rearrangement of Eq. (1) we get:

$$\varrho_{i+1}v_{i+1} = \varrho_i v_i \frac{1-c}{1+c}, \tag{2}$$

which shows that if we know the acoustic impedance in the first layer and the reflection coefficient, we can compute the acoustic impedance in the next layer. In this way the acoustic impedance of the n-th layer of a sequence can be computed from the acoustic impedance of the first layer and from the reflection coefficient sequence:

$$\varrho_n v_n = \varrho_1 v_1 \prod_{i=1}^{n-1} \frac{1-c_i}{1+c_i}. \tag{3}$$

The quotient in Eq. (3) can be written, by the series development

$$\ln \frac{1-c}{1+c} = -2\left\{c + \frac{c^3}{3} + \frac{c^5}{5} + \ldots\right\} \tag{4}$$

hence

$$\frac{1-c}{1+c} = e^{-2c} e^{-2\left\{\frac{c^3}{3} + \frac{c^5}{5} + \ldots\right\}} \approx e^{-2c} \tag{5}$$

and

$$\varrho_n v_n = \varrho_1 v_1 e^{-2\sum_{i=1}^{n-1} c_i} \tag{6}$$

This formula is called velocity transformation. Formulae (3) and (6) are directly suitable for transformation of a reflection coefficient sequence into an acoustic impedance sequence.

During seismic processing, the seismic trace comes closer to the reflection coefficient sequence. In spite of this the processed seismic trace cannot be considered as a reflection coefficient sequence—even in the most ideal case. Applying the velocity transformation formula to a processed seismic trace, we get a pseudo acoustic impedance channel.

Let us investigate the connection betweeen the real and the inverted acoustic impedance. It is essential to see the connection clearly, because the real acoustic impedance function obtained from boreholes is the bridge between geology and its seismic image. The seismic method measures the same physical property—the acoustic impedance—but the measuring methods are different. The information content of a seismic trace related to the information content of an acoustic log obtained from a borehole in the same place is less than one per

cent—even if we neglect the inevitable distortions of seismic noise. (The sampling rate in well logging is 0.2–0.4 m. The highest frequency on the seismic trace is about 50 Hz.With an interval velocity of 2000 m/s, the resolution of the subsurface information from seismic traces will be less than 40 m.) The difference between the information contents is mainly due to the band limited nature of the seismic trace.

2. Connection between the real and inverted acoustic impedance function

The main sources of error of the method are due to the deviations of the seismic trace from the reflection coefficient sequence. The reflection coefficient sequence is a transformation of the acoustic impedance sequence by Eq. (1), i.e. there exists a one-to-one correspondence between them; they contain the same geological information. It should be noted that the transformations connecting the acoustic impedance sequence with the reflection coefficient sequence (Eqs. (1) and (2)) are not linear. The same is true for the seismic trace and the pseudo acoustic impedance function computed from it.

The question is: What is the link between the real and the pseudo acoustic impedance log? First, let us investigate the connection between the functions from which the real and the pseudo acoustic impedance logs can be generated. These are the reflection coefficient sequence, and the seismic trace.

Let us compare a borehole sonic log with a nearby seismic trace *(Fig. 1/a)*. The sonic log is transformed into a time function, and resampled at a 2 ms rate. Consequently, the sampling rate is the same as in the seismic trace. In spite of the same sampling rate the sonic log contains more information than the seismic trace. Let us compare the measurements in the spectral domain *(Fig. 1/b)*. By comparing the respective power spectra of the sonic log (A), the reflection coefficient sequence (B), the seismic trace (C) and the pseudo acoustic impedance log computed from the seismic trace (D), the following observations can be made.

The spectrum of the reflection coefficient sequence deviates somewhat from that of the sonic log due, apart from other factors, to the nonlinear transformation process, but they are similar in character.

The transformation which generates the reflection coefficient sequence from the acoustic impedance log is similar to a differentiation, so the inverse transformation is similar to an integration. Investigation of the spectra shows the spectrum of the pseudo acoustic impedance log (D) being shifted toward lower frequencies with respect to the spectrum of the seismic trace.

The most remarkable feature on the spectrum of the seismic trace is the band limitation, its information content is much less than that of the above spectra. The difference is not only due to band limitation. The reason for further differences will be clear if we take into consideration the recording and processing procedures of the seismic method and the measuring technique of sonic logging. The sonic log yields a detailed velocity curve. The seismic method is sensitive to acoustic impedance, hence it contains density information as well. During seismic wave propagation there are many effects, with which we cannot deal adequa-

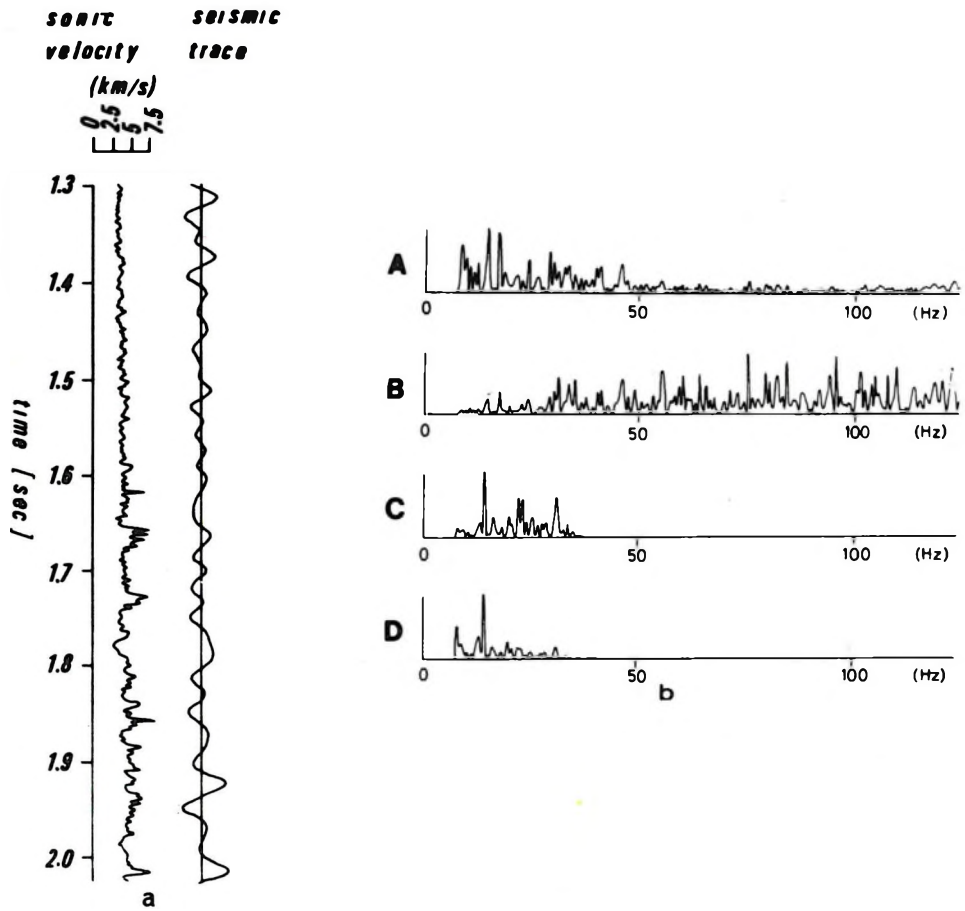

Fig. 1. Comparison of sonic log with a nearby seismic trace (a) and the power spectra (b)
A — power spectrum of the sonic log; B — power spectrum of the reflection coefficient sequence; C — power spectrum of the seismic trace; D — power spectrum of the pseudo acoustic impedance log

1. ábra. Szonikus log szelvényrészlet és ugyanazon a helyen mért szeizmikus csatorna, valamint teljesítményspektrumaik:
A — szonikus log teljesítményspektruma; B — reflexivitásfüggvény teljesítményspektruma; C — szeizmikus csatorna teljesítményspektruma; D — álakusztikus impedanciacsatorna teljesítményspektruma

Рис. 1. Сопоставление кривой АК с полученной в этом же месте сейсмической записью (a) и их энергетические спектры (b)
A — энергетический спектр кривой АК; B — энергетический спектр кривой коэффициентов отражения; C — энергетический спектр сейсмической записи; D — энергетический спектр кривой псевдоакустического импенданса

tely during seismic processing. For example: systematic noise and random noise; reflections arriving from lateral directions; migration; distortion of the wave form and amplitude, and so on. The non-linear transformation may also cause some additional distortion. In spite of all these deviations the spectrum of the seismic trace and the other spectra are still similar in character. This implies that the non-linear transformation does not alter the spectrum too severely. Moreover, the most important information content of the seismic trace concerns the velocity function of the subsurface. Recomputing the acoustic impedance function from a seismic trace which has a relatively narrow spectrum, the resulting acoustic impedance function will obviously have the same spectral width.

In the above investigation we cannot eliminate several effects influencing the seismic trace, so it is expedient to investigate the effect of the convolution and the non-linear transformation on models. Suppose for simplicity that the density is constant, moreover the only difference between the reflection coefficient sequence and the model seismic trace is the convolution by the wavelet (no noises are present). So we have an input velocity function V_1; a reflection coefficient sequence C_i computed from V_i; a wavelet and the resulting seismic model trace X_i; and a pseudo velocity log PVL_i obtained by inverting X_i. Convolving the input velocity by wavelet, and starting from the reflection coefficient sequence we get two branches. The end of the first is the pseudo velocity log, the end of the second is the wavelet filtered input velocity function $\tilde{V}_i$ *(Fig. 2)*. In

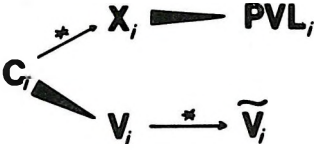

Fig. 2. *2. ábra*

Puc. 2.

both branches there are the same transformations: a linear (the convolution) and a non-linear transformation, but in reverse order. Because these are not interchangable transformations the ends of the two branches *must be different.* Although the above study of the sonic log and the seismic trace allows one to conclude that the deviations between pseudo velocity log and sonic log are not very large in the seismic frequency band, model studies are needed to clear to answer the questions. *Figure 3/a* illustrates a synthetic velocity curve (A), a seismic trace (D) computed with a wavelet of 40 Hz peak frequency (C), and a pseudo velocity log (E) computed from the synthetic trace. Multiples and other noises are not taken into account. The pseudo velocity log (E) does not show good correlation with the synthetic velocity log (A) but it is in a fair correlation with the seismic wavelet filtered synthetic velocity log (F). The power spectra of the curves of Fig. 3/a are shown in *Fig. 4/a.* Comparing spectra (E) and (F) we find an acceptable similarity in the spectral domain, too. Repeating the computation with a wavelet of 80 Hz peak frequency *(Fig. 3/b* and *Fig. 4/b)* we again find good correlation in the time domain between the pseudo velocity log (E) and the filtered velocity curve (F). Due to the higher signal peak frequency both curves give a better representation of the initial velocity function. In the spectral domain the similarity of the spectra (E) and (F) above 50 Hz is not as good as

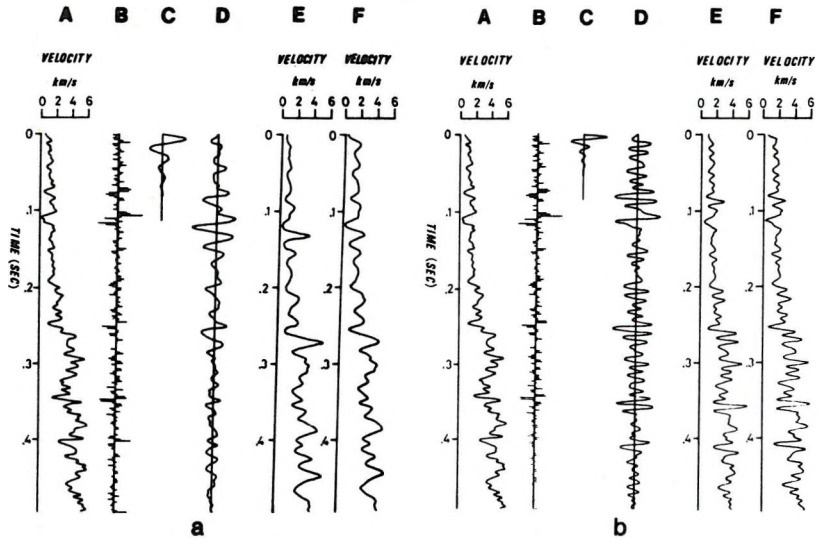

Fig. 3. Effect of bandwidth of the seismic signal on the pseudo velocity log. Model computation using a wavelet of 40 Hz peak frequency (a) and that of 80 Hz (b)
A — velocity model; B — reflection coefficient sequence computed from velocity curve (A); C — wavelet; D — synthetic seismic trace computed from wavelet (C) and reflection coefficient sequence (B), without multiples; E — pseudo velocity log computed from synthetic seismic trace (D); F — velocity curve (A) convolved by wavelet (C)

3. ábra. Modellszámítás: a jel sávszélességének hatása az álsebesség-csatornára
A — sebességmodell; B — reflexivitásfüggvény „A" sebességből számítva; C — wavelet; D — szintetikus szeizmikus csatorna „B" reflexivitásfüggvényből és „C" waveletből számítva, többszörösök nélkül; E — álsebesség-csatorna „D" szintetikus szeizmikus csatornából számítva; F — „C" wavelettel szűrt „A" sebességfüggvény

Рис. 3. Влияние ширины полосы сейсмического сигнала на кривую псевдоскоростного каротажа (модельные вычисления с использованием сигнала с пиковой частотой 40 Гц (а) и 80 Гц (b).
A — модель кривой скоростей; B — кривая коэффициентов отражения, подсчитанная по кривой скоростей A; C — сигнал; D — трасса синтетической сейсмограммы, подсчитанной по кривой коэффициентов отражения B и сигналу C без кратных отражений; E — кривая псевдоскоростного каротажа, подсчитанная по трассе синтетической сейсмограммы D; F — кривая скоростей A, профильтрованная сигналом C

below 50 Hz. But there is a similarity in character. On the other hand, above 50 Hz there is very little seismic information. It should be noted that frequencies below 8 Hz are not shown because they do not have significance in the given set up.

The following conclusions can be drawn from the model computation. The band limitation of the seismic signal implies that the speudo velocity log computed from the seismic trace is also band limitated. Here we lose significant geological information. The pseudo velocity log computed from the band limited seismic trace is very similar to the sonic log convelved by the seismic wavelet.

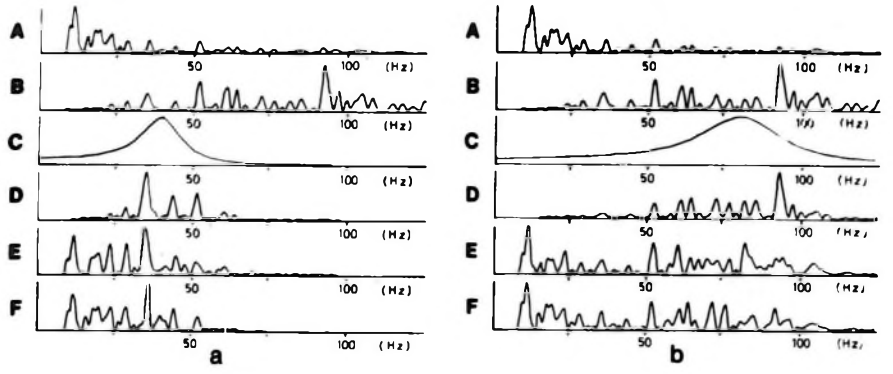

Fig. 4. a and b. Power spectra corresponding to the model traces (A)–(F) of Fig. 3 a and b

4. ábra. Teljesítményspektrumok a 3a és b ábra azonos jelzésű modellcsatornáiból számítva

Рис. 4. a и b. Энергетические спектры, соответствующие модельным трассам A – F на рис. 3, a и b.

The similarity is also seen in the spectral domain, and it is especially strong in the seismic frequency range below 50 Hz. Consequently, the two non-linear transformations and the linear transformation—namely the convolution by the seismic wavelet—do not distort significantly the reconstructed velocity function, not taking into consideration the band limitation.

In this paper we do not deal with the other earlier-mentioned distorting factors, we show one figure only to illustrate the effect of the strong multiple activity *(Fig. 5)*. It can be seen that the pseudo velocity log, computed from the synthetic trace with multiples has practically no resemblance with neither velocity curves below 2.2 s.

Application

For the application of formula (3) in seismic processing we have to know the acoustic impedance of the first layer. Moreover, the seismic trace must be scaled to match the reflection coefficient sequence. The acoustic impedance of the first layer is only a constant multiplier—as can be seen in formula (3).

The effect of the scaling of the seismic trace is not so simple. The true amplitude processing preserves the relative values of the real amplitudes in favourable conditions, but we still need a proper realing factor for the complete trace. Sometimes the amplitude of some identifiable reflection can be fitted to the correct value known from well logs, but in most cases this is not possible. In this situation we scale all the processed seismic traces so that the maximum of the amplitudes refers to a reflection coefficient of 0.25, for example, keeping in mind that the maximum of the real reflection coefficients is seldom over 0.3.

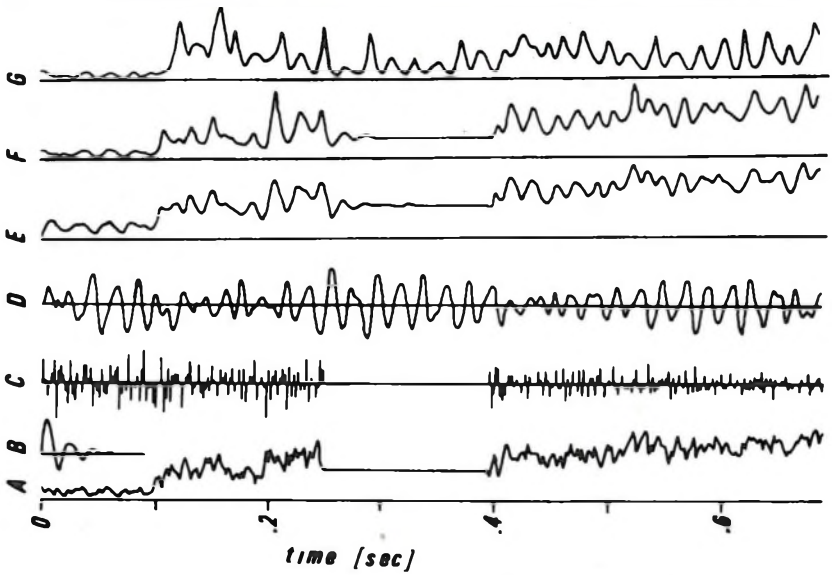

Fig. 5. Effect of multiple activity on the pseudo velocity log. (Model computation)
A — velocity model; B — wavelet; C — reflection coefficient sequence computed from velocity curve (A). Maximum of reflection coefficient: 0.32; D — synthetic seismic trace computed from wavelet (B) and reflection coefficient sequence (C), with multiples; E — velocity curve (A) filtered by wavelet (B); F — pseudo velocity log computed from primaries only; G — pseudo velocity log computed from synthetic trace (D)

5. ábra. Modellszámítás a többszörösök álsebesség-csatorna számítására gyakorolt hatásának vizsgálatára
A — sebességmodell; B — wavelet; C — reflexivitásfüggvény „A" sebességből számítva; D — szintetikus szeizmikus csatorna „C" reflexivitásfüggvényből és „B" waveletből számítva, többszörösök figyelembevételével; E — „B" wavelettel szűrt „A" sebességfüggvény; F — álsebesség-csatorna, a többszörösök figyelembevétele nélkül; G — álsebesség-csatorna a „D" szintetikus szeizmikus csatornából számítva

Рис. 5. Влияние кратных отражений на кривую псевдоскоростного каротажа (модельные вычисления)
A — модель скоростей; B — сигнал; C — кривая коэффициентов отражения, подсчитанная по кривой скоростей A; максимальный коэффициент отражения: 0.32; D — трасса синтетической сейсмограммы, подсчитанной по сигналу B и кривой коэффициентов отражения C с кратными отражениями; E — кривая скоростей A, профильтрованная сигналом B; F — кривая псевдоскоростного каротажа, подсчитанная по синтетической сейсмической записи D.

Let us now see the effect of over-scaling or under-scaling. In this case we change the values which we use as reflection coefficients, so we change the differences of acoustic impedances. Suppose that the velocities and densities increase with depth. So $C_i<0$ in formula (6), the exponent will be positive, and the value of the exponential will be larger than 1. Inverting a trace X scaled by K, in formula (6) we have to put KX_i instead of C_i:

$$\varrho_n v_n \cong \varrho_1 v_1 e^{-2\sum_i KX_i} = \varrho_1 v_1 \left[e^{-2\sum_i X_i}\right]^K$$

The scaling factor occurs as the exponent of the exponential expression. The value of the exponential function is larger than 1 so up-scaling the input trace will result in an up-sclaing of the acoustic impedance function in a degree increasing with depth. In case of under-scaling, the results will be reversed. The effect of scaling is illustrated in the model example *(Fig. 6)*. Three pseudo velocity logs are shown, with different scaling. Curve "A" results from no scaling—this corresponds, as shown above, roughly to the initial velocity curve filtered by the wavelet. The amplitude maximum on the X_i model trace is 0.18; when 0.01 is used as maximum amplitude the resulting curve is "B"; and when 0.99, the resulting curve is "C". Relative values are shown in Fig. 6 so the three pseudo velocity logs differ only in scaling.

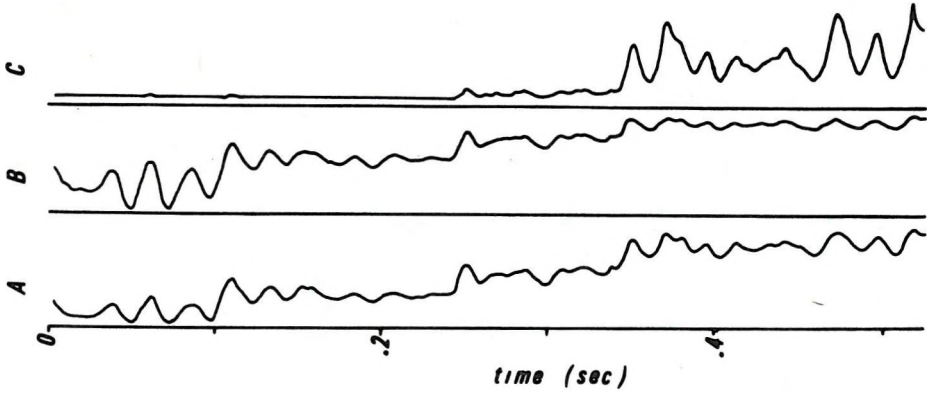

Fig. 6. Effect of scaling of the seismic trace on the computed pseudo velocity log. (Model computation)
A — pseudo velocity log, computed from correctly scaled seismic trace; B — pseudo velocity log, computed from strongly under-scaled seismic trace; C — pseudo velocity log, computed from strongly over-scaled seismic trace

6. ábra. Szeizmikus csatorna skálázásának hatása a számított álsebesség-csatornára
A — korrekt skálázással számított álsebesség-csatorna; B — erős alulskálázással számított álsebesség-csatorna; C — erős túlskálázással számított álsebesség-csatorna

Рис. 6. Влияние масштабирования сейсмической трассы на расчетную кривую псевдоскоростного каротажа (модельные вычисления)
A — кривая псевдоскоростного каротажа, подсчитанная по правильно масштабированной сейсмической трассе; B — кривая псевдоскоростного каротажа, подсчитанная по сильно недомасштабированной сейсмической трассе; C — кривая псевдоскоростного каротажа, подсчитанная по сильно перемасштабированной сейсмической трассе

The model investigation shows that the exact knowledge of the scaling factor has no essential role in computing the relative values of the inverted velocity. Moreover, the under-scaling distorts less the inverted relative velocity function than up-scaling.

The estimation of the velocity function in the seismic frequency band has been computed by the above method. The missing high frequencies are lost, their restoration from seismic measurements is not possible. There exist methods; however for the later addition of low frequencies. The missing low frequencies

may be obtained either from moveout analysis or from filtered, interpolated well logs. The low frequency trend is simply added to the inverted velocity function.

The real polarity of the seismic trace is identifiable by comparing it to a filtered sonic log. If we invert the nearest seismic trace with both polarities and the trace with the better correlation will be of the correct polarity.

Interpretation

The information content of the pseudo acoustic impedance sections—not taking into consideration the later added low frequency component—is the same as that of the seismic sections, but the seislog section can be correlated more easily with the geological build-up. Still the lithological interpretation of the pseudo acoustic impedance section is impossible without the analysis of core samples. When there is at least one borehole in the area the lithological information from it may be extrapolated by using the seislog section. In the absence of boreholes, no lithological interpretation can be given, however seislog helps to some extent in the interpretation. The interpretational value of seislogs depends on the quality of the seismic section in the first place and on the other available information. Although the most important application of seislogs is direct hydrocarbon prospecting, the pseudo acoustic impedance sections may be used in predicting abnormally pressured zones and in porosity prediction. There are no generally used methods of interpretation of seislogs, in spite of their being used for 5–6 years.

Two field sections are shown in Figs. 7 and 8 illustrating the application of the method. Both sections cross productive fields with known gas reservoirs. Since no density data or low frequency variations were applied during the inversion, we could only receive a relative pseudo acoustic impedance section. In the deconvolved section *(Fig. 7/a)* there is a strong amplitude anomaly at 1.4 s. In the seislog section *(Fig. 7/b)*—computed from the deconvolved section—at 1.4 s, where the borehole hit a gas containing layer a negative velocity anomaly appears. The deconvolved section of *Fig. 8/a* reveals a classic structure. Borehole data proves that the gas cap is at 1.52 s. In the computed seislog section *(Fig. 8/b)* the limits of the correlatable negative acoustic impedance anomaly are marked. Not regarding the two small disturbances, the negative anomaly follows the gas reservoir.

In conclusion, the band limitation of the seismic trace is one of the most important restricting factors in the computation of pseudo velocity logs, restricting the width of the spectrum of the resulting velocity log. Ignoring other distorting effects, the information content of the pseudo velocity log corresponds with that of the sonic log as restricted to the seismic frequency band with minimum alteration. For this reason a deconvolution of the best possible quality is needed. The frequency bandwidth of the seismic interpretation may be increased by a proper deconvolution. So the hidden information may be raised to the level of the detectability, both in the conventional seismic section and in the seislog sec-

tion computed from it. Because the other distorting factors cannot be completely eliminated, the interpretation of pseudo velocity logs requires much experience and as much preliminary information as possible about the exploration area.

It is to be hoped that high resolution sources, wide band registration and 3 D migration will, in the near future, give new impetus to the using of seislogs in stratigraphic and lithologic interpretations.

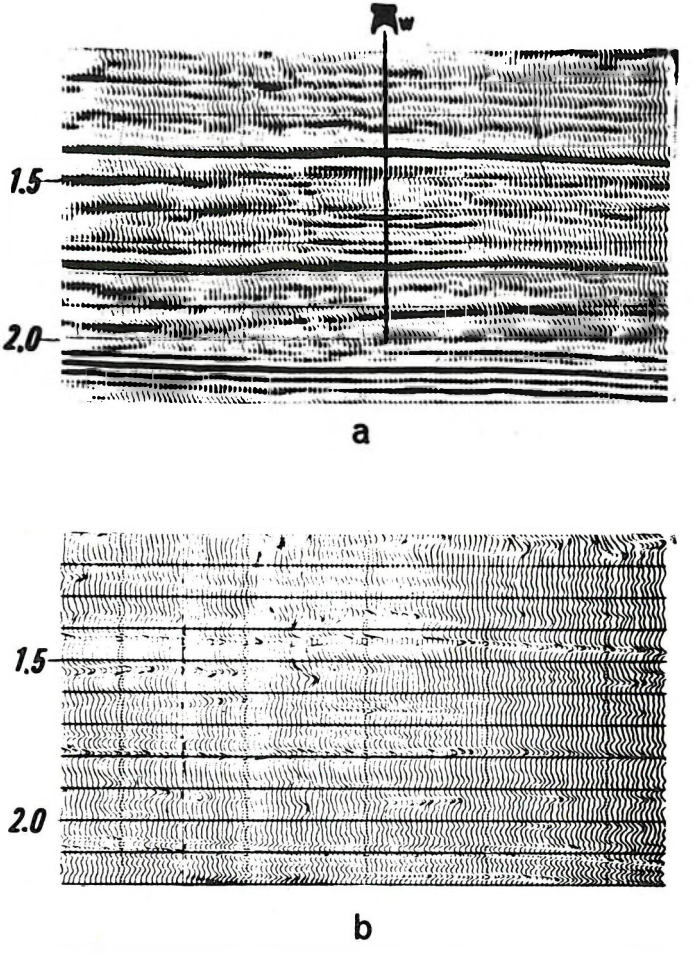

Fig. 7. Seismic section (a) and pseudo acoustic impedance section (b) crossing a gas field

7. ábra. Gáztartalmú területen mért szeizmikus szelvény (a) és ebből számított álakusztikus impedanciaszelvény (b)

Рис. 7. Сейсмический разрез (а) и кривая псевдоакустического импеданса (b) в газоносном районе.

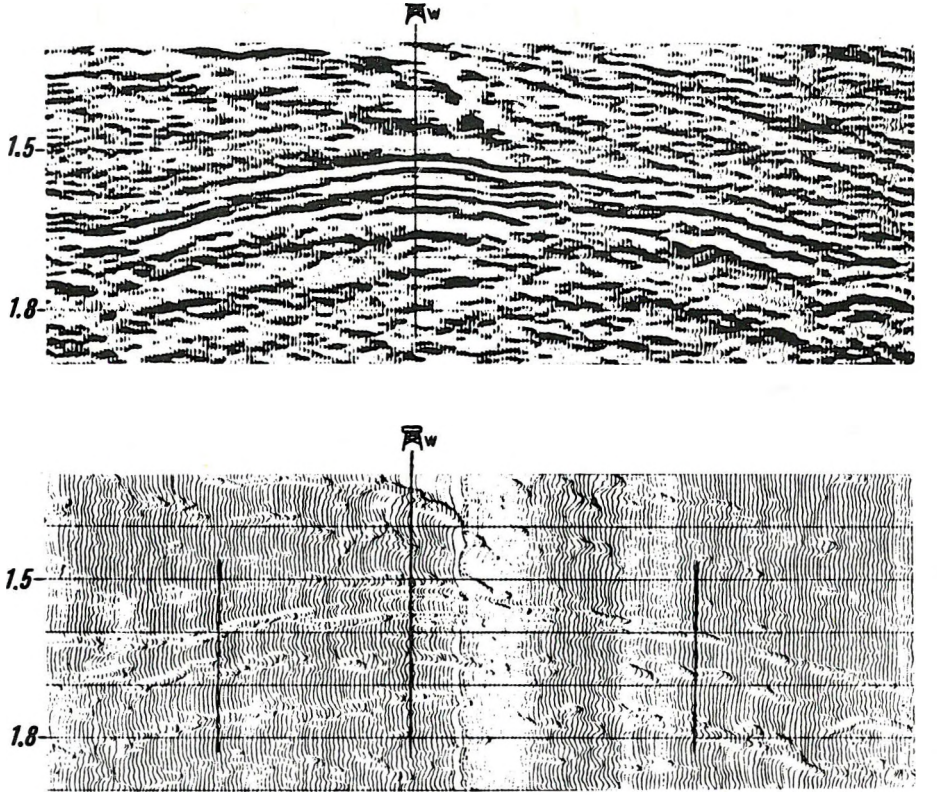

Fig. 8. Seismic section (a) and respective pseudo-acoustic impedance section (b) over a gas cap

8. ábra. Gáztartalmú terület dekonvolvált szeizmikus szelvénye (a) és álakusztikus impedanciaszelvénye (b)

Рис. 8. Сейсмический разрез (а) и соответствующая кривая псевдоакустического импеданса (b) над газовой шапкой

BIBLIOGRAPHY

BECQUEY, M., LAVERGNE, M. and WILLM, C., 1979: Acoustic impedance logs computed from seismic traces. Geophysics, **44**, 9, pp. 1485–1501.

DELAS, C., BEAUCHAMP, J. B., DE LOMBARES, G., FOURMAN, J. M. and POSTIC, A., 1970: An example of practical velocity determination from seismic traces. Presented at the 32nd Meeting of the EAEG, Edinburgh.

LAVERGNE, M., 1975: Pseudo diagraphies de vitesse en offshore profond. Geophys. Prosp., **23**, 4, pp. 695–711.

LAVERGNE, M. and WILLM, C., 1977: Inversion of seismograms and pseudo velocity logs. Geophys. Prosp., **25**, 2, pp. 231–250.

LINDSETH, R. O., 1979: Synthetic sonic logs—a process for stratigraphic interpretation. Geophysics, **44**, 1, pp. 3–26.

MARSCHALL, R., 1980: Interpretational information from seismic data. Prakla-Seismos GmbH, Hannover.

STONE, D. G., 1978: Using seismic data to extrapolate well logs. 48th Meeting of the SEG, San Francisco.

STREET, A. V., 1979: Development and application of seislogs to sub-surface lithology determination. 24th International Geophysical Symposium, Cracow.

SZULYOVSZKY IMRE

AZ ÁL-SEBESSÉG SZELVÉNYEK ÉS A SZONIKUS SZELVÉNY KAPCSOLATÁRÓL

Ideális esetben a megfelelő előfeldolgozás utáni szeizmikus anyag inverziójával kapott ál-sebesség szelvény nagyon hasonlít a szeizmikus csatorna helyén, fúrólyukban mért szonikus szelvényhez.

A dolgozat modelleken megvizsgálja, hogy a dekonvolúció utáni jel sávszélessége és a nemlineáris transzformáció hogyan befolyásolja a számított és a bemeneti sebesség szelvény kapcsolatát.

Látható, hogy a számított sebesség szelvény azonos jellegű a szeizmikus jellel szűrt szonikus szelvénnyel és a hasonlóság különösen a szeizmikus frekvenciasávban erős. A dolgozat néhány példát mutat be a módszer gyakorlati alkalmazására.

И. СУЁВСКИ

О СВЯЗИ КРИВЫХ ПСК И АК

В идеальном случае кривая псевдо-скоростного каротажа (ПСК), полученная в результате инверсии сейсмического материала после соответствующей предобработки, очень похожа на кривую акустического каротажа (АК), полученную в скважине на месте сейсмического канала.

В работе на моделях изучается эффект ширины полосы сигнала после деконволюции и нелинейной трансформации на отношение расчетной и входной скоростных функций.
Видно, что характер расчетной кривой скорости совпадает с кривой АК, профильтрованной сейсмическим сигналом, и подобие является особенно сильным в полосе сейсмических частот. Приводятся примеры практического применения метода.

EÖTVÖS LORÁND GEOPHYSICAL INSTITUTE OF HUNGARY
GEOPHYSICAL TRANSACTIONS 1982
28/1 pp. 73–85

DETERMINATION OF ATTENUATION FROM REFLECTION SEISMIC DATA AND THE INFLUENCE OF LAYERING

U. PATZER*

When developing new seismic processing techniques it is of great importance to test them with synthetic traces. Very often this step is decisive. Comparison of the obtained processing results with the known model data allows one to draw conclusions on the general performance, the optimum parameters, and the effectiveness of the technique under actual conditions.

As is demonstrated with a specific technique of attenuation determination the result obtained from such synthetic computations depends essentially on the reflection coefficient series from which the synthetic trace is computed. Unsuitable model traces can lead to incorrect assertions on the achievable accuracy and consequently on the potential practical effectiveness of the technique.

1. Problem discussion

A seismic trace $x(t)$ is considered to be the convolution of a reflectivity derived spike series with a wavelet

$$x(t) = i(t)\,s(t).$$

The spike series $i(t)$ represents the acoustic impedance distribution in the subsurface. While travelling underground the spectral composition of a seismic wavelet $s(t)$ is changed mainly as a result of attenuation. If the attenuation coefficient is to be determined from this spectral change the problem arises of extracting the wavelet spectrum from the seismic trace.

There exist several techniques to eliminate the influence of the spike series to such a degree that a sufficiently accurate estimation of the wavelet spectrum can be achieved. Their effectiveness is commonly tested with synthetic data. It is a general experience that the attenuation distribution computed from synthetic seismograms depends essentially on the used layer or velocity model (BARULI et al. 1980), in some cases the influence of the spike series may be so great that no meaningful attenuation determination can be achieved (MILLAHN and JURCZYK 1977, ENGELHARD 1978).

It is possible that the used technique does not enable a clear separation of the parts $s(t)$ and $i(t)$. Furthermore, the accuracy largely depends on the type of model used for the theoretical analyses. These two effects will be illustrated by a typical example in *Fig. 1*. First of all it can be established that the cepstrum analysis generally yields a more exact estimation of the actual wavelet spectra than the autocorrelation function technique of RAPOPORT (1969) where great deviations from the true spectra occur if an actual reflection coefficient series is applied.

* VEB Geophysik Leipzig, GDR.

Paper presented at the 26th Geophysical Symposium, Leipzig, 22–25. September, 1981.

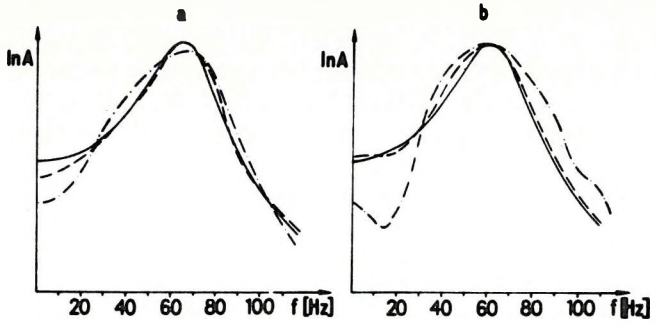

Fig. 1. Wavelet spectrum estimation from synthetic seismic traces
a — spike series of random distribution; b — actual reflection coefficient series
——— given spectrum, – – – – spectrum obtained by cepstrum analysis,
–·–·– spectrum obtained from the autocorrelation function

1. ábra. Az elemi jel spektrumának becslése szintetikus szeizmogramokból
a — véletlen eloszlás impulzussorozata; *b* — tényleges reflexiós koefficiens sorozat
——— tényleges spektrum, – – – – cepstrumanalízissel kapott spektrum, —— autokorrelációs függvénnyel számított spektrum

Фиг. 1. Оценка спектра сигнала для синтетической сейсмической трассы
a — последовательности импульсов по случайному распределению; b — реальная последовательность коэффициентов отражения
заданный спектр, – – – – спектр по кепстральному анализу, –·–·– спектр по функции автокорреляции

2. Models and test computations

Test computations were carried out on models derived from the velocity distribution of a well located in the North German–Polish Basin. No density values were available.

In model A of Fig. 5 the constant velocity layers were derived from the lithologic coloumn taking into account the acoustic log as well as petrophysical data. The mean layer thickness amounts to about 30 m. In the depth section corresponding to a traveltime range of 1.0 to 2.8 s acoustic log data were available. Models B and C, sampled at 10 m and 2 m rates, respectively, resulted from these data. All models are presented on the left part of Fig. 5 (for the traveltime interval 1.4 to 2.3 s).

In Fig. 1 the connection between the quality of spectrum estimation and the type of distribution of the used spike sequences is shown. Further special investigations were carried out based on model C. To have a better approximation of the actual conditions the data sampled with a 2 m rate were transformed into the time domain. Following Baranov and Kunetz (1960) the medium, assumed as ideally elastic, was subdivided into equal traveltime (in this case 1 ms), constant velocity layers. Thus, separate analyses of the influence of transmission and that of the multiples on the reflection coefficient series can be simultaneously made.

The randomness of the reflection coefficient series computed in this manner can be checked using the autocorrelation function. The autocorrelation function of a true random series only deviates significantly from zero for the time shift $\tau=0$. If $\tau\neq 0$ the values must be within a threshold level of significance, this threshold depends on both the false rejection probability and width of the analysed interval. The false rejection probability was selected as 5% for all investigated cases. For example, using an analysis window of 0.2 s some 15% of the peak value of the autocorrelation function corresponds to the threshold of significance.

Figure 2 shows the sampled, normalized autocorrelation function for different positions of the analysed traveltime window (the above mentioned threshold is also given). At narrow windows (0.2 and 0.4 s) significant differences in the character of the autocorrelation function can be seen for adjoining traveltime windows. In most cases there are several extrema exceeding the threshold of significance. This clearly indicates that the reflection coefficient series are generally *not* randomly distributed.

This general statement is also valid when the analysed window is enlarged up to an interval corresponding to the so-called effective time window (0.8 s) used for the attenuation determination. The intensity of the secondary extrema at time shifts $\tau\neq 0$ is somewhat lower for the summarized coefficient series (d) compared with the other ones (a, b, c). But in each case there also occur individual peaks exceeding or coming close to the threshold value.

Further analyses using actual reflection coefficient series show that in general they obey a normal distribution. This is demonstrated in more detail in PATZER et al. (1981). The evaluation given above is in good agreement with the results obtained by AGARD and GRAU (1961).

Returning to the results presented in Fig. 1, we have seen how much the quality of spectrum estimation from the autocorrelation function depended on the type of distribution. For the cepstrum analysis the most suitable type of distribution is obviously a random reflection coefficient series. However, the deviations of the actual reflection coefficient series from this type of distribution have not such a strong effect on wavelet spectrum estimation as in case of the autocorrelation function method. We have found that when using cepstrum analysis with optimally selected program parameters, it yields an approximately four times higher accuracy in attenuation determination than that achieved with the autocorrelation function technique.

3. The influence of intrabed multiples

The term "attenuation" generally describes the frequency dependent energy losses of a seismic wave due to its propagation through the medium. This energy loss is esentially caused both by the nonreversible change of mechanical energy into heat and by wave scattering at interfaces and other inhomogeneities. If a seismic signal travels through a layered medium an additional attenuation mechanism acts. It results from the combination of transmission losses at inter-

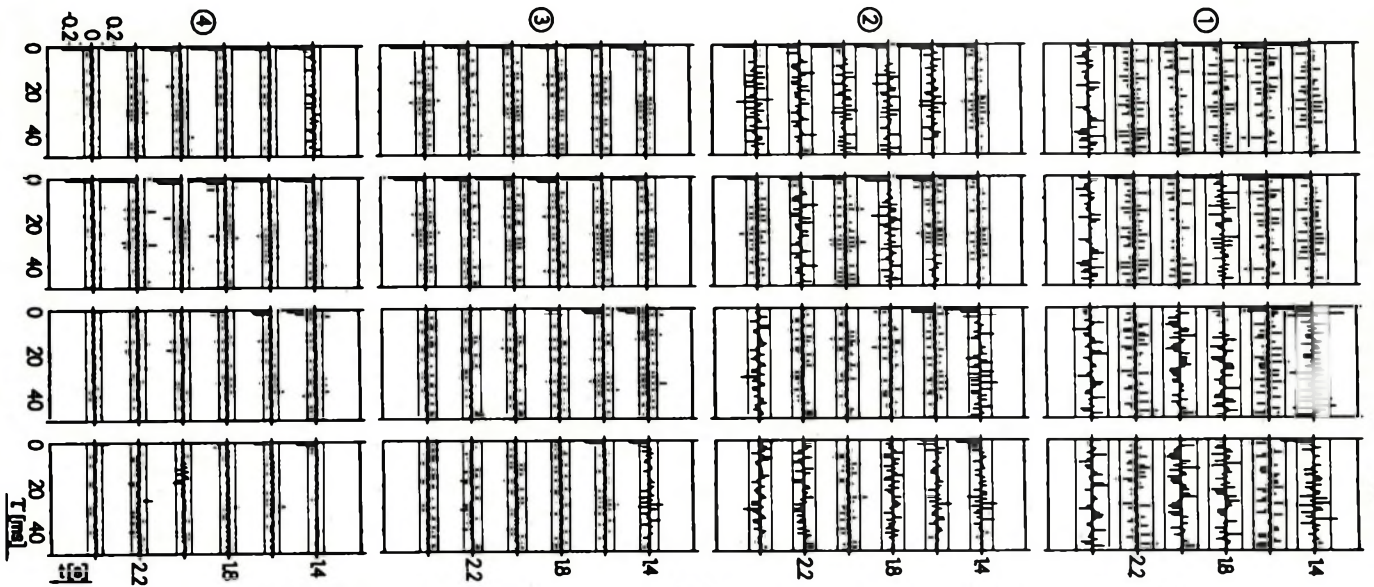

Fig. 2. Sampled autocorrelation functions of reflection coefficient sequences derived from model C
a — normal reflection coefficient sequence; b — reflection coefficient sequence including transmission loss; c — reflection coefficient sequence of multiple reflections; d — summarized reflection coefficient sequence ($b+c$)
1 — time window 0.2 s, 2 — time window 0.4 s, 3 — time window 0.6 s, 4 — time window 0.8 s

2. ábra. C modellből származtatott reflexiós koefficiens sorozatok mintavételezett autokorrelációs függvényei
a — kiinduló reflexiós koefficiens sorozat; b — reflexiós koefficiens sorozat az áthaladási veszteségek figyelembevételével; c — többszörösök reflexiós koefficiens sorozata; d — összegezett reflexiós koefficiens sorozat ($b+c$)
1 — időablak 0,2 s; 2 — időablak 0,4 s; 3 — időablak 0,6 s; 4 — időablak 0,8 s

Фиг. 2. Полученные в результате квантования функции автокорреляции для последовательности коэффициентов отражения, выведенных по модели С
а — нормальная последовательность коэффициентов отражения; b — последовательность коэффициентов отражения с учетом потерей по передаче; с — последовательность коэффициентов отражения для многократных отражений; d — накопленная последовательность коэффициентов отражения ($b+c$)
1 — временное окно 0,2 с, 2 — временное окно 0,4 с, 3 — временное окно 0,6 с, 4 — временное окно 0,8 с

faces and intrabed multiples generated therefrom. In particular, when a seismic wave travels through a stack of thin layers of strongly changing acoustic impedances an essential fraction of the signal energy gets trapped and only reappears of greater traveltimes. Hence, the maximum amplitude decreases and the predominant frequency of the signal is lowered. Although the mechanism is of an entirely different kind from that caused by inelasticity and scattering, its action on the seismic pulse is very similar. This "quasiattenuation" effect was clearly described by O'DOHERTY and ANSTEY (1971). For our investigations it is of interest to what extent this apparent attenuation due to intrabed multiples acts in the used models. The investigations were carried out again on layer model C. The reflection coefficient series was computed according to BARANOV and KUNETZ'S technique (1960).

Similarly to the method suggested by SCHOENBERGER and LEVIN (1974), the model was sealed at the bottom of the hole by an additional isolated totally reflective interface of reflection coefficient $R = -1$. In the computed reflection coefficient series involving all true and multiple reflections each reflection generated at this reflective horizon represents that energy which has travelled downward and upward through the layer model.

For computational reasons the additional reflective interface was inserted at 2 s traveltime. *Figure 3* shows that at this traveltime the multiple tail of the original model is not entirely suppressed and superimposes on the reflections gener-

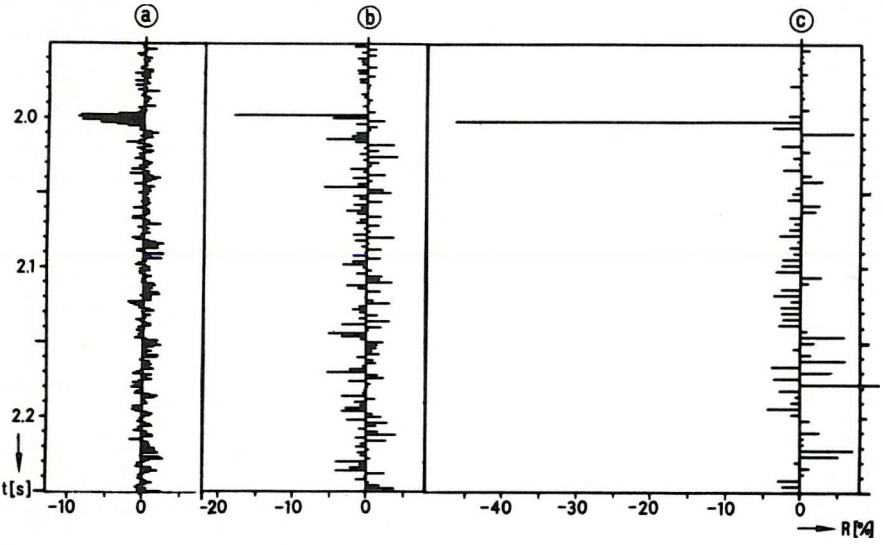

Fig. 3. Impulse response for a spike travelling twice through model C for different sampling rates
a — sampling rate 1 ms; b — sampling rate 2 ms; c — sampling rate 4 ms

3. ábra. Impulzus-válaszfüggvény, a C modellen való kétszeri áthaladás esetén, különböző mintavételezéssel
a — mintavételi köz 1 ms; b — mintavételi köz 2 ms; c — mintavételi köz 4 ms

Фиг. 3. Характеристика импульса, проходящего два раза модель слоистости С при разных шагах квантования в диапазоне времени
a — шаг квантования 1 мс; b — шаг квантования 2 мс; c — шаг квантования 4 мс

ated at the isolated reflective interface. Nevertheless, the model allows qualitative assertions about the filtering effect of the original series of layers.

As can be seen from Fig. 3, the impulse response exhibits considerable differences depending on the sampling rate used for the computation of the reflection coefficient series (see also SCHOENBERGER and LEVIN 1979).

The shift of a considerable fraction of the reflected energy towards greater traveltimes with simultaneous pulse broadening (typical for a cyclic layering according to O'DOHERTY and ANSTEY 1971) becomes clear only when applying a sampling rate of 1 ms, in spite of the great thickness of the analysed layer complex.

The amplitude spectra of the impulse responses *(Fig. 4)* show that for sampling rates greater than 2 ms the frequency dependent attenuation caused by intrabed multiples can be neglected.

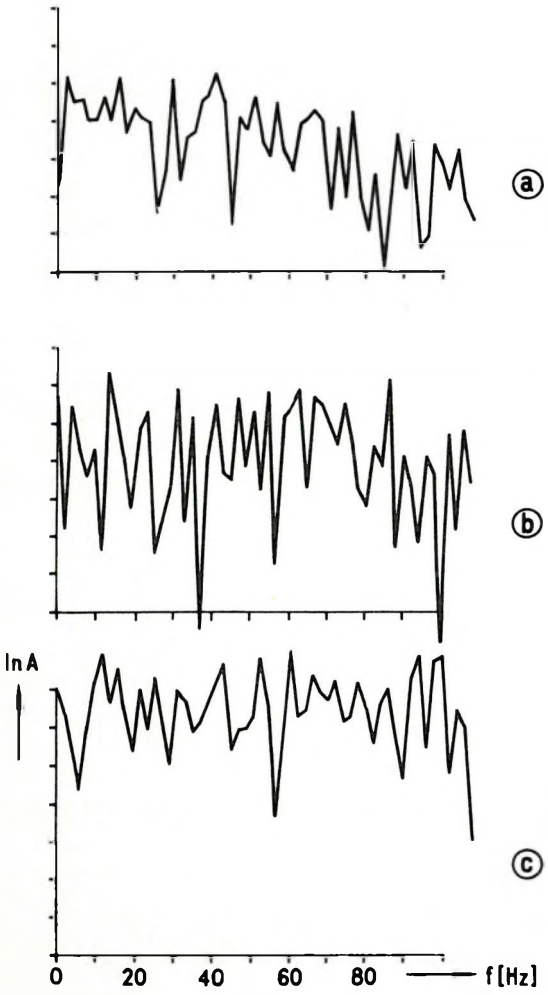

Fig. 4. Amplitude spectra of the impulse responses presented in Fig. 3
a — sampling rate 1 ms; b — sampling rate 2 ms; c — sampling rate 4 ms

4. ábra. A 3. ábrán bemutatott impulzusválaszfüggvények amplitúdóspektrumai
a — mintavételi köz 1 ms; b — mintavételi köz 2 ms; c — mintavételi köz 4 ms

Фиг. 4. Амплитудные спектра характеристик импульсов, приведенных на рис. 3
а – шаг квантования 1 мс; в – шаг квантования 2 мс; с – шаг квантования 4 мс

4. Computation of synthetic seismograms with attenuation and attenuation determination

The investigations on the influence of the selected layer model on the accuracy of attenuation determination were accomplished on synthetic traces computed by taking into account attenuation. First of all the complex frequency characteristics of the model were determined by applying Fourier transform to the spike series including all primary and multiple reflections (GOGONENKOV and ZACHAROV 1971). A linear dependence of attenuation on frequency was assumed. Velocity dispersion was taken into account according to the well-known FUTTERMAN relation connecting attenuation and dispersion. We started out from different attenuation functions, derived the spikes series for the models A to C, and convolved the results by an actual wavelet recorded near one of the shotpoints.

The computation of attenuation was carried out by the computer program ABSOR2. The signal spectrum is determined by cepstrum analysis within moving time windows shifted in 50 ms steps along the trace. The effective length of this window and hence the resolution power of attenuation determination is approximately 0.8 s. An earlier version of this technique was presented at the 22nd Geophysical Symposium held in Prague [DANCKWARDT et al. 1978]. The attenuation coefficient α is assumed to depend linearly on frequency, $\alpha(f) = k \cdot f$. The factor k of dimension $m^{-1} Hz^{-1}$ is computed in the well-known manner from the slope of the spectral ratios. This value, reflecting the change of the ratios between high- as well as low-frequency signal components is denoted by k_f.

In the extended version of the program [DANCKWARDT and PATZER 1981] the attenuation is additionally computed from the traveltime dependent amplitude decay for the same harmonic components of the signal spectrum (attenuation value k_t). Besides the determination of the individual values k_f and k_t the program also computes the summarized attenuation coefficient $k_\Sigma = 1/2(k_f + k_t)$.

5. Analysis of the influence of layering

First, the processing results obtained for model A are considered. In *Fig. 5* (upper part) it can be seen that a very high deviation occurs from the actual attenuation value. The greatest error arises in k_t, computed from the traveltime-dependent amplitude decay.

From *Fig. 6* (left part) it is clearly seen that the character of the distribution of the results is not changed if different attenuation functions are assumed. The mean deviation from the true attenuation value remains approximately constant. This means that the accuracy of the attenuation determination is independent of the actual magnitude of attenuation.

The causes of these great errors can be attributed mostly to the insufficient suppression of the spike series. The right-hand side of Fig. 6 shows the difference curves for the computed attenuation. Subtracting the curves based on the

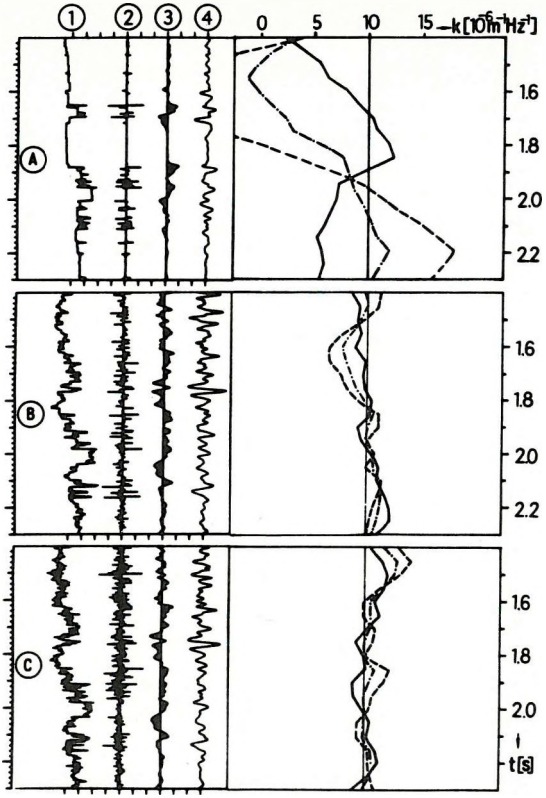

Fig. 5. Attenuation determination from synthetic traces for different velocity distributions and different models

A — based on lithology (mean layer thickness 30 m); B — resulting from acoustic log, sampling rate = 10 m; C — resulting from acoustic log, sampling rate = 2 m

1 — velocity distribution, 2 — reflection coefficient series, 3 — attenuation affected reflected impulses, 4 — synthetic trace after convolution of 3 by a wavelet (attenuation: model 1 with $k = 10$), computed values for k_f ———, k_t – – – –, k_Σ –·–·–

5. ábra. Csillapodás-meghatározás szintetikus szeizmogramokból különböző sebességeloszlásokra és különböző modellekre

A — a fúrási szelvényből (átlagos rétegvastagság 30 m); B — akusztikus szelvényből, mintavételi köz 10 m; C — akusztikus szelvényből, mintavételi köz 2 m

1 — sebességeloszlás, 2 — reflexiós koefficiens sorozat, 3 — csillapított reflektált impulzusok, 4 — szintetikus szeizmogram (3 konvolválva egy elemi hullámmal) az adott csillapítással (modell 1, $k = 10$), számított értékek: k_f ———, k_t – – – –, k_Σ –·–·–

Фиг. 5. Результаты определения поглощения по синтетическим тестовым трассам, которые получены с применением различных законов скоростей и моделей слоистости

А — по литологическому разрезу, средняя мощность пластов 30 м; В — по акустическому каротажу, шаг квантования = 10 м; С — по акустическому каротажу, шаг квантования = 2 м

1 — распределение скорости, 2 — последовательность коэффициентов отражения, 3 — импульсная трасса с учетом поглощения, 4 — синтетическая трасса после свертки импульсной трассы 3 с сейсмическим сигналом (заданное поглощение: модель 1 с к = 10), рассчитанные значения для k_f ———, k_t – – – –, k_Σ ——

attenuation functions 1 ($k = 10 \times 10^{-6}\ m^{-1}\ Hz^{-1}$) and 2 ($k = 5 \times 10^{-6}\ m^{-1}\ Hz^{-1}$), respectively the above mentioned difference curves result. As can be seen, a significant decrease of the deviation from the given attenuation model is achieved. But this correction for layering effects is only of a hypothetical value as it is not applicable to actual data.

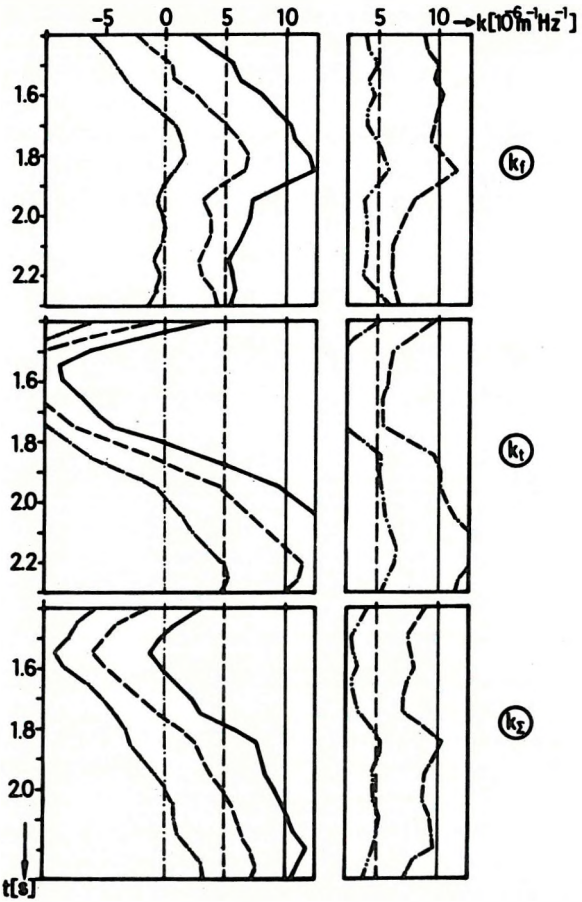

Fig. 6. Attenuation determination from synthetic traces, velocity model A
——— data for model 1 ($k = 10$), – – – – data for model 2 ($k = 5$), –·–·– data for model 3 ($k = 0$), – – ·– – difference between the values for models 1 and 3, – – ·· – – difference between the values for models 2 and 3

6. ábra. Csillapodás-meghatározás szintetikus szeizmogramokból, A sebességmodellre
——— adatok modell 1-hez ($k = 10$), – – – – adatok modell 2-höz ($k = 5$), –·–·– adatok modell 3-hoz ($k = 0$), – – ·– – 1. és 3. modellre számított értékek különbsége, – – ·· – – 2. és 3. modellre számított értékek különbsége

Фиг. 6. Результаты определения поглощения на тестовых синтетических трассах модели слоистой среды А
данные для модели 1 ($\kappa = 10$), – – – – данные для модели 2 ($\kappa = 5$), –·–·– данные для модели 3 ($\kappa = 0$), – – ·– – разница между данными моделей 1 и 3 – – ·· – – разница между данными моделей 2 и 3

If the test result obtained from this layer model had been available it would have been possible to conclude that the used technique does not enable a sufficient suppression of the spike series influence and is unsuitable for detecting attenuation anomalies under actual conditions.

But when using more detailed layer models which may be derived from acoustic log data (models B and C in Fig. 5) an essentially smaller deviation between computed and given attenuation values is achieved. According to Table I the mean deviation is only as small as about 1×10^{-6} m^{-1} Hz^{-1} for this model. If a value of 10×10^{-6} m^{-1} Hz^{-1} is taken for the average attenuation in the subsurface under normal conditions, a theoretical accuracy of about 10% is achieved in determining attenuation. Under such circumstances the application of the described technique to practical exploration problems seems more favourable than in the case of layer model A.

Table I. Accuracy of attenuation determination depending on the sampling rate of an actual velocity model

Layer model	Layer thickness		Mean deviation m_k in 10^{-6} m^{-1} Hz^{-1}		
	in m	in ms	m_{k_r}	m_{k_z}	m_k
A	≈30	≈15	2.5	9.3	4.0
B	10	≈ 5	0.9	1.2	0.9
C	2	≦ 2	0.9	1.2	0.8

6. Detection of Attenuation Anomalies

To prove the general performance of program ABSOR2 in predicting layers with increased attenuation the computations were repeated for model C using a modified attenuation function (attenuation model 4). When evaluating the data presented in *Fig. 7*, it must be considered that because of the limited vertical resolving power of the technique a strong smoothing of the attenuation distribution results. The theoretically achievable representation of the anomaly (dotted line) depends on both the magnitude of the attenuation anomaly (length 0.3 s, change of attenuation by 10×10^{-6} m^{-1} Hz^{-1}) and on the resolving power of the computation (0.8 s).

Taking these facts into account a satisfying approximation of the computed attenuation values to the theoretically achievable curve can be established for attenuation model 4. A reliable detection of attenuation changes of such a magnitude seems to be somewhat problematic for actual conditions. Obviously, such anomalies are at the lower boundary of detectability when using program ABSOR2.

The subtraction of data for attenuation function 1 (with anomaly) from those corresponding to function 4 ("normal level" of attenuation), already

demonstrated in Fig. 6, yields a decrease of deviations—but not decisive—between theoretical and computed values. Also in this case, the improvement results from the elimination of the residual layering influence. As follows from Fig. 7, this influence of the spike series for layer model C is not very high, it is in the order of the inevitable inaccuracies of the computational technique.

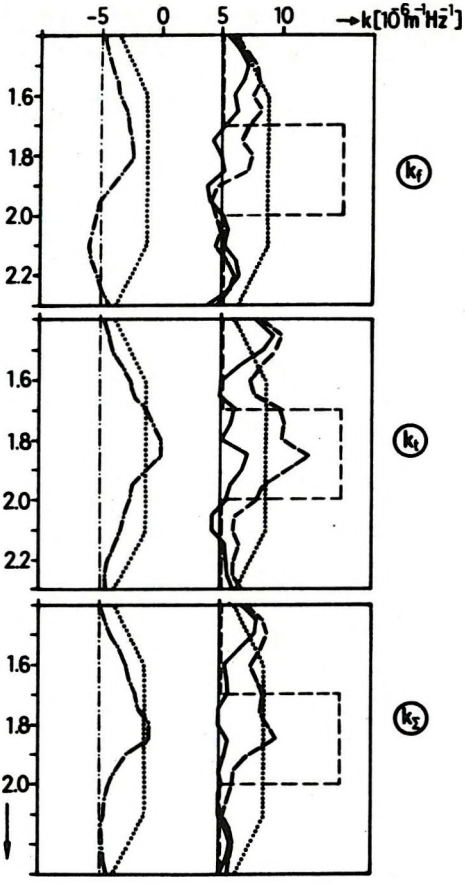

Fig. 7. Attenuation determination from synthetic traces, velocity model C
——— data for model 1 ($k=10$), – – – – data for model 4 (interval 1.7 to 2.0 s, $k=20$, outside this interval $k=10$), –·–·– difference between the values for models 1 and 4, ... theoretical distribution of the results for model 4 for the given resolving power

7. ábra. Csillapodás-meghatározás szintetikus szeizmogramokból, C sebességmodell
——— adatok modell 1-hez ($k=10$), – – – – adatok modell 4-hez (az 1,7—2,0 s intervallumon belül $k=20$, ezen kívül $k=10$), –·–·– 1. és 4. modellre számított értékek különbsége, ... az eredmények elméleti eloszlása a 4. modellre, az adott felbontóképesség mellett

Фиг. 7. Результаты определения поглощения на тестовых синтетических трассах модели слоистой среды С
данные для модели 1 ($\kappa = 10$), – – – данные для модели 4 (в интервале от 1,7 до 2,0 с, $\kappa = 20$, вне этого окна: $\kappa = 10$), –·–·– разница между данными моделей 1 и 4, ····· теоретическое распределение данных для модели 4, получаемое с учетом разрешающей способности

REFERENCES

AGARD, J. – GRAU, G., 1961: Étude statistique de sismogrammes. Geophys. Prosp., **9**, 4, pp. 503 – 525.

BARANOV, V. – KUNETZ, G., 1960: Film synthétique avec réflexions multiples; théorie et calcul pratique. Geophys. Prosp., **8**, 2, pp. 315 – 325.

БАРУЛИ, Г. И. и др.: Результаты исследования корреляционной методики прямого поиска на модели геологического строения борта Прикаспийской впадины. – Геол. и разв., Москва (1980) 3, 121–126.

DANCKWARDT, E. – LEISSRING, B. – PATZER, U., 1978: Attenuation determination from reflection seismic data. Proc. 22nd Intern. Geophys. Symp. in Prague 1977; Geofyzika n.p. Brno, 1, pp. 275 – 294.

ДАНКВАРДТ, Е.; ПАТЦЕР, У., 1981: Комбинированное определение поглощения с помощью кепстрального анализа. – Доклад на 2 Науч. Семинаре Координационного центра Интернефтегеофизика, Ереван

ENGELHARD L., 1978: Zur Bestimmung der Absorption seismischer Wellen aus Reflexions-seismogrammen. Erdöl-Erdgas-Z., **94**, 9, pp. 325 – 327.

ГОГОНЕНКОВ, Г. Н.; ЗАХАРОВ, Е. Т., 1971: Теоретические сейсмограммы в тонкослоистых поглощающих средах. – Физ. земли, Москва 2, 45–54

MILLAHN, K. O. – JURCZYK, D., 1977: Measurement of attenuation in reflection seismograms. Paper, presented at the 47th Meeting of the SEG, held in Calgary, Alberta, Canada

O'DOHERTY, R. F. – ANSTEY, N. A., 1971: Reflections on amplitudes. Geophys. Prosp., **19**, 3, pp. 430 – 458.

PATZER, U. – DANCKWARDT, E. – LEISSRING, B., 1981: Über dies statistischen Eigenschaften realer Reflexionskoeffizientenfolgen. Geoph. und Geol.; Geophys. Veröff. **2**, 3, pp. 17 – 30.

РАПОПОРТ, М. В., 1967/1969: Способ определения поглощения сейсмических волн. № пат. СССР 240 282.

SCHOENBERGER, M.–LEVIN, F. K., 1974: Apparent attenuation due to intrabed multiples. Geophysics, **39**, 3, pp. 278 – 291.

SCHOENBERGER, M. – LEVIN, F. K., 1979: The effect of subsurface sampling on one-dimensional synthetic seismograms. Geophysics, **44**, 11, pp. 1813 – 1829.

ULRICH PATZER

A RÉTEGZŐDÉS HATÁSA A CSILLAPODÁS MEGHATÁROZÁSÁNAK PONTOSSÁGÁRA

Szintetikus csatornákon végzett elméleti számításokból ismeretes, hogy a rétegzett közeg modellje jelentős hatást gyakorol a csillapodás számításának pontosságára. Az alkalmazott eljárások valószínűleg nem adnak módot ezen hatás kiküszöbölésére. Ezenkívül az elérhető pontosság jelentős mértékben függ az elméleti analíziseknél alkalmazott, rétegzett modell fajtájától.

Vizsgálatokat végeztünk olyan modelleken, amelyek különböző részletességgel tükrözték a fúrólyukakban meghatározott sebességeloszlásokat. A szelvény durva tagolása alapján kapott sebességmodell felhasználásakor igen nagy mérési hiba figyelhető meg, ez azzal kapcsolatos, hogy a modell nem elég részletesen tükrözi a valóságos viszonyokat. A rétegzett közegen — akusztikus karotázs alapján, csökkentett mintavételi közzel — végrehajtott elméleti számítások alátámasztják ezt a következtetést, a számított abszorpciós értékek sokkal kisebb mértékben térnek el a megadottaktól.

У. ПАТЦЕР

ВЛИЯНИЕ СЛОИСТОСТИ НА ТОЧНОСТЬ ОПРЕДЕЛЕНИЯ ЗАТУХАНИЯ

По теоретическим расчетам с синтетическими трассами известно, что модель слоистой среды оказывает существенное влияние на точность расчета затухания. Применяемые способы очевидно не позволяют исключить этот эффект. Кроме того, достигаемая точность в значительной мере зависит от вида слоистой модели, применяемой при теоретических анализах.

Исследования проводились на моделях, которые отражали распределения скоростей, определенные в скважине, с разной степенью детальности. При использовании модели скорости, полученной по грубому расчленению разреза, наблюдается очень большая ошибка измерения, которая получается из-за того, что модель недостаточно детально отражает реальные условия. Этот вывод потверждается теоретическими расчетами на модели слоистой среды с уменьшенным шагом квантования по акустическому каротажу, причем расчетные значения поглощения в значительно меньшей мере отличаются от заданных.

Készült a Prospektagent Gmk gondozásában,
Szedte a Nyomdaipari Fényszedő Üzem
Statisztikai Kiadó Vállalat
Felelős vezető: Kecskés József igazgató
Nyomdaüzem – 82–5265–09
Budapest, 1982
Terjedelem: 7,7 A/5 ív